Optical and Mechanical Aspects on Polysiloxane Based Electrical-Optical-Circuits-Board

Der Fakultät für Elektrotechnik und Informationstechnik

der Technische Universität Dortmund

zur Genehmigung eingereichte

Dissertation

zur Erlangung des Akademisches Grades

Doktor der Ingenieurwissenschaften

By

Dengke Cai

February 2008

1 Introduction 1

1.1 Electrical interconnect and optical interconnect 1

1.2 State-of-Art of polymer optical interconnect 2

2 EOCB fabrication and production................................. 7

2.1 Polysiloxane based EOCB lab fabrication.............................7

2.2 Polysiloxane based EOCB production 9

2.3 Overview about the thesis work 10

3 Optical aspects on EOCBs 15

3.1 Introduction...15

3.2 Experimental 16

3.3 Refractive index and bandwidth...18

3.4 Optical loss 23

3.4.1 Scattering loss 23

3.4.2 Intrinsic absorption loss by molecule vibrations........................25

3.4.3 Estimation of absorption loss 35

3.5 Processing of PDMS optical waveguides.............................43

3.5.1 Fabrication of PDMS optical waveguides 44

3.5.2 Scattering loss from mould roughness......................................48

3.5.3 Optical loss due to interlayer 50

3.5.4 Optical loss from packaging substrates 52

3.6 Summary of results of the chapter.......................................55

4 Mechanical Aspects on EOCBs 56

4.1 Introduction...56

4.2 Curing mechanism of PDMS materials 57

4.2.1 Hydrosilylation addition reactions in PDMS 58
4.2.2 Experimental characterization to PDMS curing.........................61
4.2.3 Identification of curing conditions for waveguides fabrication ...67
4.2.4 Mechanical characterization 69

4.3 Development of SAP and substrates etching 72
4.3.1 Basic concept for Surface-Adhesion-Promoter synthesis 72
4.3.2 Identification of substrate surface molecular structures 74
4.3.3 Effect of treatments on surface roughness 83
4.3.4 Effect of treatments on surface free energies of substrates......85
4.3.5 Influences from hydrophobic recovery on treated PCBs...........89

4.4 Development of EOCB fabrication based on SAPs and compatible etching method 91
4.4.1 Basic concept 90
4.4.2 Determination of SAP components and etching condition 94
4.4.3 Characterization to fabrication EOCB 96

4.5 Environmental stability of realized EOCB 102
4.5.1 Environmental accelerated testing design 102
4.5.2 Determination of simulating aging time and samples sizes 104
4.5.3 Optical stability of EOCBs...109
4.5.4 Mechanical stability of EOCBs..111

4.6 Summary of results of the chapter.......................................112

5 Conclusion and outlook.. 113

6 Liturature I

6.1 Applied liturature s..I

6.2 Own publications.. IX

1 Introduction

1.1 Electrical Interconnect and Optical Interconnect

Although higher component cost and ease of assembly continue to be challenges for the technology to substitute copper for applications with shorter transmission distances (typically within data and telecommunication systems), data transmission through optical fiber has provided significant advantages in terms of transmission distance and bandwidth compared with copper over long distances. For shorter transmission distances, the benefits of using optical technologies have been compromised by cost and performance improvements in copper based technology. Particularly in the areas of cable connecters and printed circuit board electrical performance, they are simpler, cheaper, and reliable. However, the increasing speeds being seen for optical communications are increasing the speed and frequencies being used in telecom and datacom equipment, which is causing electrical interconnection to be pushed to its limits.

The problem with electrical interconnections at higher frequencies is that the electrical losses through the copper traces become much higher; reducing the distance that the electrical signal can travel. All transmission of electrical energy results in the loss of electrical energy as the electrical current travels along the conductor. It can be lost though several ways including:

1) The heating effect generated by the resistance of the conductor.
2) The effects of the dielectric loss of the isolating dielectric materials.
3) Electrical field skin effects on the conductor – high frequency loss

This problem is well known at a large scale for electrical power transmission, where utility companies need to carefully plan how electricity is transmitted to end users without significant amounts being lost in the distribution network.[1, 2]

Optical boards solutions have been proposed for the upcoming electrical interconnect bottleneck for over 20 years. Presently, three types of optical board technology are emerging: [3-6]

- Buried Optical Glass Fiber.
- Buried Glass Waveguides.
- Buried Polymer Waveguides

There are three basic methods for the interconnection of optical technology for a system. The most suitable will depend upon the application and how far the optical element penetrates into the system itself.

Discrete Optical Fiber Interconnect

Discrete optical fiber interconnect represents one of the most common and fundamental means of interconnecting optical signals within a system today. As the title suggests, it uses discrete optical fibers and separable optical connectors to interconnect modules and components on one daughter card to another within a rack connection. Figure 1.1 illustrates a typical configuration using this approach. [1, 5]

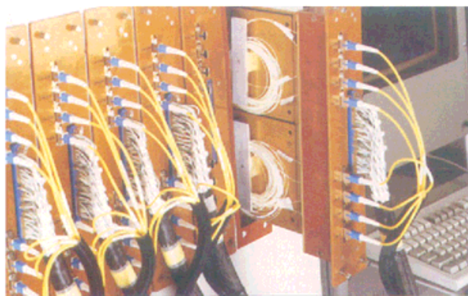

Figure 1.1 *Discrete optical fiber interconnect*

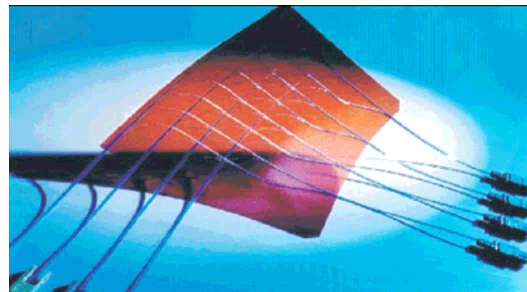

Figure 1.2 *Flexfoil optical interconnection*

A range of optical connectors is now widely available to realize such constructions. Typically MT-based multi-fiber connectors and ferrules are used including the MTP and MTRJ connector. This optical interconnect approach is simple, relatively low cost and offer high performance “point to point” interconnection for critical transmission lines within a rack system. Such an interconnection method is covered in this report, only as it represents the current interconnection point of many systems that utilize optical technology.

Flexfoil/ Buried Fiber Optical Interconnection

Advanced Interconnection Technology Incorporated (AIT) of Islip, New York, USA was one of the first companies to develop a “Flexfoil” optical interconnect technology (see Fig. 1.2). The alternative variation is to carry out a similar manufacturing process but to bury the fibers in a rigid board. This then allows the optical elements to be combined with the electronic part of the backplane system, which can then be incorporated in a cabinet format. This potentially saves converting optical signals an electrical signal and then back into an optical one when it can remain optic. This can save on electronics high cost connectors and reduce losses that are inevitable by OEO conversion. Here optics is penetrating into the system itself but here only passively. [1]

Electrical and Embedded Polymer Optical Interconnects

The third technology, which has only just recently emerged, is embedded optical waveguides in conventional printed circuit board technology, which is presently very attractive because of their potential of ease, low-cost manufacture and well compatible with SMT (Surface Mounted Technique) of standard PCB production. The final product will be the Electrical-Optical-Circuit-Board (EOCB) which is illustrated in Fig. 1.3. [7-10]

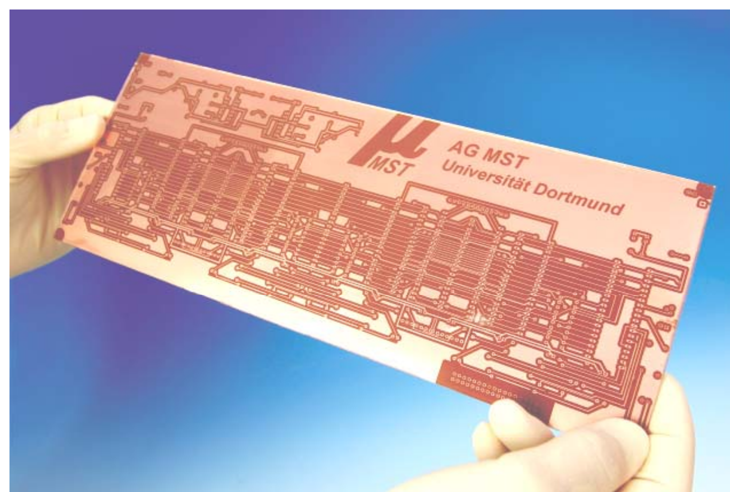

Fig. 1.3 *Electrical-Optical-Circuit-Board (AG MST)*

The basic idea of the EOCB concept is the combination of common PCB carriers with embedded polymer optical waveguides layer. But this has to be carried out with consideration of the interface processes: board fabrication and system assembling, and its basic figure are illustrated in Fig. 1.4.

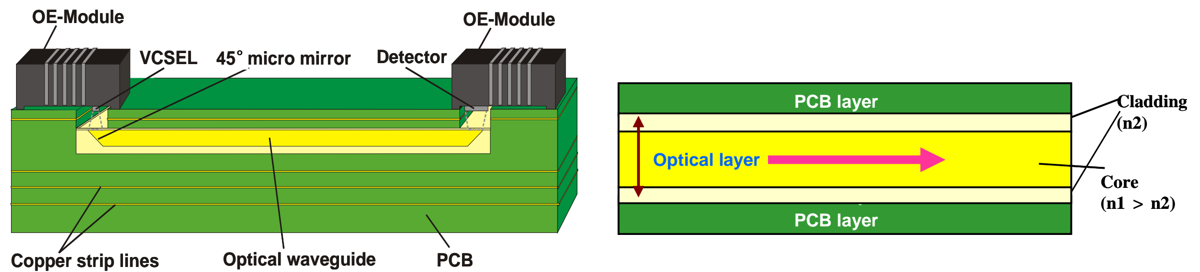

Figure 1.4 *Concept of EOCB with coupled optic-electric modules*

In the whole optical transmission system, it contains passive and active parts. The passive components involve both electrical and optical "wiring". Then active devices like VCSELs and PINs are coupled to the waveguides through 45° high reflectance mirrors. The polymer waveguide structure consists of three layers, i.e. top cladding layer, core layer and bottom cladding layer. In order to keep the light only to be transmitted in the core optical layer, the basic condition: refractive index $n_{core}>n_{cladding}$ must be fulfilled.

1.2 State-of-Art of Polymer Optical Interconnect

As mentioned, polymers have many excellent properties over silica. However, some drawbacks exist. Most polymers are unstable under high temperature and humidity conditions. Upon thermal aging, polymers can yellowish due to the oxidation. They have greater optical losses than silica and their chemical resistance is lower. However, many of these can be modified, and this makes them attractive materials for fabricating the optics on board.

Key parameters affecting the optical polymer waveguide are the core material and the waveguide index profile. The core material determines the attenuation characteristics and operating temperature, whereas the index profile limits to the maximum bandwidth (bit rate). Some of the key qualitative properties for waveguide materials are listed below. [10]

- Good refractive index control and low birefringence
- Intrinsic absorption loss, low optical scattering loss and low polarization dependent loss
- Low cost and environmental friendly material and low material processing loss
- High thermal stability, good environmental stability and good mechanical

strength

- Similar coefficient of thermal expansion (CTE) value as the other materials in use.

Nowadays in world-wide scale multiplicities of research groups at universities, institutes and in the industry are partly commercial developing optical materials (see Table. 1.1) for polymer waveguide fabrication, identifying respective fabrication procedures and are converting them into the manufacturing processes as well. In Tab. 1.2 it is listed about the results of the most important groups working in the area of the electrical-optical printed circuit board as well as the introduction of their research progress and solution which are embodied mainly on. e.g. fabrication methods, the optical propagation loss of EOCB products, temperature stability and products sizes etc.

Tab. 1.1 *Commercial optical waveguides materials*

Company/ Groups	***Material***	***Optical loss @850nm [dB/ cm]***
Exxelis Ltd./ Terahertz, GB[11, 12]	*Truemode Backplane* ™	0,04
Zen Photonics Co. Ltd., Korea[13]	*WIR30-470/WIR30-450, ZPU12-455/ZPU12-450*	0,16
Optical Crosslinks, Inc./ DuPont, USA[14]	*GuideLink*™/ *Polyguide*™	0,08
Dow Corning Corp., USA[13, 15]	Polysiloxane	0,04
Rohm & Haas Co./ Shipley, USA[16]	*LightLink*™ (Siloxane/ Silsesquioxane)	0,03
Micro resist technology, De[17]	*EpoCore/ EpoClad*	0,1-0,2
Micro resist technology, De[18]	*ORMOCER*™	0,10
MicroChem, USA[19]	*SU-8*	0,36
Luvantix Co., Ltd., Korea[20]	*EFIRON WR*-Series	0,20

Tab. 1.2 *Overview of EOCB research group*[21]

Group	***Fabrication***	***Core material***	***Size [cm]***	***Optical loss @850nm [dB/ cm]***

Group	***Fabrication***	***Core material***	***Size [cm]***	***Optical loss @850nm [dB/ cm]***
IBM[21]	UV-ML, Laser-Writting	Acrylate, Polysiloxane	50×50	0,04
DChr[22]	Laser-Writting	N. A.	103	0,04
Gemfire[23]	Laser-Writting	Polysiloxane	10	0,05
Intel[24]	Photo-Bleaching	Acrylate	20	0,10
ETRI (1)[25]	Hot Embossing	COC	8	0,10
NTT[26]	UV-ML	Epoxy	1	0,10
OPERA[27]	UV-Embossing	UV-Glue	N.A.	0,10
ITRI (2)[28]	Injection	Opt. Glue	17	0,12
TUDD[29]	Injection	Acrylate-Glue	6	0,12
IMEC[30]	Laser-Ablation	Truemode™	7	0,13
Hitachi[31]	UV-ML	Epoxy	6	0,15
UTex (1)[13]	Softlithography	Fluor. Acrylate, ZenPhotonics	N.A.	0,16
Fujitsu[32]	UV-ML	Epoxy, Nippon Steel Chem.	15	0,20
Gatech (1)[33]	UV-ML	Epoxy-Siloxane	14	0,24[1]
IZM[34]	Hot Embossing	UV-Glue in COC	12	0,30
KAIST[35]	UV-ML	SU-8™	5	0,36
Gatech (2)[36]	UV-ML	BCB	N.A.	0,36[1]
ETRI (2)[37]	UV-Embossing	ZPU, ZenPhotonics	N.A.	0,40[2]
ULin[38]	UV-ML	Omocer™	10×10, 60×60	0,50
VTT[39]	UV-ML	SU-8™	10	0,60
UTex (2)[40]	Softlithography	SU-8™	4	0,60
ITRI (1)[41]	UV-ML	SU-8™	10	N.A.
GE[42]	UV-ML	Epoxy-Polysulfone	N.A.	N.A.

2 EOCB Fabrication and Production

Actually, the Arbeitsgebiet Mikrostrukturtechnik (AG MST) has developed a new optical layer fabrication technology based on transparent silicones which comprises all essential features for a low cost mass production of large area electrical-optical circuits boards.[43, 44] This technology is becoming transferred to a worldwide first industrial production of EOCBs within the frame of a BMBF project named "Prospeos" which stands for "Prozesssichere Stückzahlproduktion elektrisch-optischer Schaltungsträger".

2.1 Polysiloxane Based EOCB Lab Fabrication

Reactive ion etching and UV-curing have been reported for polysiloxanes waveguide fabrication. With respect to our fabrication technology, we have adopted casting in combination with the doctor blade technique as a new polysiloxane waveguide fabrication method. The main advantages of this technology are that there are no restrictions on the waveguide cross-sections, which is important for multimode waveguides, and that it has the unique feature of simultaneously fabricating optical waveguides together with integrated micro mirrors and passive alignment structures for OE-module coupling. First a casting mould for the waveguide core layer is generated. This is accomplished by SU-8-photolithography. The resist is dried and exposed through a photolithographic mask. After development of the resist the master mould is finished (Fig. 2.1). In the reported experiments standard 6"-photoresist technology has been applied, and the extension to larger formats (300 mm × 400 mm) is realized as well. In case of large area formats (Fig. 2.2), doctor blading is used instead of spin coating because of the better thickness uniformity of the resist on rectangular substrates.

The basic prerequisite for the replication process is a robust mould or stamp. A further special requirement for optical waveguide fabrication is an extremely low

surface roughness (< 40 nm) to guarantee low scattering loss. Taking advantage of its high resolution and and chemical resistance we are employing SU-8 photoresist patterns directly as mould. No special release layers are required to separate the polysiloxane materials from the mould.

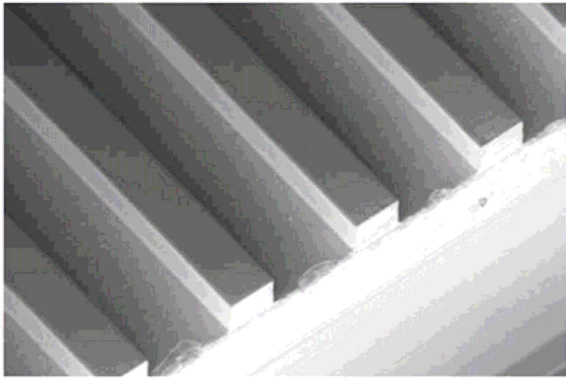

Fig.2.1 *SU-8 master form with straight channels*

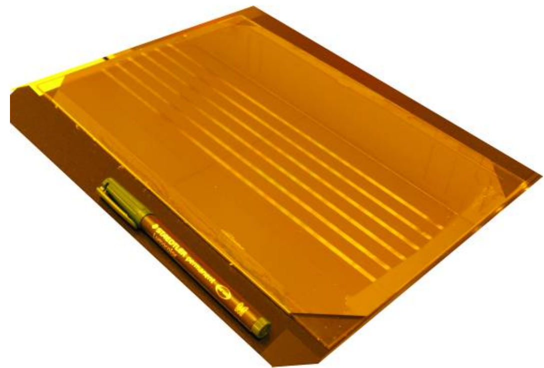

Fig.2.2 *Large size SU-8 master form*

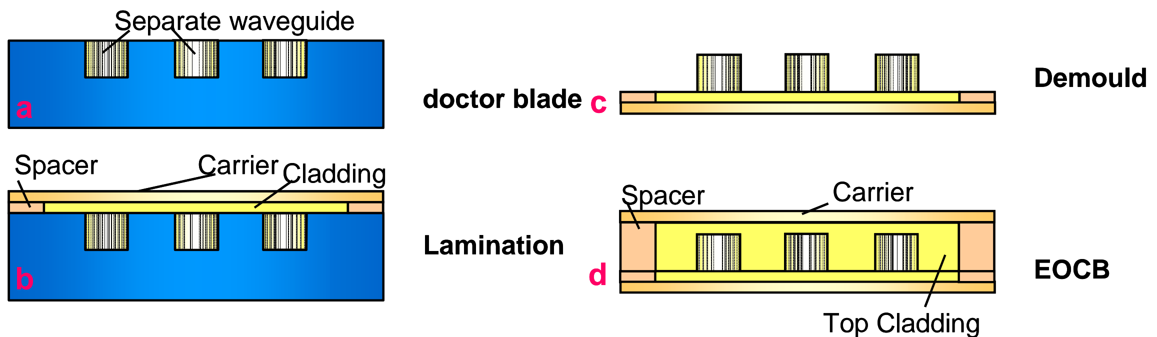

Fig.2.3 *Fabrication and self-packaging process of PDMS based optical layer*

The fabrication process starts with groove filling and blading of the core material (Fig 2.3a). The blading may be realized by hand or a stencil printer (Fig. 2.4) which is originally implemented in SMD techniques for reliably controlled process conditions e.g. control of blading angle, pressure and velocity for large size mould. After curing of the core material, the first cladding layer is applied. In the next step the first carrier (FR4, Kapton or copper) is laminated to the waveguide sandwich when the cladding is still in the liquid prepolymer state (Fig. 2.3b). After a second thermal curing, the complete core-cladding-carrier sandwich is demoulded (Fig. 2.3c). In the last step the second cladding layer is applied by casting and the second carrier is laminated on the liquid cladding material. After a third curing step the self-packaged optical layer is finalized (Fig. 2.3d). After fabrication, the optical layer embedded between two standard PCB-carriers can be integrated into any

conventional electrical multilayer board by using standard PCB production processes.

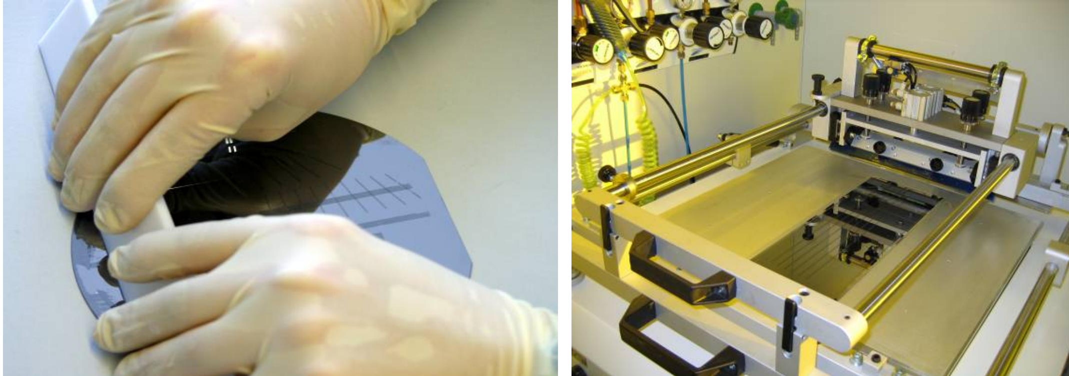

Fig. 2.4 *doctor blading by hand and stencil printer applied for controlled blading*

2.2 Polysiloxane Based EOCB Production

The described fabrication process above developed in laboratory scale at the University of Dortmund now is transferred to an industrial production line (format 460 × 305 mm2) within the framework of the BMBF-founded research project "Prospeos". In Fig. 2.5 a preliminary set-up of EOCB production machine and line is shown. A mobile stacker is placed in front and at the end of the line for easy sample handling and transportation.

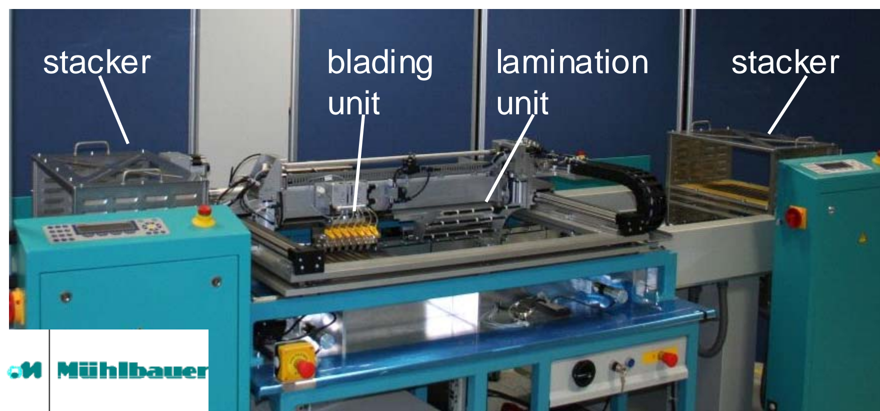

Fig. 2.5 *Preliminary set-up of EOCB production machine*

The samples (14 samples at once) are stored in the stacker after one production cycle and inserted at the beginning again. The production unit consists of three main elements: A spray coater, a blading unit and a curing oven. In between there

is space for manual operations like sample handling and retooling works. The first unit is a spray coater (Systronic/ Mühlbauer) where the moulds are coated with polysiloxanes and adhesion promoter, respectively. The automated blading unit is specially developed by ASEM GmbH in close cooperation with the University of Dortmund. Here the core material is applied by a peristaltic delivery, followed by blading and carrier lamination. In the curing oven the polymers are cross linked. Alternatively to inline curing the whole stacker could be placed into a fan oven. For producing the complete optical layer four cycles are necessary. In order to be processable by the shown processing techniques the basic polysiloxane materials had to be modified. To enable spray coating, the cladding material was blended by silicone oil to lower the viscosity to values < 1000 mPas. By spray coating polysiloxanes layer thicknesses between 20 and 200 µm could be achieved. To extend the pot life of the processable polysiloxanes materials from a few hours to some days inhibitors have been used. A critical point in using polysiloxanes materials in EOCBs is the realization of a mechanically stable interface between the optical PDMS layer and the adjacent PCB materials like FR4 or Kapton.

2.3 Overview about the Thesis Work

The industrial production line of polysiloxane based Electrical-Optical-Circuits-Board (EOCB) is under development within the German national industrial project Prospeos. However, in order to produce highly qualified EOCBs and assure their long-term reliable operation, it is necessary to identify the critical quality aspects on EOCBs and consequently pursue the respective quality control from these aspects. Considering from EOCB application environments, the quality control will be performed mainly from optical and mechanical two aspects.

Additionally, the important quality requirements from market requests and PCB compatibility etc. can be summed up from the following items:

- Bandwidth of 10 Gbps
- Low loss optical layer fabrication (loss< 10 dB/ m at 850 nm)
- Optical layer lamination to Printed Circuit Boards (T= 180 °C/ 2h)
- Lead-free soldering process (T> 250 °C/ 10s)
- Environmentally stable

In terms of the identified quality aspects and quality requirements the influences of the materials, processes, and reliability etc. on the optical, mechanical and thermal performances of the final EOCBs should be focused and studied. Quality

monitoring methods as well as test and optimization procedures need to be identified and verified as well.

In detailed, first in chapter 3 the optical aspects in EOCBs will be discussed.

In this aspect, the main problem is how to realize the low optical waveguide loss of EOCB after the whole process under meeting the request of bandwidth. The low optical waveguide loss may be affected from the following quality factors.

(1). Refractive index and Bandwidth

Guided wave optics confines radiation in the optical waveguides through the phenomenon of total internal reflection (TIR), where the core material is surrounded by a cladding material with a lower refractive index. The coupling and propagation characteristic of the waveguide i.e. bandwidth is thus defined by the core-cladding index difference. The respective refractive indices of practically applied core and cladding polysiloxanes in Prospeos project will be studied and measured as well as their numerical aperture and its thermal stability considering the operation environmental change of EOCB. Additionally, the bandwidth of EOCB also needs to be verified in terms of request of 10 Gbps/ 1m.

(2). Optical loss

In general, all optical waveguide devices need to have low optical loss, in particular at the major communication wavelengths. Actually, two main losses contribute to optical waveguide loss of EOCB, and one is the material intrinsic loss, e.g. scattering loss, electronic transition loss and molecular vibration absorption etc. The other is responsible for extrinsic loss which can be traced back to contaminating dust, pores, crystallites and core-clad interface roughness from the fabrication process.

First, with respect to material intrinsic loss various mechanism and reasons causing the optical loss in polysiloxanes will be identified from molecular views through optical spectroscopy methods e.g. FTIR. After that, some modification and improvement methods will also be proposed in order to fulfil the technical request of 10 dB/ m.

Additionally, within EOCB fabrication process core-clad interface roughness, structural interlayer between core and cladding layer, and packaging substrates are identified to be the main loss contributors. So, in the part their influences will be identified and respective controlling and improvement methods will be proposed as well in terms of the request of 10 dB/ m.

In chapter 4 the mechanical aspects in EOCBs will be focused.

It is vital for the reliable operation of EOCB to realize mechanically stable interfaces between core and cladding layers, cladding layers and the whole optical PDMS layers and the adjacent PCB substrate materials like FR4, Kapton and copper coated boards etc. In case of bubbles and insufficient interfacial adhesion among them, thermal stress due to CTE (Coefficient of Thermal Expansion) and Young's modulus mismatch will lead to delamination and resulting damage of the boards when processed for lamination and soldering etc.

The main work in the chapter is divided into two parts:

(1). Realization of EOCB robust packaging

First curing mechanism of polysiloxanes is studied. After that, with respect to core and cladding polysiloxanes different curing conditions within waveguide fabrication process will be defined and optimal conditions will be proposed as well to achieve mechanically stable interfaces in optical layer, i.e. core and cladding layers, and 1st cladding layer and 2nd cladding layer. Furthermore, in order to realize one robust packaging of polysiloxanes optical layer between PCB layers one highly efficient surface adhesion promoter will be studied and identified. PCB surfaces (e.g. elements distribution and topography etc.) will also be studied as main points to identify appropriate etching conditions and to match with the adhesion promoter from chemistry view. In the end, based on the aforementioned methods one novel EOCB packaging solution will be proposed and transferred to the real production line.

(2). Design for reliability

For an industrial implementation of EOCBs, a reliable production technology as well as a corresponding quality management must be developed. Consequently the environmental stability of the optical and mechanical properties of fabricated PDMS based EOCBs will be necessary to be verified.

Due to potential operation environments and long-term reliability of EOCBs, and also referring to the standards for optical components in telecommunications (Telcordia) and general PCB tests (IPC and IEC) experimental stability verification design will be done and the test items should be determined as follow, e.g. dry heating, damp heating and thermal shock etc.

With respect to different test items, different acceleration models will be built considering their different physical properties and phenomena. Additionally the

respective operation life will be estimated based on the defined aging conditions as well.

Moreover, considering from practical application market and referring to other similar products, one reliability objective for EOCB products will be defined based on the deduced acceleration factors above. Thereafter, the sample sizes will be determined with one set statistical confidence, e.g. 90%. Thus, in terms of the sample sizes, the experimental samples with respect to different test items will be prepared for the acceleration aging tests.

In chapter 5, one summary of the whole work and the brief outlook to future work will be presented.

This page is blank!

3 Optical Aspects on EOCB

3.1 Introduction

In the optical communication field, polymethylmethacrylate (PMMA), polystyrene (PS), polycarbonate (PC), epoxy, polyimide, perfluorocyclobutyl (PFCB)-based polymers, and polysiloxane etc. have been widely used as multimode waveguides materials for short-distance datacom applications, e.g., with polymer optical fibres (POF) in filtering and routing devices and others. However, their implementation in applications for the datacom market is still critical and restricted due to various factors such as high cost, shrinking, thermal instability etc., despite the fact that these materials all show the required optical transparency in the common datacom region (600 - 1600 nm).[45-53] Recently, two component addition curing polysiloxane e.g. Polydimethylsiloxane (PDMS), frequently referred to by the generic name silicones, are polymers with a unique combination of properties resulting from the presence of an inorganic siloxane backbone and organic methyl groups attached to silicon. Thermally robust SiO units are the backbone of those materials and thermal stability can be up to 300 °C, their refractive indices can range from 1.39 to 1.50 (at a wavelength of 589 nm at 20 °C) by varying the concentration of vinyl groups in the base component.[53-55] The chemical configuration produces silicone polymers which have low glass transition temperatures, and hence are fluids over a wide range of temperatures, have good thermal stability, good oxidative resistance, good optical properties down to 300 nm and good chemical stability. In addition, due to easy and low cost (≤ 50 euro/ l) thermal casting and injection techniques under no shrinking, and also such PDMS show minimal insertion loss compared to multimode PMMA and glass waveguides, thus they were received much interest for application in waveguide based devices.

The bands in the spectral VIS-NIR region are primarily overtones and combinations of the fundamental bands found in the classical mid-infrared region. Most chemical bonds have negligible harmonic absorption compared with so-called X-H subgroup

bonds, i.e., C-H, N-H and O-H. Among the latter, the absorption losses from N-H and O-H subgroups are usually 10 - 20 times larger than those arising from C-H vibrations, so for the pre-selection of optical siloxane-based polymers, no N-H and O-H bonds should exist. With the growing interest in addition-thermal curing two-component siloxane-based materials for optical datacom applications e.g. EOCB production project: Prospeos, however, until now only very few reports have been devoted to the characterization of their optical characteristics in the visible and near-infrared (VIS - NIR) region, which is the most important wavelength range for datacom and telecom applications.

In this chapter, commonly used PDMS –also practically applied materials in EOCB prospeos project- was selected for this study with regard to the bandwidth applicability. An empirical equation for estimating the wavelengths with the most significant intrinsic absorption loss due to the corresponding vibration band was formulated, which was found to agree well with the experimental data. It provides a relationship between the integral band strength and the intrinsic absorption loss, thus furnishing us with estimates of the loss limit in such materials when implementation in data- and telecom devices is strived for. For such purpose, singlemode and multimode waveguides were fabricated and their respective optical insertion loss was also measured at 1300 nm and 850 nm, as well their thermal stability verified.

3.2 Experimental

Polymer formulation

The key functional group of the PDMS polymers is $–SiO(CH_3)_2$ which can be considered as an organically modified quartz, i.e., two oxygen atoms attached to every silicon atom have been replaced by methyl groups. This changes the structure from the three-dimensional backbone of quartz to linear polymer molecules. Here, the methyl groups are free to rotate about the -Si-O-Si- chain. As a derivative, other groups instead of methyl groups can be attached to the silicon-oxygen backbone. The linear silicone polymers can be crosslinked to each other by different extents, i.e., covalently via groups containing different atoms. This explains the wide range of optical, mechanical and chemical properties of the corresponding silicones.

A two-component commercial PDMS polymer called RT 601 (Wacker Chemie, Burghausen, Germany) was used as cladding material. In close cooperation with

our group, the PDMS core material was especially developed by Wacker Chemie (provisional product name SLM 77522), with a few methyl groups substituted by phenyl groups for obtaining a higher refractive index as required for waveguiding. Both materials were prepared from two components by means of a cross-linking procedure through a hydrosilylation reaction by thermal curing using a platinum catalyst. The addition reaction occurs mainly on the terminal carbon and is catalysed by organometallic Pt colloid complexes. The following mechanism, as illustrated in Fig. 3.1, has been proposed after the oxidative addition of the SiH groups in the coupling agent by means of the Pt catalyst with a following hydrogen transfer onto the double bond and a reductive elimination in the product (for simplification, other Pt ligands and Si-substituents are omitted).

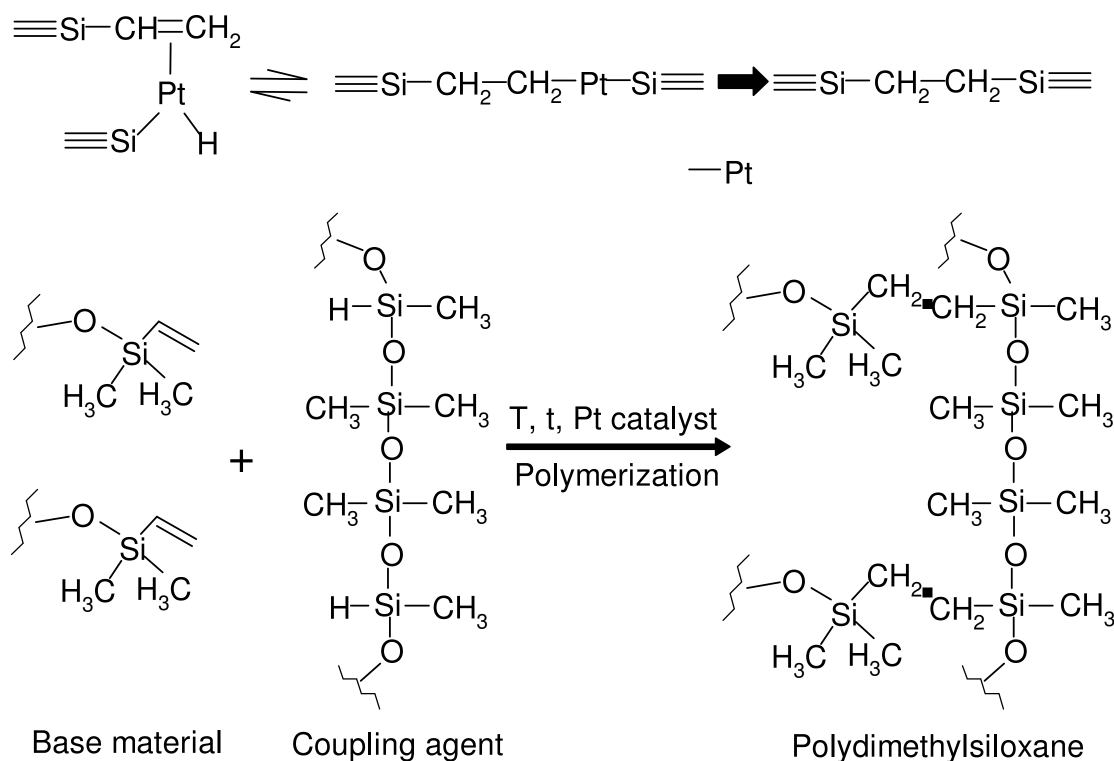

Fig. 3.1 *PDMS polymerisation scheme based on a two-component set. The first scheme illustrates the reaction principle (the symbol in the above formula '≡' represents two methyl groups and the rest of the polymer chain).*

To study the optical properties of amorphous PDMS cladding and core polymers, it was necessary to purify the raw material before the curing process to avoid extrinsic losses, e.g., by particle scattering. The base material and coupling agent were both filtered using a cellulose-mixester membrane filter of pore size of 0.2 µm. After purification, they were mixed in the ratio of 19:1 for cladding and 9:1 for core

materials, respectively, and deaerated through vacuumizing. Subsequently, the mixed polymers were cured in a clean oven for 2 hrs at 70 °C to obtain samples for the optical characterisation. All experiments were performed under clean room (class 100 and 10) conditions.

Spectrometers used for optical characterisation

For mid-infrared measurements, a PE-2000 FTIR-Spectrometer (Perkin-Elmer, Überlingen, Germany) was available. As measurement conditions, 500 scans were coadded for spectral recording at a spectral resolution of 2 cm^{-1}. Transmission measurements were carried out with solid films on a ZnSe window. Near-infrared and visible optical absorption measurements were made using a FT-NIR-spectrometer Vector 22N from Bruker Optics (Ettlingen, Germany) equipped with a Ge-diode as detector (1500 scans coadded, spectral resolution of 64 cm^{-1} and Norton-Beer (strong) apodization) and, secondly, a spectrometer Cary 5 from Varian (Darmstadt, Germany), based on a scanning double monochromator (scan rate 60 nm/ min; slit width 2 nm). Samples were prepared with optically flat surfaces, and their thickness varied between 3 mm and 30 mm. The measurements were carried out in a temperature controlled environment of 23 ^{o}C ± 2 °C.

For Raman measurements, a portable HoloSpec Raman spectrometer from Kaiser Optical Systems, Inc., provided with a diode laser (λ = 785 nm, 50 mW) from SDL, Inc. and a liquid-N_2 cooled CCD detector from RS Roper Scientific were used. Part of the spectrometer is a non-scanning polychromator that is equipped with a fiber-optic probe, usable also for remote-measurements. It combines robustness and high detectivity with reasonable resolution. The following measurement conditions were used: integration time of 25 s with 10 spectral frame accumulations at a laser power of 10 mW.

Refractive index measurements

Wavelength dependent measurements in the visible and near-infrared spectral range were carried out on RT 601 PDMS intended as cladding and SLM 77522 as core material. An "ABBE-Refractometer" from Zeiss (Jena, German.) was applied to measure the different refractive indices by using the limit angle of total reflection at different wavelengths. For this, a sodium emission lamp with filter at 589 nm was used, and a halogen tungsten lamp with different filters at 515 nm, 632 nm, 852 nm, 1300 nm and 1550 nm, respectively, under a constant temperature of 20 °C.

3.3 Refractive Index and Bandwidth

Optical waveguiding was first referred to as 'light piping' in 1880 by Wheeler. This effect of light transmitted through a glass pipe medium is what is now described with fibre-optics technology. Guided wave optics confines radiation in the optical waveguides through the phenomenon of total internal reflection (TIR), where the core material is surrounded by a cladding material with a lower refractive index. The coupling and propagation characteristic of the waveguide is thus defined by the core-cladding index difference.

The refractive index of polymers mainly depends on the molecular polarizability, the molecular volume and the difference between the used optical wavelength and the maximum absorption wavelength of polymers. In terms of the PDMS polymer used in the paper, the core material has an intrinsic higher refractive index than the cladding material through the introduction of phenyl groups that are substituting methyl groups in the side chain of the PDMS backbone which will be described in detailed elsewhere. The ratio of methyl to phenyl units can be varied to obtain a broader refractive indices interval. [56]

With the refractive indices measured at several wavelengths, there are various dispersion formulas available that could be used for the fitting refractive index data, e.g., equations provided by Hartman, Conrady, Herzberger, Schott Optical Glass, Inc., and Sellmeier.[57-59] But some of the formulas, e.g., by Conrady, Schott or Herzberger, are linear in their fitting constants, which means they can be fitted easily using a classical least-squares procedure; from this, it should be clear that the fitting accuracy should be the dominant aspect in choosing the most appropriate dispersion formula. From this point of view, the Sellmeier equation is especially suited for the coverage of the refractive index in the wavelength range from the UV through the visible to the mid-IR range (up to 2.3 µm) due to its high accuracy and applicability. The Sellmeier formula is derived from the classical dispersion theory and allows the description of the progression of refractive index throughout the total transmission region with one set of parameters and the calculation of accurate interpolated values. Presently, it has been found that a 3-term Sellmeier formula is generally a necessary and sufficient descriptor for satisfactorily fitting almost all refractive index data of materials in practical use within their main transparent region. Equation (3.1a) describes the three-term Sellmeier formula:

$$n^2 = 1 + \frac{B_1\lambda^2}{\lambda^2 - C_1} + \frac{B_2\lambda^2}{\lambda^2 - C_2} + \frac{B_3\lambda^2}{\lambda^2 - C_3} \qquad (3.1a)$$

where n is the optical index at wavelength λ, B_1 - B_3 and C_1 - C_3 are the constants to be determined by the fitting process.

In Fig. 3.2A and B, the refractive index measurement results of the cladding and core PDMS materials with the Sellmeier fitting curves and the calculated A_N values (numeric aperture, $A_N = \sqrt{n_{core}^2 - n_{cladding}^2}$) at different wavelengths are shown, respectively. The Sellmeier formular for the two fitting curves of cladding and core are shown in equations 3.1b and 3.1c.

$$n^2 = 1 + \frac{-2.30744 \times \lambda^2}{\lambda^2 + 0.02605} + \frac{1.85952 \times \lambda^2}{\lambda^2 + 0.01362} + \frac{1.39944 \times \lambda^2}{\lambda^2 + 0.01349} \qquad (3.1b)$$

$$n^2 = 1 + \frac{-0.1432 \times \lambda^2}{\lambda^2 + 0.69379} + \frac{1.01366 \times \lambda^2}{\lambda^2 - 0.01304} + \frac{0.14158 \times \lambda^2}{\lambda^2 + 0.58129} \qquad (3.1c)$$

In addition, by varying the temperature from 20 ℃ to 55 ℃ the respective thermo-optic coefficients (TOC) of core and cladding were obtained and displayed in Fig. 4, where the core TOC is $-3.59 \cdot 10^{-4}$/ K and that of the cladding material is $-3.65 \cdot 10^{-4}$/ K. Whilst as seen, the A_N values are quite stable with a rise in temperature, for the PDMS waveguides the temperature is possibly not stable enough due to environmental changes and variation from active elements, e.g. the optical laser and photodiode etc.

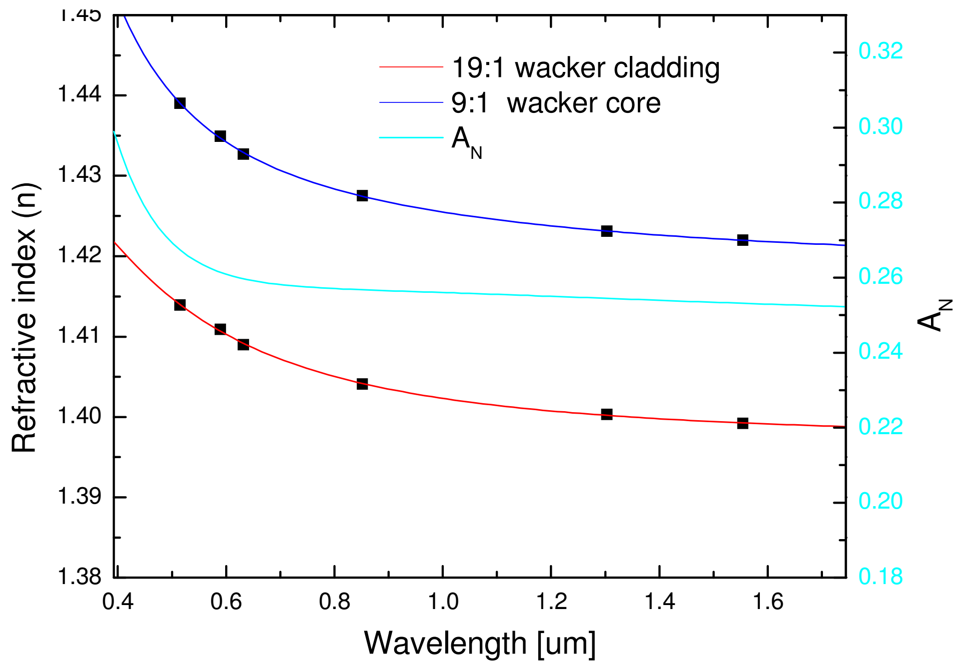

Fig. 3.2*A* *Wavelength dependency of the refractive indices of the PDMS core and cladding materials (left ordinate scale) and the numerical aperture calculated for this combination of materials (right ordinate scale);*

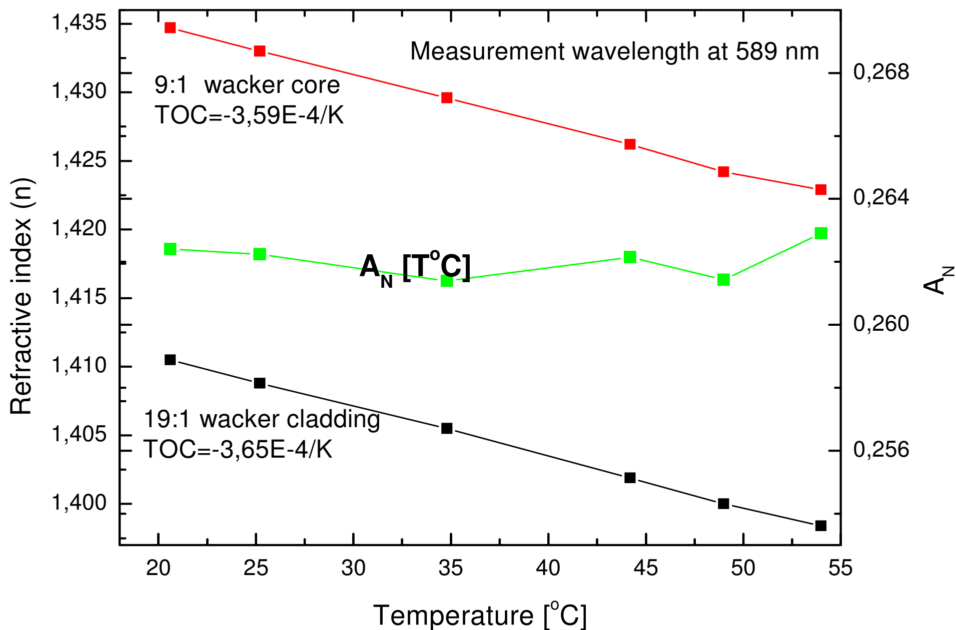

Fig. 3.2B *Temperature dependence for the refractive indices of both materials and of the corresponding numerical aperture at 589 nm.*

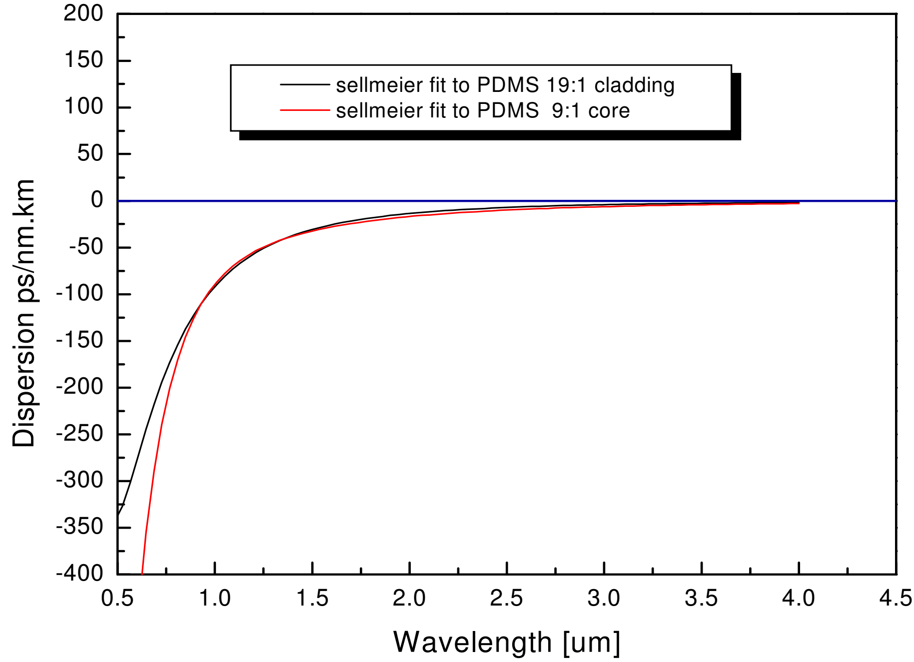

Fig. 3.3 *Calculated wavelength dependent dispersion for PDMS clad and core materials*

In optical waveguides, mode dispersion (different propagation constants for each mode) and material dispersion are the main effects which limit the bandwidth of the optical waveguide transmission. Based on the obtained Sellmeier fitting curves, as shown in Fig. 3.2A, the material dispersion curves of the PDMS cladding and core were both obtained using the material dispersion equations below (c/n is the light velocity).

$$M(\lambda) = -(\frac{n \times \lambda}{c}) \times (\frac{d^2 n}{d\lambda^2}) \qquad (3.2)$$

As seen, the material dispersion of the core PDMS is -144.9 ps/ (nm.km) and -45.01 ps/ (nm.km) and of the clad material is -136.87 ps/ (nm.km) and -45.96 ps/ (nm.km) at 850 and 1300 nm wavelengths, respectively.

For multimode waveguides, apart from the material dispersion, there also exists mode dispersion, which is the maximal time delay $\Delta t_{g\max}$ between the longest and shortest rays through the core of the PDMS waveguide. This can be expressed by Eq.3.3:[4]

$$\Delta t_{g\max} = LA_N^2 / (2cn_{core}), \qquad (3.3)$$

where L is the length of the polymer waveguide layer, A_N is numeric aperture of the

step-index waveguide, c is the light speed in vacuum and n_{core} is the refractive index of the core material at the work wavelength.

Also, the relation between dispersion and bandwidth may be simplified with Eq. 3.4:

$$B \approx 0{,}443 / \Delta t_{g\max} \qquad (3.4)$$

According to the Nyquist rule[60] the maximum data rate is $R_{\max} = 2B\log_2 V$ bps where B is the bandwidth and V is the number of states encoded. In our case is V=2, so $R_{\max} = 2B$, with B and Δt substituted equation (3.4) and (3.3), respectively, leading to,

$$R_{\max} = \frac{1.772 \times c \times n_{core}}{L \cdot A_N^2} \qquad (3.5)$$

For such a PDMS waveguide system, assuming a transmission speed of 10 Gbps at 850 nm wavelength and a 20 ℃ work temperature, it can be concluded that its optical pathway should be below 1.14 m, which is the precondition for using such PDMS polymers for optical waveguiding. If longer optical interconnect is required, the material design can be achieved through varying the ratio of phenyl and methyl groups in PDMS to decrease the index difference between core and cladding material.[53, 61]

3.4 Optical Loss

In general, all optical waveguide devices need to have low optical loss, in particular at the major communication wavelengths, e.g. 850 and 980 nm for datacom, or 1310 and 1550 nm for telecom applications. Normally, four kinds of attenuation loss phenomena contribute to the propagation loss in optical polymer materials within the VIS - NIR region: first, in the far ultraviolet region with a wavelength less than 200 nm the molecules with single bonds (predominantly molecular groups with aliphatic hydrogen atoms) can undergo $\sigma \rightarrow \sigma^*$ transitions, but this is not of interest to us. In addition there are absorptions arising from $\pi \rightarrow \pi^*$ or $n \rightarrow \pi^*$ electronic transitions caused by double bond structural units, e.g., >C=C< or >C=O etc. Theses usually appear in the ultraviolet wavelength region and influence the propagation loss of optical polymer materials still in the visible wavelength region through their absorption tails (200 - 400 nm). Secondly, molecular vibration absorption exists due to the higher harmonics (overtones) of fundamental

stretching vibrations and combination bands with corresponding bending vibrations, which are main contributors to the absorption losses as found in amorphous polymers at wavelengths beyond 600 nm. Furthermore, the third significant loss factor is due to Rayleigh scattering, caused by fluctuations of the density and the refractive index in such polymer materials. The three loss phenomena mentioned above explain intrinsic propagation losses. Other sources that are responsible for extrinsic loss can be traced back to contaminating dust, pores and crystallites from the fabrication process. Of particular importance, especially for polymer waveguide systems, is the scattering due to the core–clad interface roughness as another source of extrinsic loss.[62]

3.4.1 Scattering Loss

Extrinsic loss arising from scattering in polymers can result from unfiltered particles, dust, dissolved bubbles and uncreated monomer. For eliminating this source of extrinsic scattering it is necessary to follow rigorously ultimate procedures in the preparation of polymer formulations, e.g. by filtering and deaeration etc., and to perform all preparations in a clean room environment.

As scattering often arises from a number of sources, the experimental scattering data often fits with an empirical law of the form: [56]

$$\alpha_{scatter} = A + B/\lambda^2 + C/\lambda^4 \qquad (3.6)$$

where A is the contribution from large particle scattering (i.e., with their diameters >> λ), B the contribution from inhomogeneities in the order of λ in size (Mie scattering), and C the contribution from smaller inhomogeneities (size << λ, Rayleigh-like).

The material of RTV 2 PDMS is a kind of elastomer polymer with a very low glass-transition temperature (around – 50 ^{o}C) which means that it is in the liquid state at the normal operation temperature. In addition, its base components have been filtered and deaerated before thermal curing, so Rayleigh scattering loss will be negligible compared with other intrinsic losses, e.g. from vibrational overtone absorptions beyond 600 nm.

Then RTV 2 PDMS is polymerized through a hydrosilation reaction by thermal curing using a platinum catalyst (see also Fig. 3.1) and after hydrosilylation, the Pt catalyst complex will be a by-product. The Pt catalyst complex is possibly bonded with some left over polar components in cured PDMS, e.g. vinyl groups as found in

the base component to form a more stable and larger size colloid with increasing temperature and continuous curing. This will result in PDMS compositional inhomogeneities in even larger length scales giving rise to optical scattering. To investigate and confirm the influence of Pt on the optical loss, a commercial Pt catalyst complex (Catalyst EP from Wacker, Chemie) and a pure filtered PDMS polymer (RT 601, Wacker, including 30 - 40 ppm of Pt in the base component), not containing other impurities like silicon oil and inhibitors etc., were selected for studying its contribution to the loss budget.

It was identified in Fig. 3.4A that the optical scattering loss of PDMS increased gradually as a larger platinum concentration was chosen. From Fig.3.4B, it was also found that Pt colloids changed peak shifts from 260 nm to 325 nm due to size change or so due to more platinum catalyst added and higher temperature treatment. Whilst it also proves that PDMS with the increased addition of Pt catalyst shows brownness and yellowness due to the blue light scattered out. In order to improve the PDMS optical stability and decrease the scattering loss, the Pt concentration should get controlled in a preliminary step before reaching its final applications.

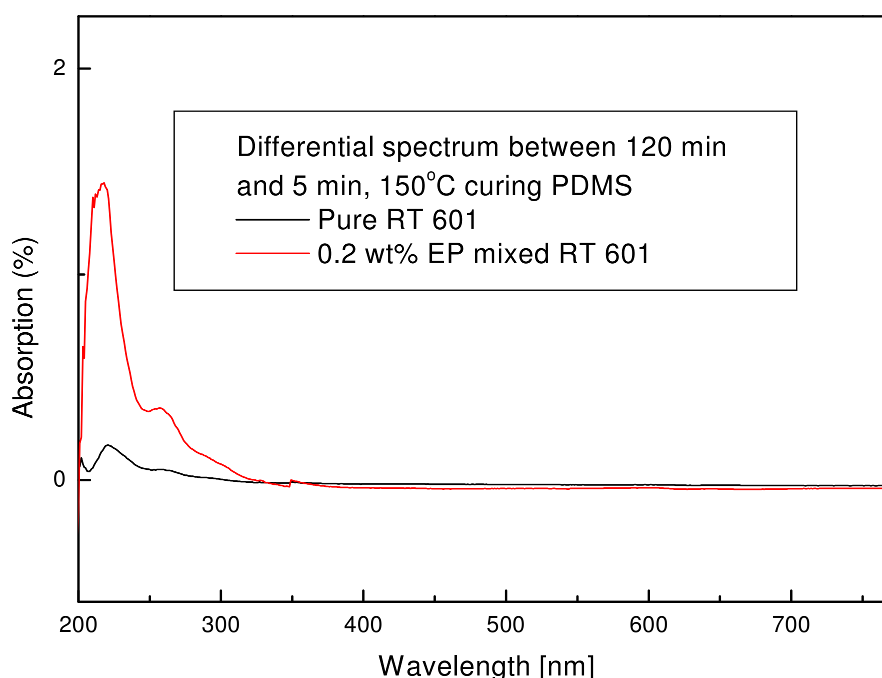

Fig. 3.4 A *optical scattering loss of PDMS with different Pt concentrations;*

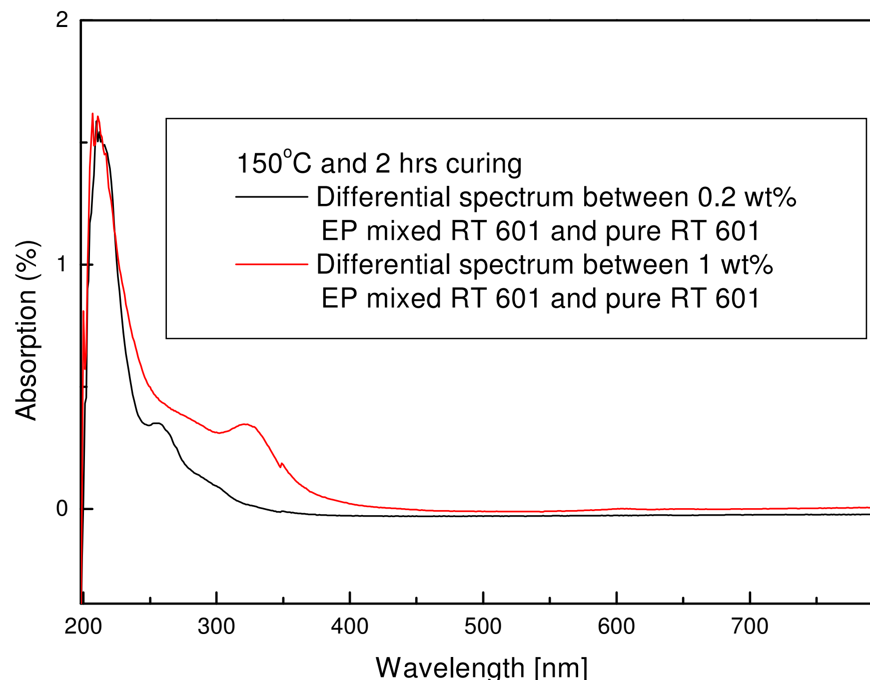

Fig. 3.4 B *size change due to different Pt concentrations*

3.4.2 Intrinsic Absorption Loss by Molecule Vibrations

For polymer materials, both electronic and vibrational absorptions are likely to contribute to optical loss. Polymeric media generally have large absorptions in the ultraviolet owing to fundamental excitations of their electrons. These absorptions tend to be in the deep ultraviolet (less than 200 nm) for polymers with predominantly aliphatic hydrogen atoms, and in the near UV ranging from 200 to 400 nm for polymers with significant numbers of aromatic hydrogens.

Then in the VIS-NIR region, absorptions coming from overtones and combinations of the fundamental bands found in the classical mid-infrared region are dominant. Since the strength of the absorption tends to decrease by approximately an order of magnitude between each harmonic order, higher harmonics are generally weak enough to not be of concern (at least for waveguide applications). Clearly, the highest energy vibrations will be those that have high spring constants (stiff bonds, such as double bonds) or small reduced masses. The smallest reduced mass occurs when one of the atoms is hydrogen. Thus for most chemical bonds, they have negligible harmonic absorption compared with some X-H bonds (C-H, N-H and O-H), in addition among them the absorption losses from N-H and O-H are 10-20 times larger than C-H, so in the pre-selection of optical polymers, they

should contain less N-H and O-H bonds.[53]

Determination of the anharmonicity constants of PDMS

PDMS system as studied belongs to the category of addition thermal curing RTV 2 silicone resins, and after polymerization electronic transition absorption can be neglected in the optical loss analysis of PDMS after 600 nm wavelengths. In addition, once Pt concentration is controlled in from 10 to 50 ppm which can ensure the basic curing of PDMS, consequently, most of the intrinsic attenuation losses of PDMS arise from overtone and combination bands of molecular vibrations.

From mid-IR spectra of cladding and core were, the band assignment of measured with FTIR and FTRaman spectroscopies and illustrated in Fig. 3.5, furthermore we assigned the fundamental bands of various chemical bonds in PDMS e.g. Si-O and Si-C etc., respectively, which are observed at longer wavelength in the mid-IR region and shown in Table 3.1. Absorption bands due to these chemical bonds can be neglected in the VIS-NIR wavelength region, compared with vibrations of the C-H bonds within them, e.g. polyatomic $–CH_3$ methyl, $-CH_2$ methylene and C=C vinyl and CH phenyl (in core material- SLM 77522) groups etc.

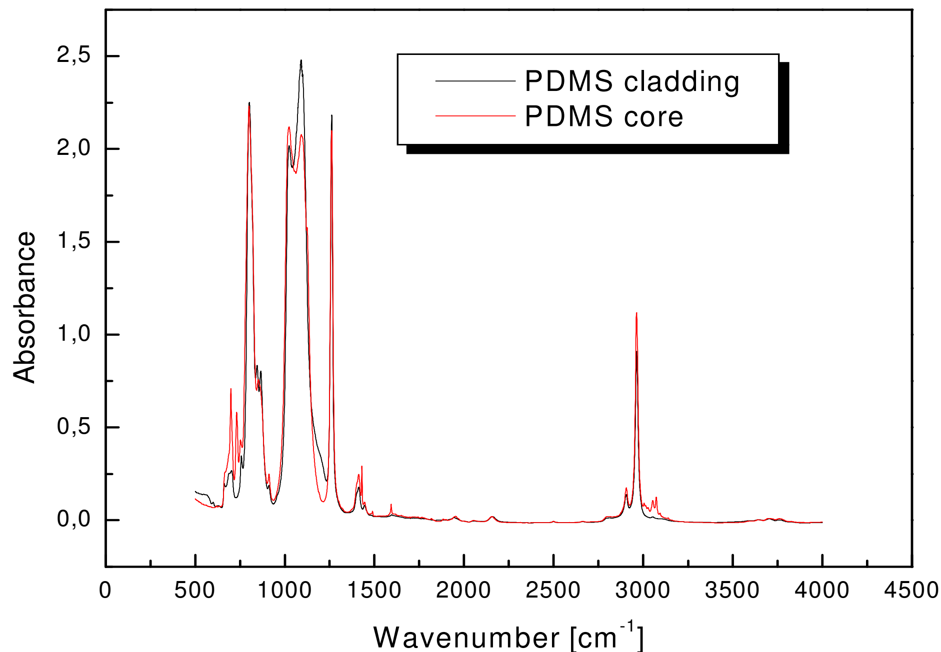

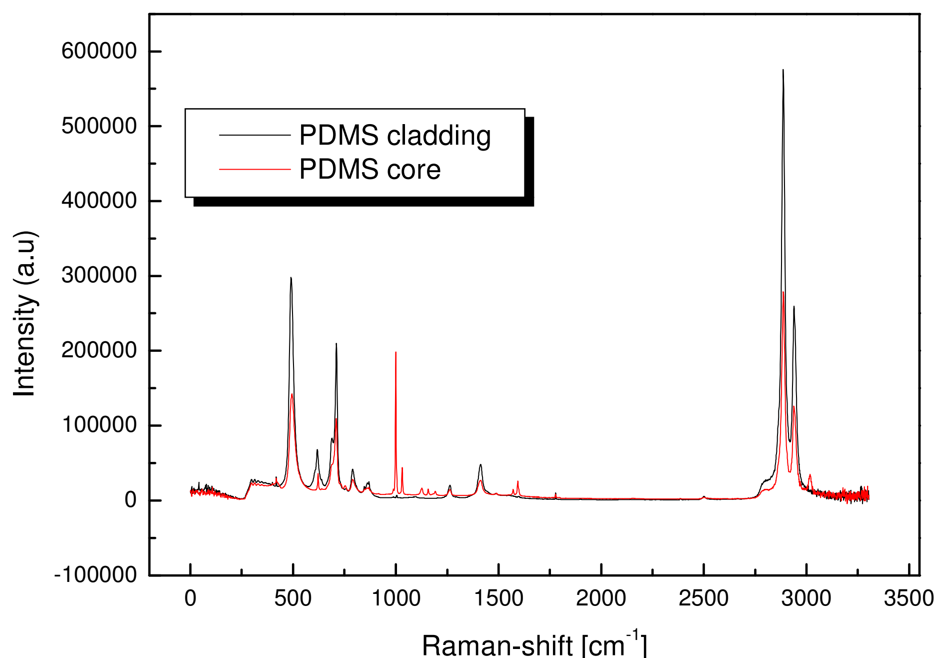

Fig. 3.5 *FTIR and FTRaman spectra of clad and core PDMS*

To polyatomic molecules, the anharmonicity causes not only the appearance of overtones but combination bands as well. When the fundamental are related to C-H, N-H and O-H functional groups that occur between 4000 and 2500 cm^{-1}, the overtones and combinations make up the backbone of what is called the "near-infrared". Thus this region of the spectrum is not really difficult and can be predicted by the rules of spectroscopy as well as any other "normal" region.

Table 3.1 *Infrared and Raman spectral bands assignment of PDMS* [63-64]

Assignment	Cladding ($\tilde{\nu}_{exp}/cm^{-1}$)	Core ($\tilde{\nu}_{exp}/cm^{-1}$)
Si-C - Valence, sy, $Si(CH_3)_2$	664	664
Si-C - Valence, as, $Si(CH_3)_3$	687	687
CH_3 - rocking, sy, $Si(CH_3)_3$	758	758
Si-C - Valence, as, $Si(CH_3)_2$	799	799
CH_3 - rocking, sy, $Si(CH_3)_2$	815	815
CH_3 - rocking, as, $Si(CH_3)_3$	844	844

CH_3 - rocking, as, $Si(CH_3)_2$	866	866
Si-C stretching and CH_3 rocking	802	800
CH_2 wag	912	911
Si-O-Si stretching vibration.	1023-1100	1024-1100
$\delta_s(CH_3)$	1263	1261
CH_2 asymm waging	1342	1337
CH_2 symm waging, C-C stretching	1367	1372
$\delta_{as}(CH_3)$	1412	1412
Si-Phenyl	ND	1430
CH_2 symm. Bending	1446	1446
CH_2 asymm. Bending	1475	1479
$Si\text{-}CH{=}CH_2$	1597	1593
Si-H	2159	2156
$\nu_s(CH_3)$	2905	2905
$\nu_{as}(CH_3)$	2963	2963
$\nu_s(CH_2)$	2840	2840
$\nu_{as}(CH_2)$	2928	2928
$\nu_s(=CH_2)$	2970	2970
$\nu_{as}(=CH_2)$	3041	3043
aromatic $\nu_s(CH)$ stretching	ND	3052
aromatic $\nu_{as}(CH)$ stretching	ND	3072

Taking into account the anharmonicity terms (higher than quadratic terms, cubic, quartic…), the general formula (without degenerate vibrations) for combination and overtone vibrational energy levels of a polyatomic group (term scheme is given in wavenumber units) is: [63]

$$G(\mathrm{v}_1, \mathrm{v}_2 \ \ldots) = \sum_i \bar{\nu}_i (\mathrm{v}_i + \frac{1}{2}) + \sum_i \sum_{k \geq i} X_{ik} (\mathrm{v}_i + \frac{1}{2}) (\mathrm{v}_k + \frac{1}{2}) + \ \ldots\ldots\ldots\ldots (3.7)$$

Where $\tilde{\nu}$ i is the corresponding frequency of the symmetrical stretching and bending, asymmetrical stretching and deformation fundamental vibrations etc. (also

called normal vibrations) measured in units of cm^{-1}, and the X_{ik} are their anharmonicity constants.

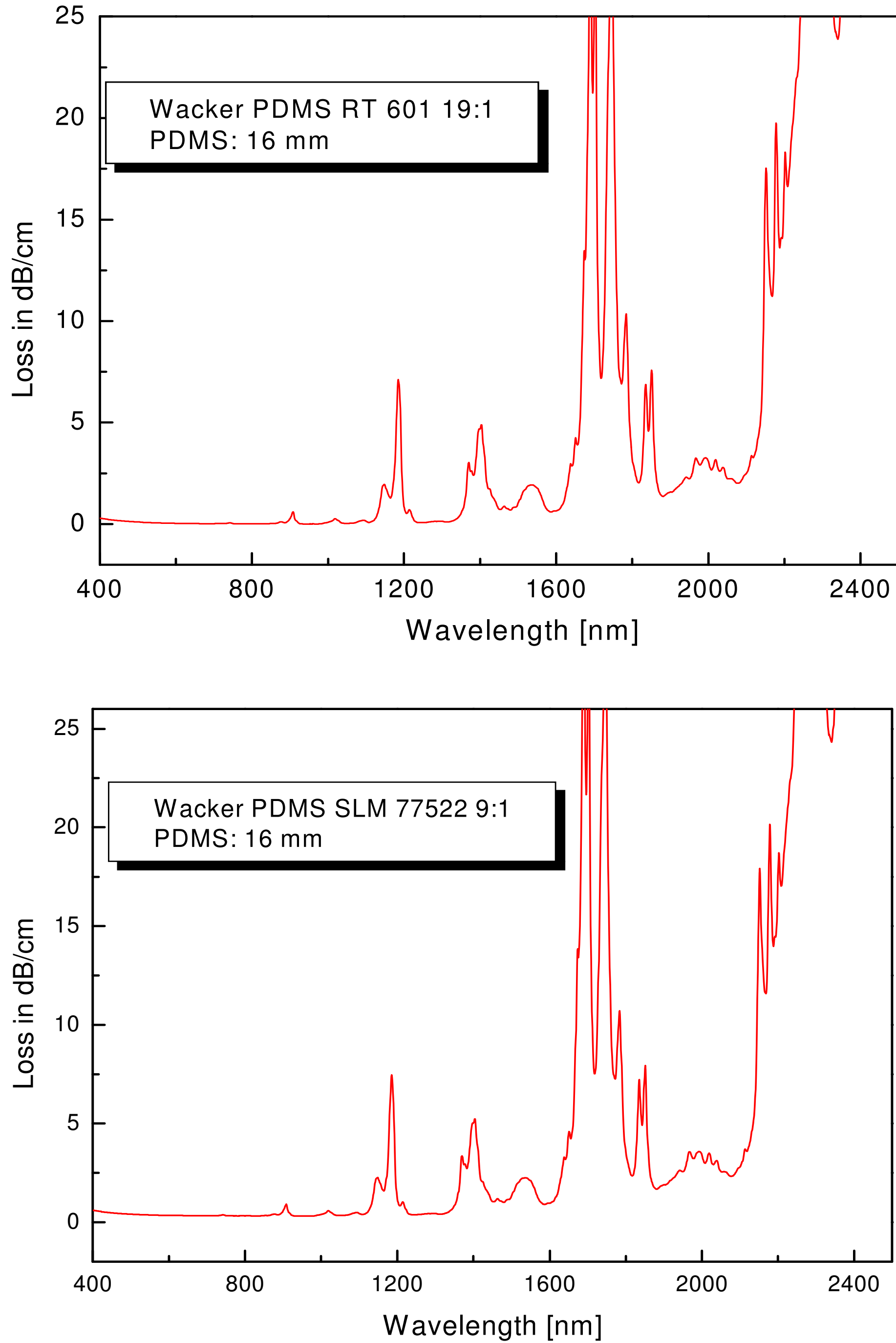

Fig. 3.6 *FTNIR loss spectra of clad and core PDMS*

CH_3 methyl group was selected for study and then the approach for determination of the anharmonicity constants is also valid to other molecular groups. For the assignment of higher overtone and combination bands, as well as the fundamental bands of the CH_3-group vibrations in cladding and core PDMS polymers, their NIR spectra were measured as well, which are presented in Fig. 3.6.

A molecule containing a number, N, atoms will have (3N-6) vibrational degrees of freedom (3N-5 for linear molecules). The PDMS molecular structure contains four atoms in the polyatomic CH_3- group, and thus the latter holds six vibrational degrees of freedom; among them, and in order to simplify the calculations, we are considering only four normal vibrations, i.e. the symmetric and asymmetric stretching and deformation vibrations, called ν_1, ν_2, ν_3, ν_4, since further two are both found at longer wavelength and show relatively low intensity. Thus, their influence on the VIS-NIR region will be negligible. With our previous assignments, we can also calculate the anharmonicity constants. For example, the wavenumber associated with the frequency of the ν_1 vibration is given by the following term differences:

$$\overline{\nu_1^{01}} = G(1,0,0,0) - G(0,0,0,0) = \overline{\nu_1} + 2X_{11} + \frac{1}{2}X_{12} + \frac{1}{2}X_{13} + \frac{1}{2}X_{14} \qquad (3.8a)$$

And, for the first overtone of vibration ν_1, also called $2\nu_1$, with $v_1 = 2$, $v_2 = 0$, $v_3 = 0$ and $v_4 = 0$:

$$\overline{\nu_1^{02}} = G(2,0,0,0) - G(0,0,0,0) = 2\overline{\nu_1} + 6X_{11} + X_{12} + X_{13} + X_{14} = 2\overline{\nu_1^{01}} + 2X_{11} \qquad (3.8b)$$

In the case of the CH_3-group, the fundamental $\nu1$ is located at 2905 cm^{-1} and its first overtone is observed at 5725 cm^{-1}, and X11 can be easily calculated:

$$X_{11} = [5725 - 2\times(2905)]/2 = -42.5 .$$

With respect to combination bands, e.g. $\nu_1+\nu_2$, the following formula applies:

$$(\overline{\nu_1} + \overline{\nu_2}) = G(1,1,0,0) - G(0,0,0,0) = \overline{\nu_1^{01}} + \overline{\nu_2^{01}} + X_{12} \qquad (3.8c)$$

Here, the combination band $\nu_1+\nu_2$ is located at 5725 cm^{-1} and the two fundamentals are found at 2905 cm^{-1} and 2963 cm^{-1} respectively, and thus the coupling constant X_{12} may be easily obtained.

Altogether, the parameters from the further overtone and combination bands can be deduced by analogy and the vibrational energy levels of CH_3-group vibrations in RT 601 PDMS can be described by:

$$G(v_1,v_2,v_3,v_4) = \overline{\nu_1}(v_1+\frac{1}{2})+\overline{\nu_2}(v_2+\frac{1}{2})+\overline{\nu_3}(v_3+\frac{1}{2})+\overline{\nu_4}(v_4+\frac{1}{2})-42.5\ (v_1+\frac{1}{2})^2-26.5\ (v_2+\frac{1}{2})^2$$
$$-13\ (v_3+\frac{1}{2})^2+4.5\ (v_4+\frac{1}{2})^2-143\ (v_1+\frac{1}{2})(v_2+\frac{1}{2})\ -4\ (v_1+\frac{1}{2})(v_3+\frac{1}{2}) \quad (3.9)$$
$$+7.5\ (v_1+\frac{1}{2})(v_4+\frac{1}{2})-10\ (v_2+\frac{1}{2})(v_3+\frac{1}{2})-4\ (v_2+\frac{1}{2})(v_4+\frac{1}{2})-5\ (v_3+\frac{1}{2})(v_4+\frac{1}{2})$$

The vibrational energy level of CH_3-group vibrations in SLM 77522 PDMS is obtained with the same approach and can be described by:

$$G(v_1,v_2,v_3,v_4) = \overline{\nu_1}(v_1+\frac{1}{2})+\overline{\nu_2}(v_2+\frac{1}{2})+\overline{\nu_3}(v_3+\frac{1}{2})+\overline{\nu_4}(v_4+\frac{1}{2})-42.5\ (v_1+\frac{1}{2})^2-26.5\ (v_2+\frac{1}{2})^2$$
$$-11\ (v_3+\frac{1}{2})^2+8.5\ (v_4+\frac{1}{2})^2-143\ (v_1+\frac{1}{2})(v_2+\frac{1}{2})\ -2\ (v_1+\frac{1}{2})(v_3+\frac{1}{2}) \quad (3.10)$$
$$+1.5\ (v_1+\frac{1}{2})(v_4+\frac{1}{2})-8\ (v_2+\frac{1}{2})(v_3+\frac{1}{2})-6\ (v_2+\frac{1}{2})(v_4+\frac{1}{2})-5\ (v_3+\frac{1}{2})(v_4+\frac{1}{2})$$

From the equations above, we can calculate the wavenumbers of overtone and combination bands of CH_3-group vibrations from 600 nm to 1800 nm in such two PDMS. The wavenumbers of the four methyl group normal vibrations to RT 601 are: ν_1 = 2905 cm^{-1}, ν_2 = 2963 cm^{-1}, ν_3 = 1263 cm^{-1}, and ν_4 = 1412 cm^{-1}. To SLM 77522, they are ν_1 = 2905 cm^{-1}, ν_2 = 2963 cm^{-1}, ν_3 = 1261 cm^{-1}, and ν_4 = 1412 cm^{-1} respectively. The calculated results with experimentally observed band positions for core and cladding are summarized in Tab. 3.2 for the overtone vibrational band assignments.

Table 3.2A *Spectral positions of CH_3-group vibrations in NIR and VIS region. S, m, and w indicate strong, medium or weak absorption for a given band*

Assignment	***Cladding***		***Core***		***Intensity***
	λ /nm	***λ***			
$\nu_1+\nu_3$	2402	2402	2402	2402	s
$\nu_2+\nu_3$	2372	2372	2372	2372	s
$\nu_2+\nu_4$	2295	2295	2295	2295	s
$\nu_1+2\nu_3$	1853	1849	1852	1851	m
$\nu_2+2\nu_3$	1837	1839	1836	1835	m
$\nu_2+\nu_3+\nu_4$	1783	1783	1784	1784	m

$2\nu_1$	1746	1746	1746	1746	s
$\nu_1+\nu_2$	1746	1746	1744	1744	s
$2\nu_2$	1703	1703	1703	1703	s
$\nu_1+3\nu_3$	1515	1539	1512	1539	m
$\nu_2+3\nu_3$	1506	1526	1503	1526	m
$2\nu_1+\nu_4$	1401	1401	1403	1403	m
$2\nu_2+\nu_4$	1376	1371	1377	1369	m
$3\nu_1$	1183	1186	1183	1186	m
$3\nu_2$	1146	1152	1146	1148	m
$2\nu_1+3\nu_3$	1063	1094	1061	1091	w
$3\nu_1+\nu_3$	1029	1020	1029	1019	w
$4\nu_1$	901	907	901	908	w
$2\nu_1+2\nu_2$	906	897	906	904	w
$4\nu_2$	868	880	868	877	w
$5\nu_1$	731	741	731	742	w
$3\nu_1+2\nu_2$	742	730	742	728	w
$5\nu_2$	701	715	701	709	w
$6\nu_1$	620	633	620	632	w

Furthermore, the higher overtone and combination bands of other vibrations with involvement of CH containing groups' vibrations in RT 601 and SLM 77522 i.e. methylene group, vinyl group and phenyl group etc. are also assigned from the NIR spectrum shown in Fig. 3.6. Results are summarized in Tabs. 3.2B, C and D respectively. From the assignment table, it can be pointed out that the absorption loss near 850 nm- the most used wavelength for datacom transmission in multimode waveguide system- is mainly due to the 3rd overtone of C-H asymmetric stretching in vinyl group and 3rd overtone of CH in phenyl group.

Table 3.2B *Spectral positions of CH_2-group vibrations in NIR and VIS region*

Assignment	λ_{exp} ***/nm***	$\tilde{\nu}_{exp}$ ***/cm^{-1}***	***Intensity***
$\nu_1+\nu_3$	2330	4290	s
$2\nu_1$	1789	5408	m
$2\nu_2$	1735	5408	s
$2\nu_1+\nu_3$	1426	7013	m
$3\nu_1$	1214	8237	w
$3\nu_2$	1181	8489	m
$4\nu_1$	918	10893	w
$4\nu_2$	895	11173	w
$5\nu_1$	754	13263	W
$5\nu_2$	719	13908	W
$6\nu_1$	637	15699	W

Table 3.2C *Spectral positions of vinyl group vibrations in NIR and VIS region*

Assignment	λ_{exp} ***/nm***	$\tilde{\nu}_{exp}$ ***/cm^{-1}***	***Intensity***
$\nu_1(-CH_2)+\nu_3(=CH_2)$	2350	4255	S
$\nu_1(-CH_2)+\nu_1(C=C)$	2195	4560	M
$\nu_1(C=C)+\nu_1(=CH_2)$	2145	4660	M
$2\nu_1$	1673	5977	S
$2\nu_2$	1650	6061	M
$3\nu_1$	1144	8741	W
$3\nu_2$	1133	8826	M
$4\nu_1$	871	11481	W
$4\nu_2$	847	11737	W
$5\nu_1$	728	13736	W
$5\nu_2$	708	14124	W

***6ν*₁**	624	15949	W

Table 3.2D *Spectral positions of CH (phenyl group) vibrations in NIR and VIS region*

Assignment	***λ_{exp}/nm***	***$\tilde{\nu}_{exp}$/cm^{-1}***	***Intensity***
$2\nu_1$	1690	5917	s
$2\nu_1$(CH stret.)+ν_2(CH bend)	1461	6845	m
$2\nu_1$(CH stret.)+$2\nu_1$(C-C stret.)	1425	7018	m
$3\nu_1$	1151	8688	m
$4\nu_1$	853	11723	w
$5\nu_1$	711	14065	w
$6\nu_1$	628	15924	w

3.4.3 Estimation of Absorption Loss

Estimations of the absorption loss in amorphous acrylic based polymers have been carried out by several authors, providing detailed procedures for such calculations. However, their empirical equations were deduced for acrylic polymers, using additionally the assumption of same band shapes of the absorption bands. Thus, it was our intention to derive an optical loss equation that is applicable for siloxane-based materials, considering the integrated band intensities.

In order to evaluate the maximum optical losses D_{max} in terms of dB/ cm, the integral band strengths have to be correlated with the corresponding absorption loss. An equation for the integral band strength (in cm/mol) for C-X stretching vibrations (X= H, D, Cl and F, and aromatic C-H) in dependence of the integral band absorbance, as well as for the ratio of the integral band strengths of overtones to the related fundamental vibration were derived by Groh. Under the assumption that the same band shape, but different half-widths for the calculated overtone vibrations existed, his equations were used by us, using the following expression: [17]

$$D_{\max} = \alpha \cdot \frac{\rho}{M_G} \cdot \frac{n_c}{\Delta\bar{\nu}} \cdot \frac{E_v^{CX}}{E_1^{CH}} \quad \text{in dB/ cm,} \qquad (3.11)$$

where α is a constant, ρ (g/ cm^{-3}) is the density of the polymer, M_G (g/ mol) is the

molecular mass of the polymer repeat unit, n_c is the number of C-X bonds in this repeat unit, $\Delta\tilde{\nu}$ is the band half-width in cm^{-1}, and E_v^{CX}/ E_1^{CH} is the ratio of the band strength of the C-X vibration overtone and that of the fundamental C-H vibration band.

According to the near-infrared loss spectrum of core PDMS, we selected two similar shape overtone bands for comparison and calculation, i.e., the $4\nu_1$ and $5\nu_1$ overtones of the CH_3-group vibrations (Figs. 3.7A and B). The maximum optical loss of D_{max} ($4\nu_1$) and D_{max} ($5\nu_1$) can be measured from these spectra, for which values of about 0.601 and 0.049 dB/ cm were found. The estimated band half-widths are 86.07 and 208.6 cm^{-1} respectively from its curve fitting spectra ranging from 600 nm to 1250 nm shown in Fig. 3.8 A and B. The detailed assignment and band half-widths etc. in the wavelengths are also summarized in Table 3.3A and B respectively.

The density of cured core PDMS SLM 77522 is ρ= 0.98 g/ cm^3, the number of C-H bonds is six and the molecular mass of the PDMS repeat unit is 74 g/ mol. In addition, referring to the corresponding theoretically calculated values of E_v^{CH}/ E_1^{CH} for the $4\nu_1$ and $5\nu_1$ overtones of the CH_3-group vibration, i.e. $7.2\cdot 10^{-4}$ and $9.1\cdot 10^{-5}$, respectively, and then substituting these parameters together with the experimentally derived optical loss values within the last equation, the constant α is calculated to be $0.906\cdot 10^6$ and $1.41\cdot 10^6$, providing an average value of $1.15\cdot 10^6$. The latter value is used for defining the relationship between the maximum optical loss and the band strength ratio, which can be summarized as:

$$D_{\max} = 1.15 \cdot 10^6 \cdot \frac{\rho}{M_G} \cdot \frac{n_c}{\Delta\bar{\nu}} \cdot \frac{E_v^{CH}}{E_1^{CH}} \quad dB/cm \qquad (3.12)$$

To check the equation's applicability, optical loss due to the $3\nu_1$ overtone of the CH_3 group vibration is measured and identified to have band half-width of 87.19 cm^{-1}. Based on the equation above and the theoretical value of E_v^{CH}/ E_1^{CH} the calculated value is 7.10 dB/ cm compared with the measurement result of 6.98 dB/ cm. This result means that the agreement between experiment and theoretical calculation is astonishingly satisfactory.

Additionally, with respect to the PDMS core material, the optical loss at 850 nm –the most used operation wavelength for datacom- is measured to be 0.019 dB/ cm from its loss spectra shown in Fig. 3.6, and the loss of molecular vibration at 853 nm is measured to be 0.0144dB/ cm from fitting curve Fig. 3.8B, whilst in the wavelength the electronic absorption can be neglected for it is far away with the

absorption band in UV region, so we can conclude the rayleigh scattering in the wavelength is 0.0046 dB/ cm.

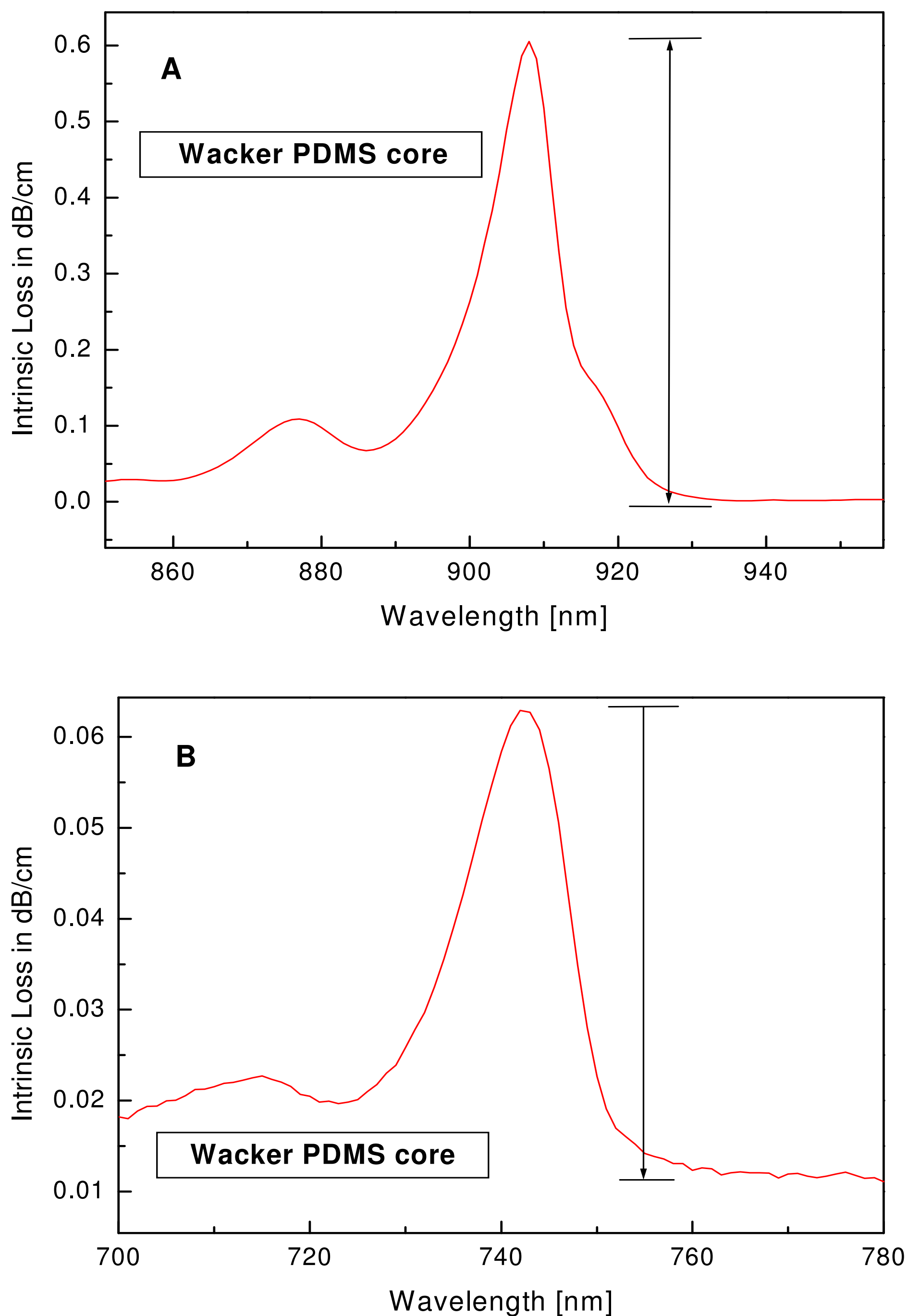

Fig. 3.7 *A and B $4\nu_1$ and $5\nu_1$ overtones of the CH_3-group vibrations in loss spectra*

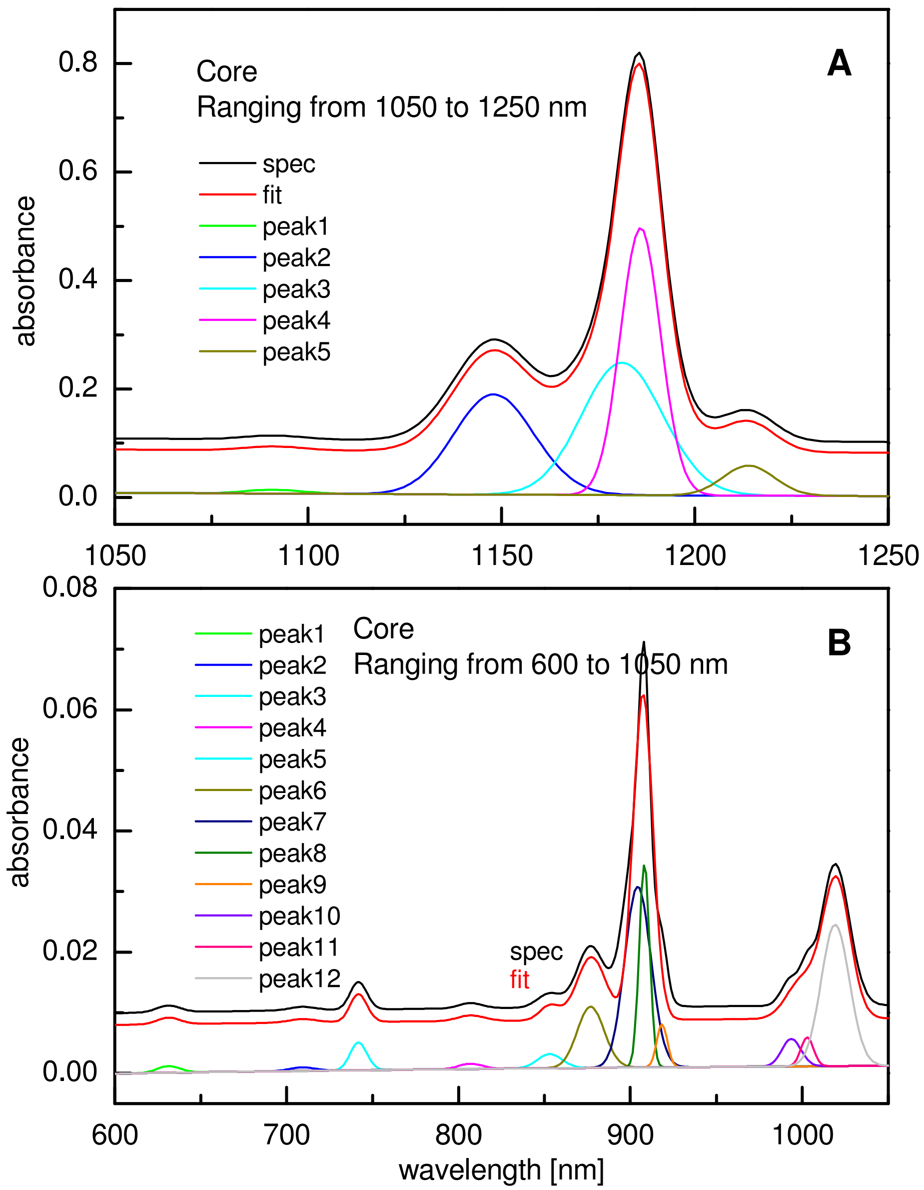

A
Core
Ranging from 1050 to 1250 nm
spec
fit
peak1
peak2
peak3
peak4
peak5
absorbance
0.0
0.2
0.4
0.6
0.8
1050
1100
1150
1200
1250
B
Core
Ranging from 600 to 1050 nm
peak1
peak2
peak3
peak4
peak5
peak6
peak7
peak8
peak9
peak10
peak11
peak12
spec
fit
absorbance
0.00
0.02
0.04
0.06
0.08
600
700
800
900
1000
wavelength [nm]

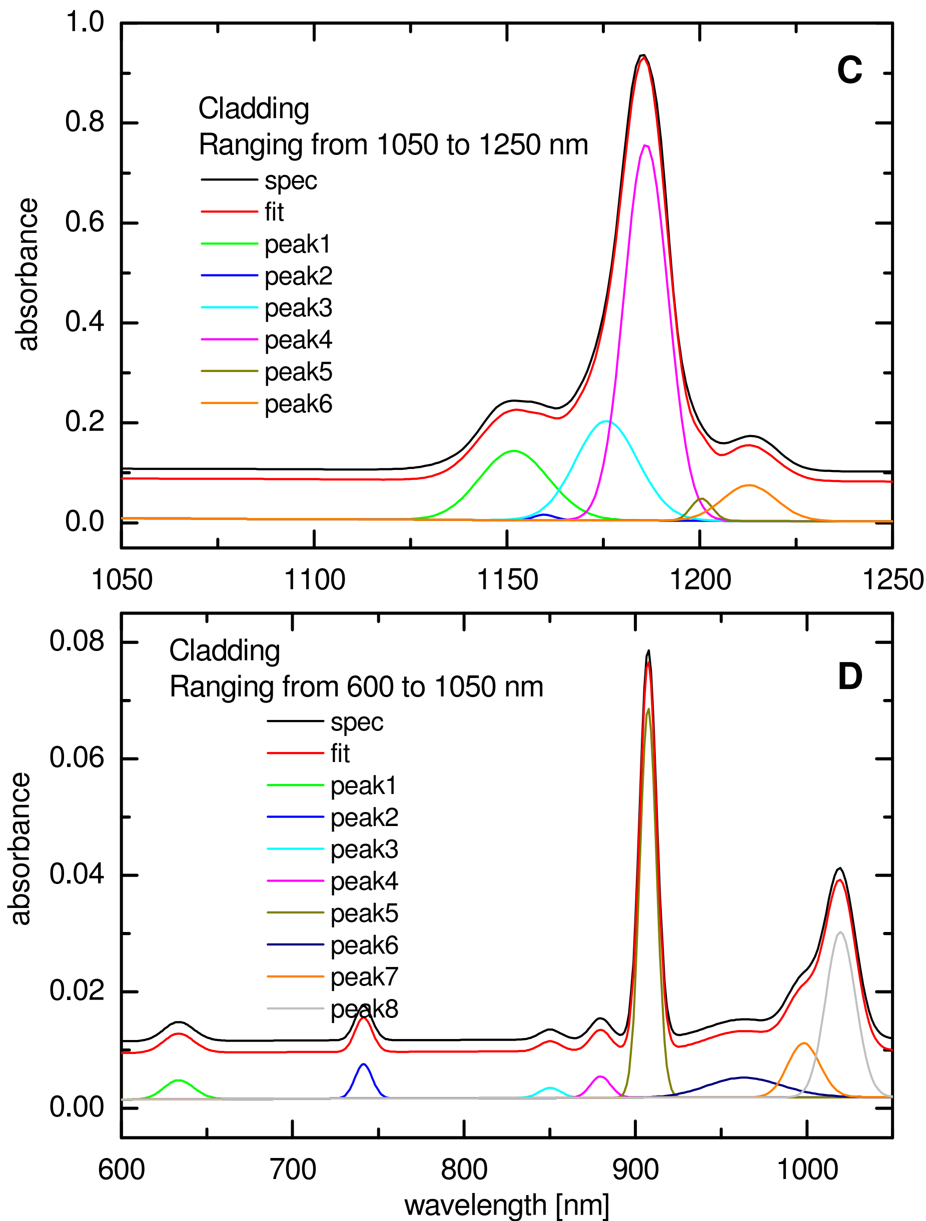

Fig. 3.8 *Curve fitting of PDMS core (A and B) and cladding (C and D) absorbance spectra ranging from 600 to 1250 nm*

According to the near-infrared loss spectrum of cladding PDMS, we also selected two similar shape overtone bands for comparison and calculation, i.e., the $4\nu_1$ and $5\nu_1$ overtones of the CH_3-group vibrations for study. The maximum optical loss of D_{max} $(4\nu_1)$ and D_{max} $(5\nu_1)$ can be measured from these spectra, for which values of about 0.599 dB/ cm and 0.0504 dB/ cm were found. The band half-widths are also

found to be 138.83 and 214.03 cm^{-1} respectively from the curve fitting spectra ranging from 600 nm to 1250 nm shown in Fig. 3.8 C and D. The detailed assignment and band half-widths etc. in the wavelengths are summarized in Table 3.3C and D respectively.

The density of cured cladding PDMS RT 601 is ρ= 1.02 g/ cm^3, the number of C-H bonds is six and the molecular mass of the PDMS repeat unit is 74 g/ mol. In addition, referring to the corresponding theoretically calculated values of E_v^{CH}/ E_1^{CH} for the $4\nu_1$ and $5\nu_1$ overtones of the CH_3-group vibration, i.e. $7.2\cdot 10^{-4}$ and $9.1\cdot 10^{-5}$, respectively, and then substituting these parameters together with the experimentally derived optical loss values within the last equation 3.11, the constant α is calculated to be $1.40\cdot 10^6$ and $1.43\cdot 10^6$, providing an average value of $1.415\cdot 10^6$. The latter value is used for defining the relationship between the maximum optical loss and the band strength ratio, which can be summarized as:

$$D_{\max} = 1.415 \cdot 10^6 \cdot \frac{\rho}{M_G} \cdot \frac{n_c}{\Delta\overline{\nu}} \cdot \frac{E_v^{CH}}{E_1^{CH}} \quad dB/cm \tag{3.13}$$

To check the equation's applicability, also the measured optical loss due to the $3\nu_1$ overtone of the CH_3 group vibration, with an fitted band half-width of 116.13 cm^{-1}, is also compared with the calculated results based on the equation above and the theoretical value of E_v^{CH}/ E_1^{CH}. The measured loss is 6.34 dB/ cm, taking into account band overlap from the neighboured band, while the calculated value is 6.8 dB/ cm. Like core material, this result means that the agreement between experiment and theoretical calculation is also very good.

Table 3.3A *Peak report of core material (From 1050 nm to 1250 nm)*

Gaussian	*Assignment*	*Area FIT*	*Peak center (nm)*	*Height*	*Half Width (cm^{-1})*
Peak 1	$2\nu_1$+$3\nu_3$ (CH_3)	1.11	1091	0.0070	149.11
Peak 2	$3\nu_2$(CH_3)	36.38	1148	0.19	184.90
Peak 3	$3\nu_2$(CH_2)	46.27	1181	0.24	177.91
Peak 4	$3\nu_1$(CH_3)	45.77	1186	0.49	87.19
Peak 5	$3\nu_1$(CH_2)	6.26	1214	0.055	106.33

Table 3.3B *Peak report of core material (From 600 nm to 1050 nm)*

Gaussian	***Assignment***	***Area FIT***	***Peak centre (nm)***	***Height***	***Half Width (cm^{-1})***
Peak 1	$6\nu_1(CH_3)$	0.47	631	0.010	399.77
Peak 2	$5\nu_2(CH_3)$	0.21	709	0.0056	349.77
Peak 3	$5\nu_1(CH_3)$	1.00	742	0.045	208.62
Peak 4	$5\nu_1(CH_2)$	0.23	807	0.00087	245.43
Peak 5	$4\nu_1$(Ar) $4\nu_2$(Vinyl)	0.57	853	0.0023	229.51
Peak 6	$4\nu_2(CH_3)$	2.57	877	0.01	239.42
Peak 7	$2\nu_1+2\nu_2\ (CH_3)$	6.94	904	0.030	218.26
Peak 8	$4\nu_1(CH_3)$	3.07	908	0.034	86.07
Peak 9	$4\nu_1(CH_2)$	0.65	918	0.0071	86.24
Peak 10	N.A	0.64	994	0.0046	132.03
Peak 11	N.A	0.44	1003	0.0048	85.68
Peak 12	$3\nu_1+\nu_3\ (CH_3)$	4.63	1019	0.023	186.01

Table 3.3C *Peak report of cladding material (From 1050 nm to 1250 nm)*

Gaussian	***Assignment***	***Area FIT***	***Peak center (nm)***	***Height***	***Half Width (cm^{-1})***
Peak 1	$3\nu_2(CH_3)$	23.33	1152	0.14	158.36
Peak 2	$3\nu_1$(Ar)	0.54	1160	0.011	45.01
Peak 3	$3\nu_2(CH_2)$	29.04	1176	0.20	137.04
Peak 4	$3\nu_1(CH_3)$	76.32	1186	0.75	116.13
Peak 5	$2\nu_1+\nu_2\ (CH_3)$	2.10	1200	0.45	44.08
Peak 6	$3\nu_1(CH_2)$	8.39	1213	0.072	110.25

Table 3.3D *Peak report of cladding material (From 600 nm to 1050 nm)*

Gaussian	***Assignment***	***Area FIT***	***Peak center (nm)***	***Height***	***Half Width (cm^{-1})***

Peak 1	$6\nu_1(CH_3)$	1.79	633	0.0033	514.38
Peak 2	$5\nu_1(CH_3)$	1.34	741	0.0059	214.03
Peak 3	$4\nu_1$(Ar) $4\nu_2$(Vinyl)	0.37	847	0.0017	202.05
Peak 4	$4\nu_2(CH_3)$	0.69	880	0.0036	178.17
Peak 5	$4\nu_1(CH_3)$	9.88	907	0.067	138.83
Peak 6	N.A	1.97	963	0.0034	545.73
Peak 7	N.A	2.18	998	0.0093	220.74
Peak 8	$3\nu_1+\nu_3$ (CH_3)	5.94	1020	0.028	196.61

Based on the measured optical loss and its theoretical calculation, PDMS will be a very good choice - owing to its low cost, easy mass production and high thermal stability - for short haul data communication application (from several centimetres to one meter) like Electrical-Optical-Circuit-Boards (EOCB) or some short distance interconnections. However, once also relatively longer distances need to be served, PDMS has to be modified for decreasing the relatively high optical loss from overtone and combination band absorption in the visible/near-infrared (VIS-NIR) region. Presently, deuteration and halogenation are the main two options to decrease the optical loss, since the CD and CX (halogen elements, e.g. F, Cl etc.) fundamental absorption bands (in particular, the stretching vibrations) in the mid-infrared region are shifted to longer wavelengths (ν(CD): 2230 cm^{-1}, ν(CF): 1250 cm^{-1} and ν(CCl): 770 cm^{-1}). Notably, also smaller anharmonicity constants exist compared with CH bond vibrations, so that finally a much lower optical loss will result for the VIS-NIR region.

After obtaining the correlation equation above and in combination with the detailed calculation results, as previously published for the ratios of E_v^{CX}/ E_1^{CH}, we can roughly estimate also the optical loss in deuterated or halogenated core PDMS within the VIS-NIR region. For example, $4\nu_1$ of the CD-stretching vibration is located at 1160 nm and the E_4^{CD}/ E_1^{CH} ratio is $1.3\cdot 10^{-4}$, and assuming its band half-width of 150 cm^{-1} being similar to that of $4\nu_1$ of the C-H bond vibration, we can find the corresponding CD stretch overtone loss value to be only 0.109 dB/ cm. This must be compared with the $3\nu_1$ of the CH-stretching vibration located at 1183 nm, as discussed above for the normal isotopic material with its optical loss found about 60 - 70 times larger than for the $4\nu_1$ of CD stretch overtone loss. Whilst from

a theoretical view deuteration and halogenation in siloxane-based materials are proving their applicability to render even more transparent materials, practical aspects about the use of such materials must still be investigated.

In addition, in terms of core PDMS and with respect to the siloxane polymer design, assuming a ratio of ρ/ M_G = 0.01 mol/ cm^{-3} based on possible deuteration or halogenation and n_c = 6, an absorption loss of 0.001 dB/cm could be achieved when referring to a quotient of $E_v^{CX}/ (E_1^{CH} \cdot \Delta\bar{\nu})$ of $1.09 \cdot 10^{-8}$. Furthermore, specifically to 850 nm, the optical loss at 850 nm of polysiloxanes will be mainly from rayleigh scattering e.g. 0.0046 dB/ cm to PDMS SLM core material once the absorption peaks near 850 nm are shifted due to deuteration or halogenation, therefore the inhomogeneities in polysiloxanes should be also controlled to obtain higher optical transparency, e.g Pt catalyst concentration and curing conditions etc. After knowing the optical loss limit, it is very important and helpful for the optical material design for decreasing the loss by appropriate hydrogen substitution, but even amplification (which can be reached with doping the PDMS material with some rare-earth metal materials showing luminescence at the requested signal wavelength) may be necessary.

3.5 Processing of PDMS Waveguides

The technique and relevant issues for processing polymer optical waveguides are quite similar to those for polymers in microelectronic packaging. Spin coating, doctor blading, extrusion and lamination etc. are all the normal techniques for casting polymer films. Then it differs with their application in microelectronic packaging, in waveguide fabrication it concerns more on film uniformity and controllable desirable thickness, free of bubbles and striations, and adhere to substrates or not etc.

Furthermore, in general, waveguide fabrication by means of replication techniques comprises the following steps:
-Fabrication of a mould with the desired waveguide pattern in form of ridges;

-Replication of the waveguide pattern into a polymer substrate which contains the waveguide structure in form of grooves;

-Filling of the grooves by a liquid core polymer which has a higher refractive index than the substrate and subsequent curing of the core polymer by UV-light or heat.

3.5.1 Fabrication of PDMS Optical Waveguides

It is well known that several properties of PDMS material are instrumental in the formation of high-quality patterns and structures. First it shows extremely high temperature stability with respect to material degradation as well as to optically transparent down to about 300 nm. Second, PDMS is one typical elastomer and can conform to the surface of the mould over a relatively large are and is excellent materials for replication processes since they can be released easily from moulds, even from complex and fragile structures, and are able to replicate structures down to the nm-range due to its elastic characteristic. Third PDMS provides a low surface energy surface when it is cured (ca. 21.6×10^{-3} J/ m^2) and chemically inert, in addition its surface properties can be readily modified by thermal treatment, UV/ O_3, gas plasma and chemical treatments to give requested interfacial properties based on different requirements. [65]

For fabrication of waveguides by using this optical material, casting is adopted as the suitable technology with regard to the PDMS properties. The first basic prerequisite for the replication process is a robust mould or stamp with low sidewall surface roughness (< 30 nm) to guarantee a low scattering loss, e.g. 6” Nickel casting mould in Fig. 3.9.

The fabrication starts by filling the waveguide grooves with the liquid core polymer which is done using a blading process (Fig. 3.10a). The choice of PMMA or POM as blading material was guided by the demands of the blade softness, flexibility, but long lasting endurance. This process step is finished by thermal curing of the core polymer. As the second step, liquid cladding material is poured onto the whole mould area (Fig. 3.10b). After curing, first cladding and core are together separated from the mould (Fig. 3.10c). This half-open structure is then filled with cladding material (second cladding). A final curing step d terminates the production process of the wave guiding laminate and after this and the optical layer can be packaged.

In the single mode fabrication, due to the small core size two issues are worth mentioning: one is the curing temperature which is proposed to be 70 ℃, since the PDMS parts will shrink if the PDMS prepolymer is cured at higher temperature, not ensuring a satisfactory pattern transfer. The other aspect is the influence of the substrate on the crosslinking rate to the PDMS thin film (for example, below 15 µm). Simpson et al.[66] proposed that the dependence of the first-order coefficient for the PDMS hydrosilylation crosslinking reaction on the type of interface is probably the result of an interfacial segregation and complexation of the Pt catalyst.

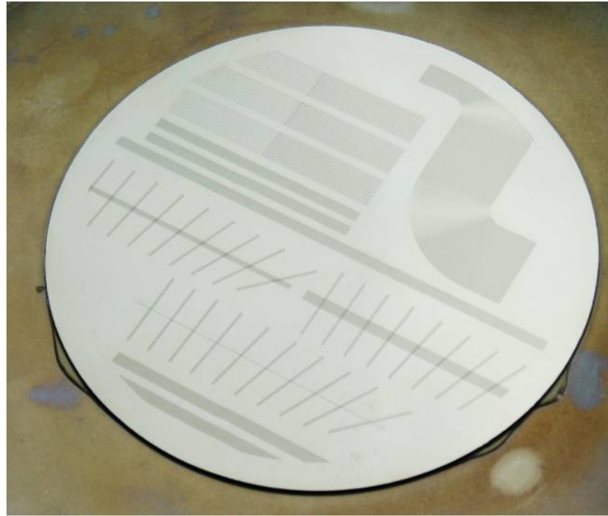

Fig. 3.9 *6" Nickel casting mould*

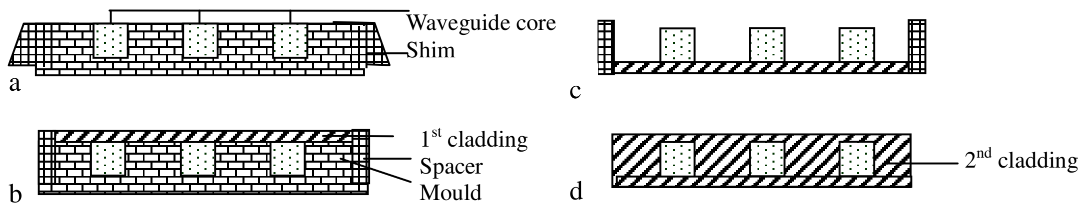

Fig. 3.10 *Schematics of the waveguide fabrication using PDMS*

Single mode

The waveguide sandwich will be cut by a razor blade at both end faces to prepare the sample for optical characterization. The cross section of a fabricated PDMS singlemode waveguides is illustrated in Fig. 3.10 which has core sizes of 6 × 6 µm^2. With these standard commercial PDMS materials (see Figure 3.11) a PDMS singlemode waveguide loss of 0.17 dB/ cm could be obtained at 1300 nm. Further reduction of transmission loss may achievable by using aforementioned introduced partially halogenated materials.

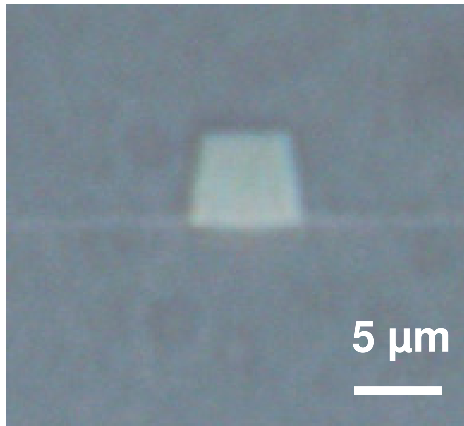

Fig. 3.11 *cross section of a fabricated PDMS singlemode waveguide*

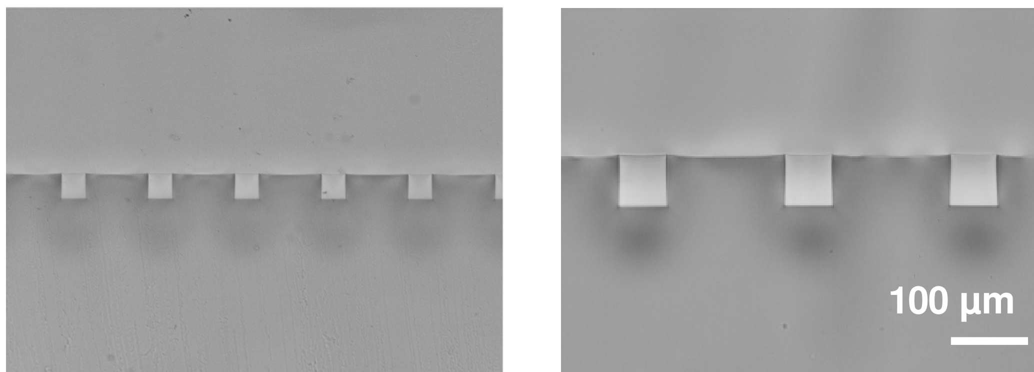

Fig. 3.12 *cross section of a fabricated PDMS multimode waveguide*

Multimode

The cross section of a fabricated PDMS multimode waveguides is illustrated in Fig. 3.12 which has core sizes of 70 × 70 µm^2.

The optical insertion loss measurement of PDMS waveguides were measured at 850 nm which is commercially used for optical datacom transmission in multimode waveguides. The detailed schematic set-up is shown in Figure 3.13.

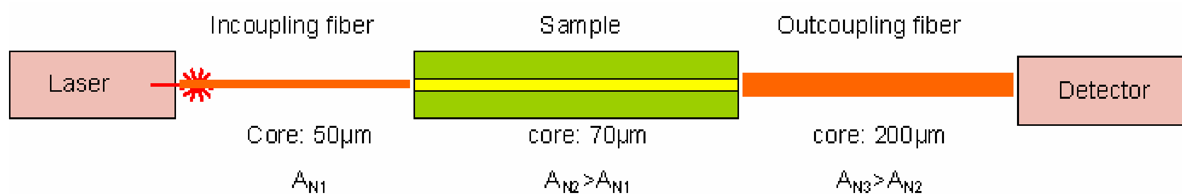

Fig. 3.13 *schematic set-up of optical loss measurement*

The instrument OMS150 of the company "Wavetek Wandel Goltermann" (Enirrgen

uA, Germany) was used for optical loss measurement, which contains of two laser sources and a detector. For our experiments a dual laser arrangement with wavelengths of 650 nm and 850 nm was applied. The spectral range was independent of the operating temperature with tolerances of ± 10 nm. The laser radiation sources were operated in the WDM mode, so that a synchronous measurement of the two wavelengths was possible. The laser light was launched into the waveguides through a butt-in-coupling 50 µm GI fibre (See Fig. 3.14) and a 200 µm SI fibre for butt-out-coupling.

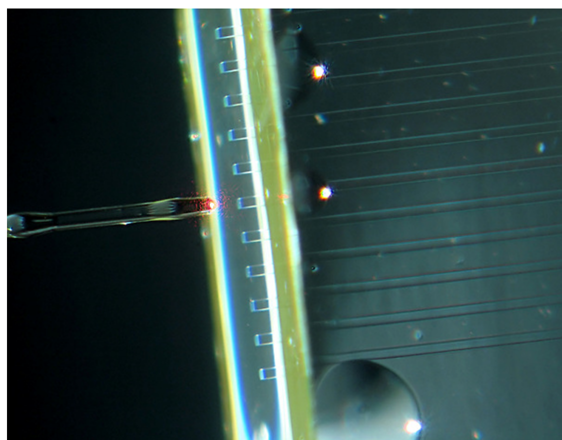

Fig. 3.14 *Measurement of PDMS waveguides insertion loss*

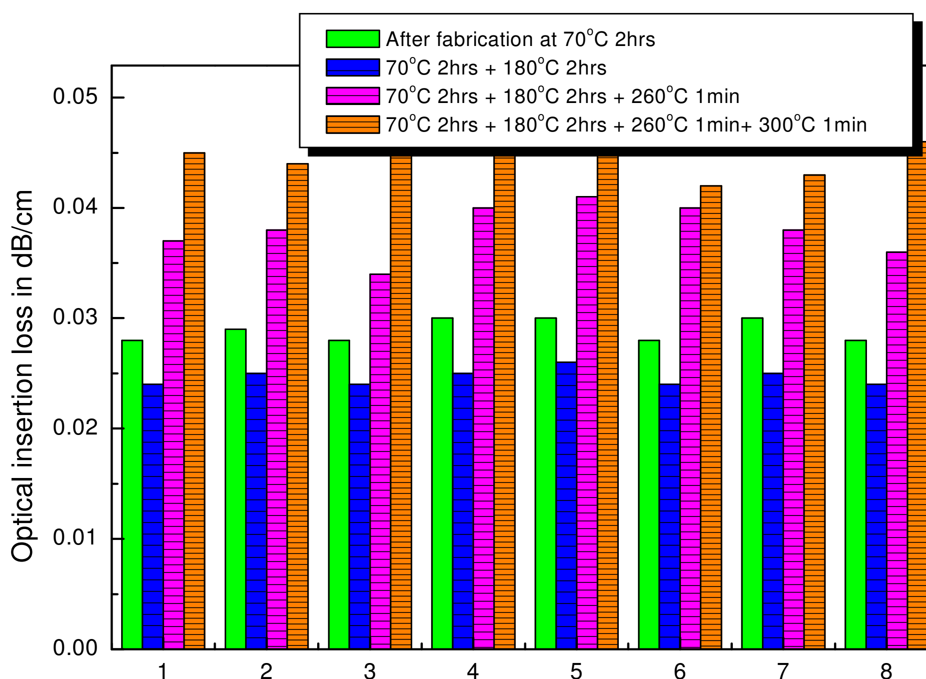

Fig. 3.15 *Optical insertion loss of PDMS multimode waveguides*

The measured optical insertion loss of PDMS waveguides after curing and different temperature treatments are shown in Fig. 3.15 and the transmission loss of multimode waveguides based on such 2 component thermal curing wacker PDMS is below 0.05 dB/ cm even after temperature treatment up to 300 ℃. The optical loss after 180 ℃ for 2 hrs is decreased possibly due to the decrease of vinyl group concentration with the further curing of PDMS. Summarily, it proves such PDMS material appropriate for short distance optical data transmission in even high temperature environments replacing other thermal modified high cost optical polymers such as acrylate and epoxy-based materials.

3.5.2 Scattering Loss from Mould Roughness

Like aforementioned, core–clad interface roughness is another source of extrinsic loss. Actually, except scattering loss, roughness and inhomogeneity also can generate unwanted mode coupling and modulation of mode coupling in devices and beating/ coupling length. Thus extrinsic loss in waveguide system typically result from core–clad interface roughness needs to be identified. Referring to the casting method for PDMS waveguide fabrication, actually the interface roughness is the copy of grooves and defects from the sidewalls of casting moulds. Additional attenuation (scattering loss) which is from continuous coupling from bound modes to the radiation field may be caused due to these surface defects and roughness. A white-light-interferometer named Veeco NT 1000 is used to quantify the roughness of casting moulds (Fig. 3.16) and SEM is adopted for direct topography observation (Fig. 3.17).

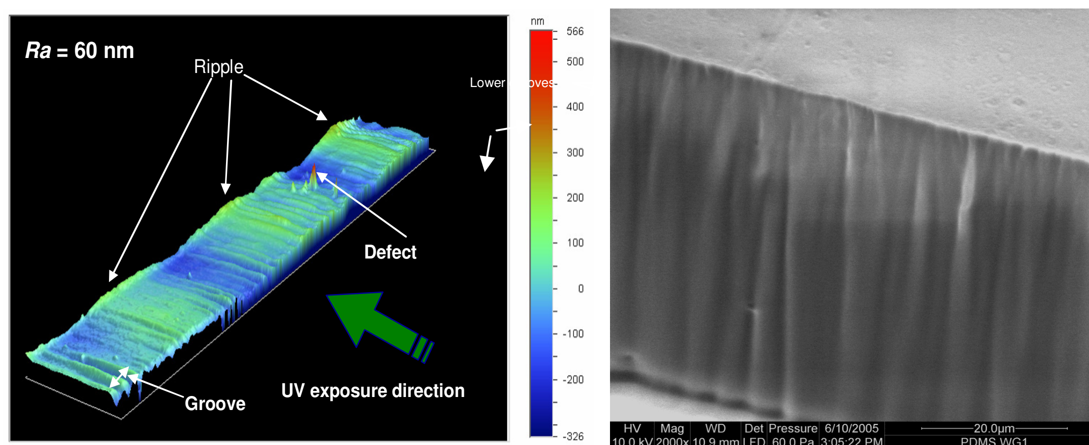

Fig. 3.16 Roughness of casting mould sidewall **Fig. 3. 17** Topography of casting mould sidewall

The optical intrinsic absorption of core and cladding PDMS are measured with NIR

spectrometer and the spectra are illustrated in Fig. 3.6 already. From their NIR spectra, the largest optical losses in the region from 842 to 855 nm where measurement laser will work are measured and calculated based on Lambert' law. Optical intrinsic loss of PDMS core is 0.0192 dB/ cm and cladding loss is 0.0176 dB/ cm respectively, which core material has relatively higher loss than cladding possibly due to its higher concentration of phenyl group whose 3rd overtone of Ar-CH is just in that region.

Additionally, in such cross-section PDMS waveguide system (RI of cladding and core: 1.4041 and 1.4275 at 589 nm and 20 ^{o}C), to simplify the calculation of waveguide loss attributed to PDMS, considering 10 % light will transmit in cladding layer it is assumed that 90 % contribution of waveguide loss is from core material and the other 10 % is from cladding Hence, the waveguide loss is 0.01904 dB/ cm.

Differently qualified SU-8 casting moulds are fabricated from different masks which directly determinate the sidewall surface qualities of moulds. Their roughness is quantified with Veeco NT 1000, where 10 spots are measured per waveguide; in addition PDMS optical waveguides of 8 cm length are fabricated based on these different quality moulds. The optical insertion loss of these obtained PDMS waveguides with different core-clad interface roughness are measured at 850 nm wavelength. Compared with sidewall roughness, the top and bottom interfaces between core and cladding can be neglected. Hereby we consider the interface roughness is main from the two sidewalls between them, in addition it is also assumed the edge qualities of lines in every mask are identical. Theoretically, the optical propagation loss due to scattering will be increased evidently when average roughness of waveguide sidewalls is more than λ(wavelength)/ 20, and hence to 850 nm wavelength, the critical transition Ra is 42.5 nm, and from the measured diagram shown in Fig. 3.18, the experimental critical transition Ra is about 50 nm.

Also, from the diagram it can help us determine the quality of mask based on different optical quality requirements to PDMS waveguides because the mould roughness is directly related with the mask. For example, supposed optical waveguide loss to be less than 0.05 dB/ cm, the average roughness of casting mould should be controlled below 40 nm and thus relevant quality mask should be selected.

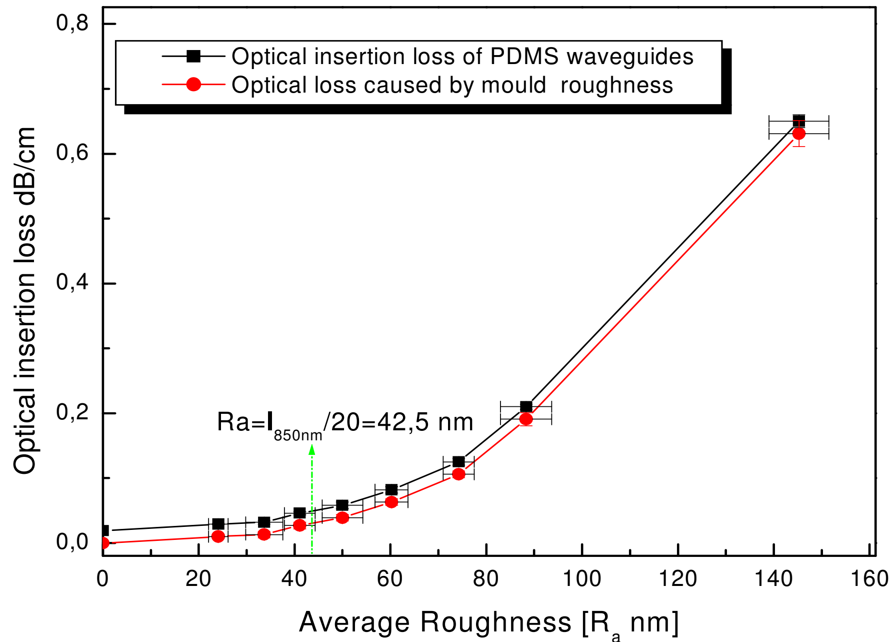

Fig. 3.18 *Relationship between sidewall roughness and optical waveguide loss at 850 nm*

3.5.3 Optical Loss due to Interlayer

Based on PDMS casting technique, the interlayer will form if over filling PDMS core and incomplete blading etc. (See Fig.3.19). Mainly the interlayer may be divided into two kinds, one is structure 3.20B in Fig.3.20, where two waveguides or more are connected by the interlay which causes the optical crosstalk and brings extra optical loss consequently, and the other is pure interlayer i.e. no connection with other waveguides: structure 3.20C, though no caused crosstalk due to it, it will lead to some extra mode dispersion and some light into cladding layer, and ultimately bring optical loss.

In the part, through modifying flatness of casting mould and blading pressure and angle etc., different thick interlayers are formed and respectively the thicknesses of different interlayers are measured by ellipsometer. Additionally, the fabricated waveguides are characterized with optical laser measurement at 850 nm wavelength and the relationship between interlayer thickness and optical loss is illustrated in Fig. 3.20 also including the ray-tracing based simulation results in terms the respective interlayer thickness. Basically one good agreement is achievement. It is concluded as well that the interlayer thickness should be less 500 nm for achieving the basic low optical loss requirement.

In order to meet the basic quality requirement of optical loss, in terms of different moulds appropriate blading angle and pressure and surface treatments of casting mould are necessary to be checked and controlled experimentally, for example it is identified that blading conditions for SU8 mould are 2 bar pressure, POM material based blade and blading angle of 60° etc.

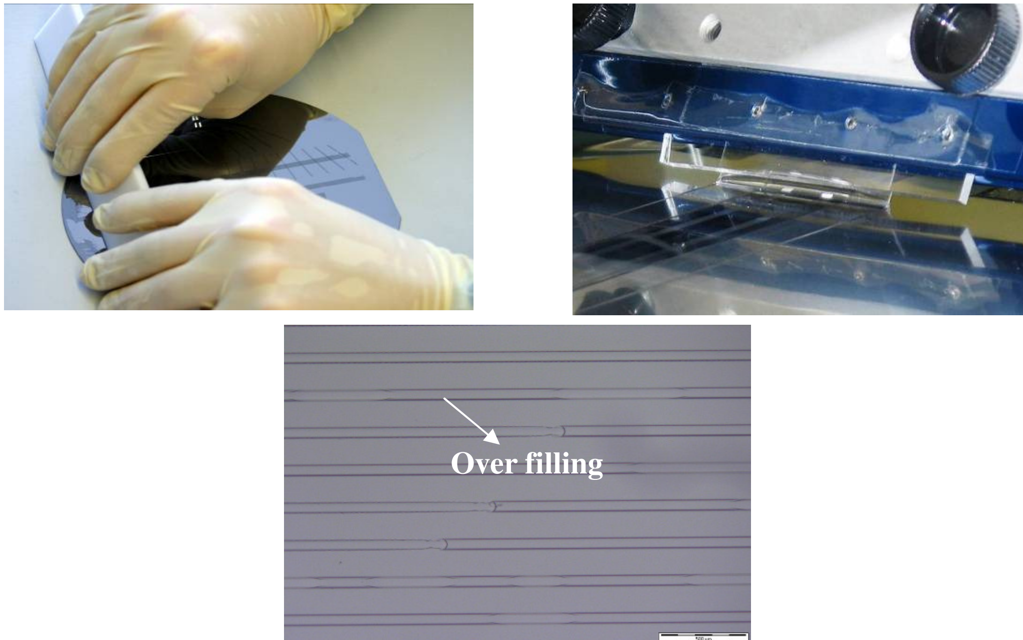

Fig. 3.19 *blading step during waveguide fabrication and overfilling due to incomplete blading*

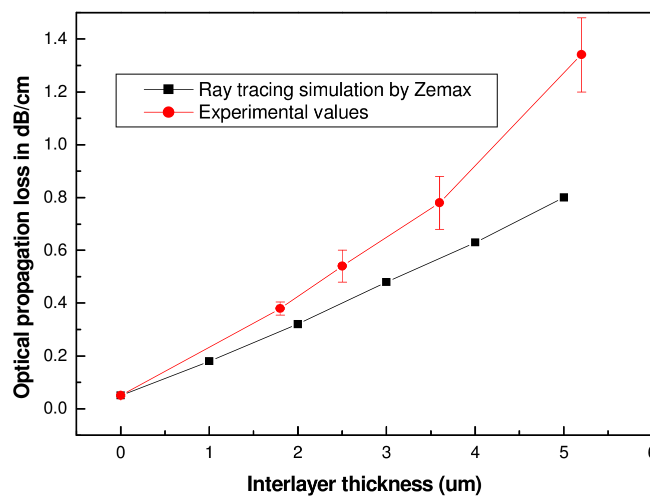

Fig. 3.20 *cross section of fabricated waveguides and interlayers*

3.5.4 Optical Loss from Packaging Substrates

Nowadays, in PCB industry, polymer based PCBs e.g. epoxy, Polyimide, PolyBenzImidazole , PolyEtherEtherKetone (PEEK), Polyester, Polycarbonate and PolyAmide-Imide are widely applied due to their good insulation properties, low cost and familiar production techniques with high stability and reliability etc., however with respect to EOCB production, their chemical compatibilities with PDMS materials of optical layer will be one important quality aspect based on EOCB production technique, e.g. outgas from heated organic PCBs.

FR4 (Glass reinforced Epoxy) series are strongly preferably recommended due to their popular use in market, low cost and familiar process and technologies etc.

As we knew, FR is the abbreviation of Flame Resistant and 4 is the class of flame retardment, and in order to improve the ability of flame retardment, some inorganic-based fillers and organic additives are added into epoxy materials in term of forms of composites and chemical synthesizing (reaction in the backbone of epoxy polymer), e.g. ATH ($Al(OH)_3$), $Mg(OH)_2$, halogen-based epoxy, phosphorous-based epoxy and nitrogenous-based epoxy etc. In order to resist flame under the condition of high temperature (e.g. lamination and soldering), they will give out various gases for preventing the flame continuous development, e.g. H_2O, noxious hydrogen halides, HPO_2, HPO and N_2 etc. as well as including some other gases from substrate materials, e.g. CO, CO_2, aromatic and alkyl CH containing gases, and even furan and dioxin etc. [67-68]

In order to identify the influences from FR4 boards on optical layer, PDMS waveguide foils without and with two different FR4 carriers (Halogen FR4 and Halogen-free FR4) kindly supported by ILFA, Hanover, Germany, are prepared based on one kind of specifically developed packaging method in our group which will be in detailed introduced in next chapter, and these fabricated waveguide laminates have dimensions of 40 × 100 mm. The thickness of PDMS layer is about 300 µm. The waveguides cross-section is 70 × 70 μm^2. The waveguide pitch is 250 µm which is from the normal pitch of commercial VCSEL-arrays. A cross-section of such PDMS waveguide foil with FR4 carrier is shown in Fig. 3.21.

After curing at 70 ℃, 180 ℃ for 2h (simulated lamination process) and 260 ℃ for 1min (lead-free soldering process) optical characterization with 850 nm laser is performed again and the detailed results of the PDMS waveguides without and with different kinds of FR4 foils are illustrated in Fig. 3.22.

From the results, the influence from halogen containing FR4 is obvious and leads

to optical loss increased to be over 0.1 dB/ cm. Optical measurement (See Fig. 3.23) of PDMS core material covered with the kind of halogen FR4 board with FTNIR spectroscopy were performed before and after 180 ℃ for 2 hrs treatment to identify the change. From the spectrums, some increased vibrational overtone and combination bands peaks from 840 nm to 880 nm are found which also fits with aforementioned optical insertion loss measurement results.

Then, it is also observed that the optical insertion loss changes very small, when the halogen FR4 board is deposited with copper as barrier layer and the result is shown in Fig.3.24, which is for the prevention of outgas from heated halogen containing FR4 by the diffused copper.

In addition, obviously compared with PDMS waveguides without any carrier layer stress optical loss is not so important due to CTE and young's modulus mismatch between FR4 and PDMS boards. Therefore, we propose that the higher optical loss possibly is due to steam, some CH overtone and combination band vibration in double carbon bond existing gases e.g. furan and dioxin emitted from halogen FR4, for such two emitted small volume gases can easily diffuse into largely expanded PDMS matrix (CTE: 300 ppm/ K) because of their high molecular volume, which finally cause the loss due to their light absorption near 850 nm (overtone of OH, $4\nu_2$ (Vinyl)- 847 nm and $4\nu_1$ (Phenyl)- 853 nm)).

So, in the future EOCB system, the selection of organic PCB boards will also play a vital role in optical quality aspect of EOCBs, and halogen free boards are recommended. Further, one copper deposition layer may also be considered as gas-resist layer.

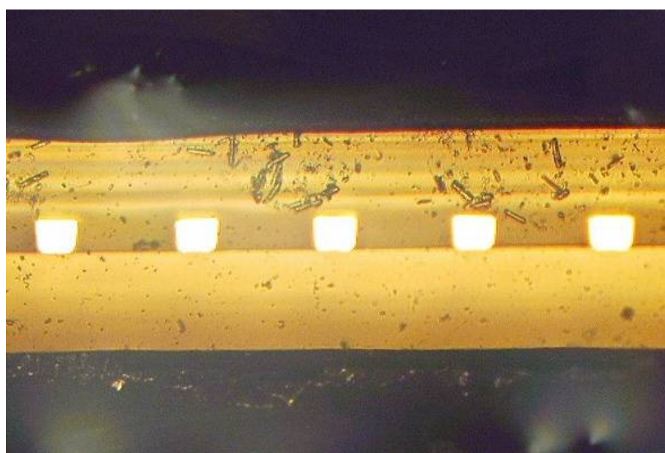

Fig. 3.21 *Cross-section of a PDMS waveguide foil with FR4 carrier*

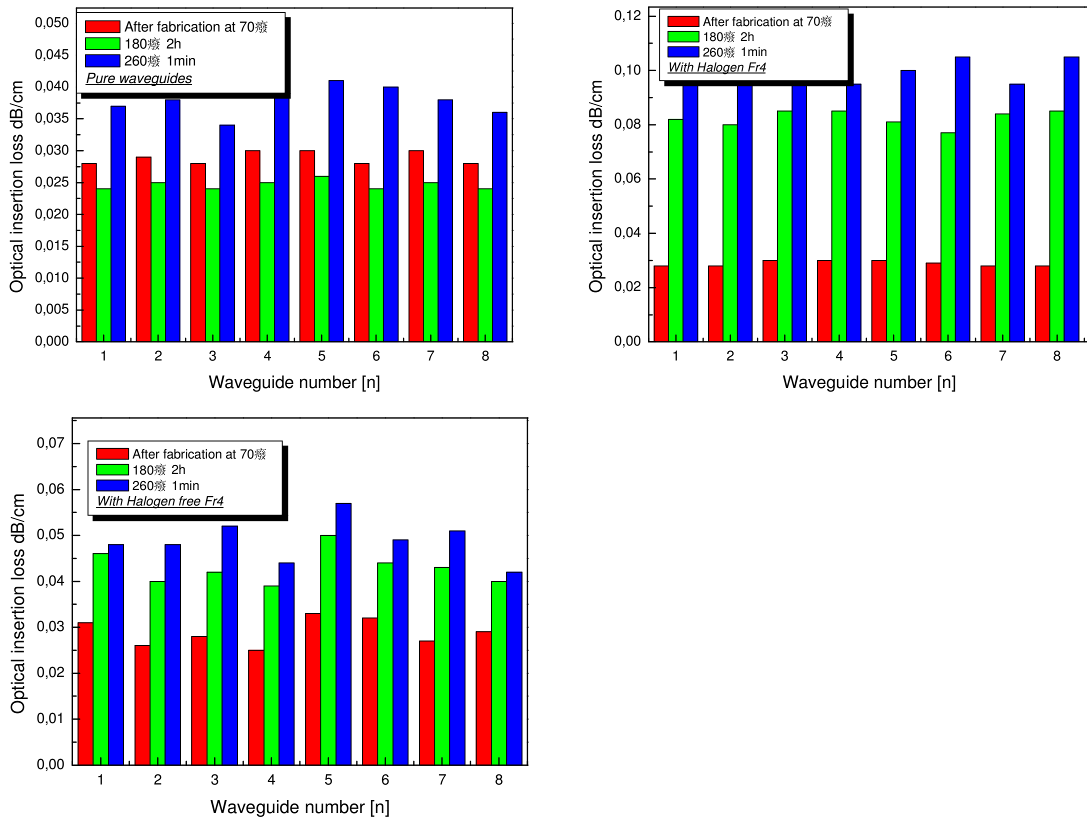

Fig. 3.22 *Optical insertion loss results of PDMS multimode waveguides without and with different carriers*

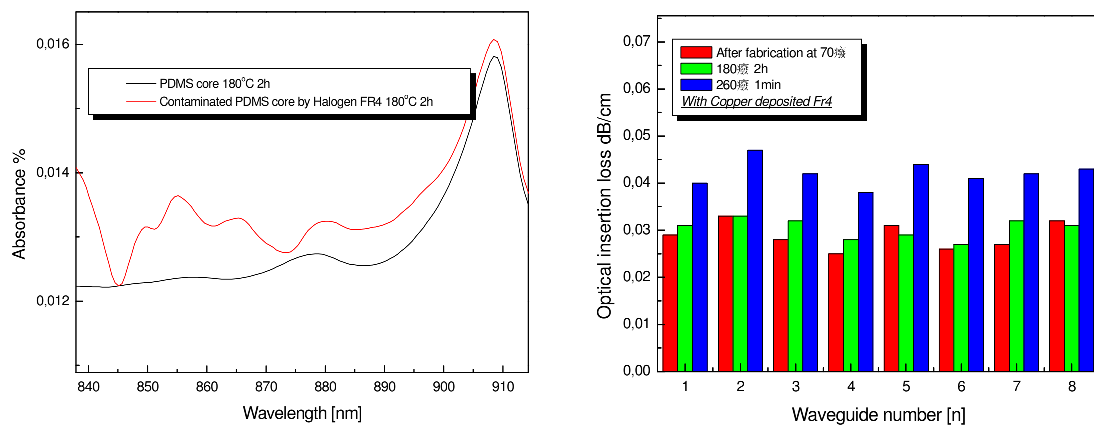

Fig.3.23 *FTNIR spectra of PDMS core material with and without cover of halogen FR4 after thermal treatment*

Fig.3.24 *Optical insertion loss of PDMS waveguides covered with copper foil FR4 boards*

3.6 Summary and review

In the chapter, the numerical aperture of polysiloxanes based waveguides was verified to be less 0.275 and fulfilled the basic bandwidth requirement of 10 Gbps/ 1m. Additionally, considering from different operation environments and thermal conduction influences from surrounding active elements e.g. VCSEL and PD the thermal stability of numerical aperture was also verified and to be proved to be very stable.

In broad wavelengths, the optical intrinsic loss of polysiloxanes and the deterministic factors were studied both. With respect to core polysiloxane at 850 nm, which is mostly used for datacom, the optical loss is 0.019 dB/ cm and found that the loss of 0.0144 dB/ cm is from the molecular vibration and the left 0.0056 dB/ cm is from rayleigh scattering.

Furthermore, experimentally it was found that average roughness of casting mould applied in waveguide fabrication should be controlled to be less 40 nm and the interlayer thickness due to incomplete blading within waveguide fabrication should be less 500 nm in order to obtain eligible EOCBs. Also, the halogen containing packaging substrates can give out gas which will absorb optical light near 850 nm wavelength and should be neglected, and halogen-free containing boards or copper covered boards are recommended for EOCB packaging.

4 Mechanical Aspects on EOCBs

4.1 Introduction

Introduced in chapter 2 and 3, our group has developed a new EOCB fabrication technology (patent pending) based on casting of thermal addition curing of two-component silicone rubber: PDMS (polydimethylsiloxane). This material has outstanding optical, thermal, and mechanical properties, an extremely favorable price (50 €/ l) and low shrinking (< 0.3 %) during polymerization. However, three critical points exist in PDMS based EOCB fabrication and products qualities. First it is the bonding quality between core and cladding, then cladding and cladding layer and the last is between two cladding layers and general PCB substrates (See Fig. 4.1). It is vital for the reliable operation of EOCBs to realize mechanically stable interfaces between core and cladding layers, cladding layers and the whole optical PDMS layers and the adjacent PCB substrate materials like FR4, Kapton and copper coated boards etc. In case of bubbles and insufficient interfacial adhesion among them, thermal stress due to CTE (Coefficient of Thermal Expansion) and Young's modulus mismatch will lead to delamination and resulting damage of the boards.

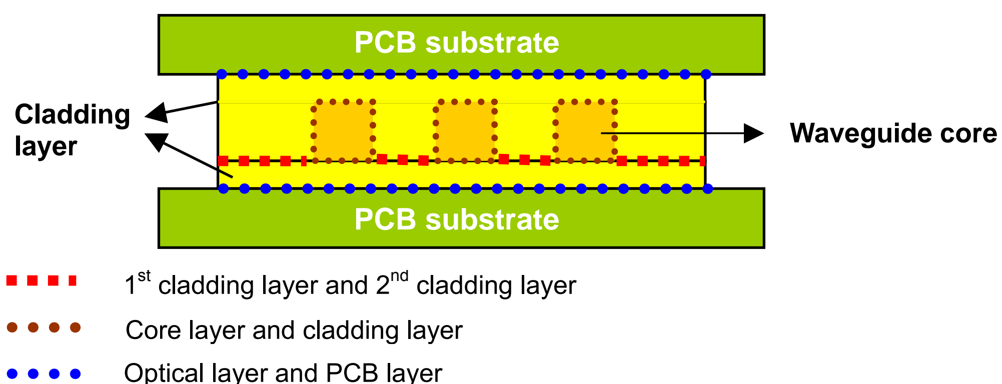

Fig. 4.1 *Basic structure of EOCB and mechanically critical interfaces*

The actually used two-component PDMS prepolymer is well known for its reluctance to adhere to most of the substrates including cured PDMS surfaces.[69] Unfortunately this property prevents the realization of self-packaged EOCBs. To overcome this problem and to achieve good adhesion between PDMS and PDMS, and PDMS and general PCB substrates applied in EOCB packaging appropriate curing conditions for core and cladding PDMS prepolymer are identified and special Surface-Adhesion-Promoters (SAP) have been developed both based on the researches on PDMS curing mechanism. In addition, the used PCB substrates are studied respectively from molecular to topography and various compatible treatment methods to these substrates are also developed in terms of the SAP molecular structural properties. By applying this procedure, we achieved – in one fabrication step - perfect curing of the liquid PDMS prepolymer without bubbles, although staying in contact with packaging substrates, as well as a good bonding between boards and PDMS layers. After curing, the well integrated PDMS optical layer is automatically laminated and packaged by two PCB carriers resulting in real-sense self-packaged EOCBs.

4.2 Curing Mechanism of Polydimethylsiloxane

Most biomolecular chemical reactions can be adapted to produce cross-linking provided the molecules are designed to form a three dimensional network as a result of the cross-linking reaction i.e., at least one of the molecules must be trifunctional. Given the relative ease with which organic functionalities can be attached as side chains to a polysiloxane backbone one would expect some adaptation of conventional organic cross-linking chemistries to be applied to the problem of cross-linking siloxanes. For these chemistries to be useful it is essential that the desired reaction occurs as expected when the organic functionalities are attached on the polymer, and the resulting cross-link should not impair the predominantly siloxane characteristics of the material.[70]

However, because silicon is such a strong eletropositive element its position relative to the organic substituent is critical in terms of the behavior of the attached orgainc substituent. Thus an organic substituent placed on the carbon β to the silicon can, because of the so-called β-effect, participate in totally unexpected reactions. The general effect of silicon substitution on an organic functional group can be illustrated by the effect of tri-methyl silyl substitution on the acidity of aliphatic carboxylic acids. The electron donating effect of the tri-methyl silyl group tends to weaken the acid and this effect is not lost until there are three carbons

between the silicon and the carboxy group. A similar pattern is observed in substituted aliphatic amines, although in the case the tri-methyl silyl group increases the basicity of the amine. Thus in general a reactive organic substituent must be located at least three carbons away from the silicon in order to preserve its normal reaction behavior.[71]

It is clear that each cross-link would contain a large number of methylene and other groups which would introduce a significant degree of organic character to the resulting cross-linked material, especially when the number of functional groups is optimized to give the degree of cross-linking needed to produce the desired physical properties and acceptable cure times. Thus it is clear that the siloxane character of the material would be significantly impaired if this or similar reactions were used as the cross-linking reactions. These reactions, therefore, tend to find utility where the intention is to modify the properties of organic materials by the incorporation of siloxanes, where additional organic character is not a problem, or in the formation of siloxane organic-copolymers.

Thus the cross-linking reactions, which will be described in more detail, are those which leave the siloxane properties virtually unchanged and produce materials, usually rubbers and coatings, which retain the desirable properties of the polydimethysiloxanes, namely their thermal and chemical stability and their ability to remain flexible at low temperature.

There are four classes of reaction which are widely used to cross-link siloxanes in commercial applications: [70]

1. Peroxide-induced free radical reactions
2. Condensation reactions
3. Hydrosilylation addition reactions
4. Hydridosilane/ silanol reaction.

In my thesis, it is mainly focused on PDMS based polymers and hydrosilylation addition reactions.

4.2.1 Hydrosilylation Addition Reactions in PDMS Materials

The Si-H bond is polar, long, and weak, and therefore, very reactive. [70] Its addition across a double bond (hydrosilylation) is an important reaction not only in organosilicon chemistry but also in organic synthesis and dendrimer and polymer chemistry. The hydrosilylation reaction, which involves the addition of a silicon

hydrogen (SiH) bond to an unsaturated carbon carbond bond, catalytzed by a noble metal, typically e.g. Pt is a well-known and versatile reaction in organosilicon chemistry. Additionally it has been widely used in the synthesis of organofunctional siloxanes and in the cross-linking of siloxane polymers. Many studies have been devoted to the soluble platinum catalyzed hydrosilylation reaction (eq. 4.1) since its discovery by speier in the late 1950. Industrially, the reaction is employed in the synthesis of silane coupling agents and UV screeners. It is also utilized in the formation of three-dimensional networks from the crosslinking reaction of multifunctional silicone hydride polymers with multifunctional silicon vinyl polymers. Product applications include silicone rubbers, liquid injection molding compounds, paper release coatings, and pressure sensitive adhesives etc.[66, 70]

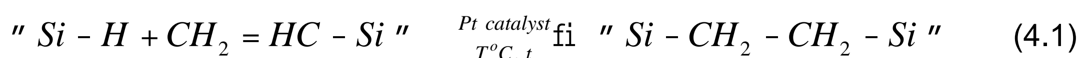

$$\equiv Si - H + CH_2 = HC - Si \equiv \xrightarrow[T^oC,\, t]{Pt\ catalyst} \equiv Si - CH_2 - CH_2 - Si \equiv \qquad (4.1)$$

Hydrosilylation reaction is a catalytic reaction for which a large variety of catalysts is available. They control the regio- and stereoselectivity including the enantioselectivity. Most of these catalysts operate according to the well established Chalk-Harrod mechanism or one of its variants resulting in the cis addition of a Si-H bond to an alkene. The Chalk-Harrod mechanism is the most commonly accepted mechanism for platinum-catalyzed hydrosilylation. In the classical Chalk-Harrod mechanism of olefin hydrosilylation a Si-H bond adds oxidatively to the metal atom of an olefin complex (Fig. 4.2). Migration of the hydride ligand onto the coordinated olefin generates the silyl alkyl intermediate, which undergoes reductive elimination to form the Si-C bond of the product. Normally, reactions following Chalk-Harrod-type mechanisms are accompanied by isomerization and scrambling of deuterium labels.[72-74]

In PDMS curing, the silyl (SiH) groups of the crosslinker reacted with vinyl groups through the hydrosilylation reaction. Simultaneously, but at a much slower rate, SiH groups are consumed through secondary crosslinking reactions that occur between SiH and SiOH groups newly-formed by the hydrolysis of SiH groups. (Some SiH groups might also react with chemical functionalities existing on the surface of the substrate.) These secondary reactions are favored when an excess of SiH over vinyl functionalities is used, and mainly occur after the completion of the primary hydrosilylation reaction. In this chapter, we will refer to the hydrosilylation reaction as the "crosslinking reaction" and to the secondary reactions that consume SiH as "post-cure reactions".

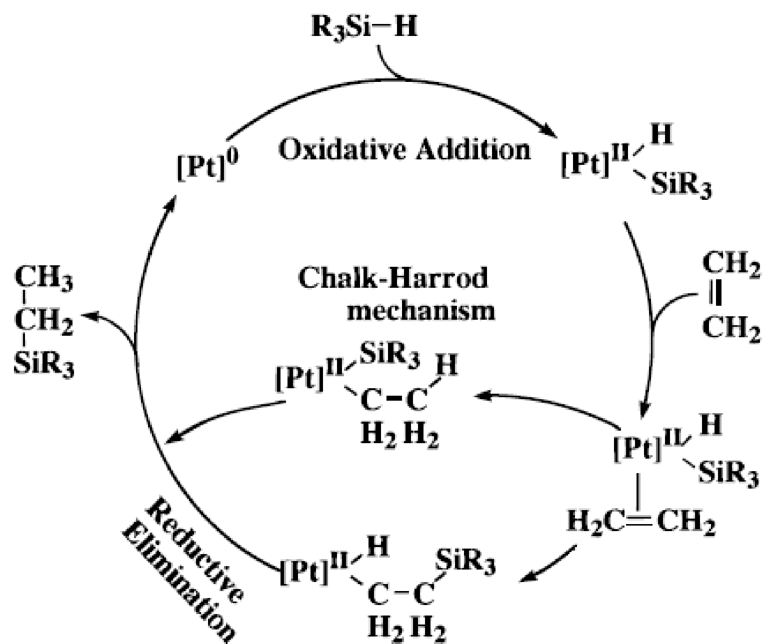

Figure 4.2 *Chalk-Harrod mechanism of olefin hydrosilylation*

The nature and concentration of both the catalyst and the inhibitor, as well as the concentration of vinyl and SiH groups influence the reaction rate. At high temperature (ca. 70 °C) with a catalyst concentration of 50 ppm (Pt), the hydrosilylation crosslinking reaction is completed within tenths minutes.

Thereby, secondary reactions also occur, when they are favored with an excess of crosslinker and in the so-called "post-cure" stage and it has been verified experimentally through blending Si-H groups containing polysiloxane, Pt catalyst and water together. The mechanism of this reaction first requires the catalyzed hydrolysis of SiH groups:

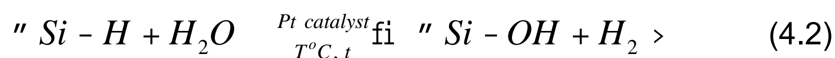

$$\equiv Si - H + H_2O \xrightarrow[T^oC,\, t]{Pt\ catalyst} \equiv Si - OH + H_2 \uparrow \qquad (4.2)$$

One of crosslinking reactions in the stage is the condensation of two silanol groups (which are created in reaction 4.2):

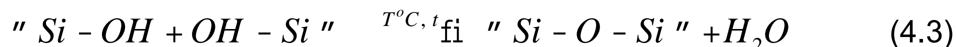

$$\equiv Si - OH + OH - Si \equiv \xrightarrow{T^oC,\, t} \equiv Si - O - Si \equiv + H_2O \qquad (4.3)$$

The other type of crosslinking reaction occurs in this post-cure stage via the creation of Si-O-Si bonds, when the newly-formed silanol groups (SiOH) catalytically react with remaining SiH groups:

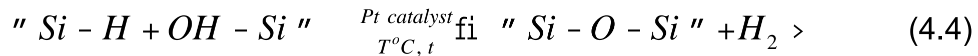

$$\equiv Si - H + OH - Si \equiv \xrightarrow[T^oC,\, t]{Pt\ catalyst} \equiv Si - O - Si \equiv + H_2 \uparrow \qquad (4.4)$$

The platinum-catalysed reactions 4.2 and 4.4 are much slower than the primary crosslinking reaction shown in Eq. 4.1. It is expected that the silanol condensation reaction (Eq. 4.3) is even slower than the SiH reactions (Eq. 4.2 and 4.4). Reactions shown in Eq. 4.2, 4.3 and 4.4 are jointly referred to herein as "post-cure reactions" as they occur when the system is allowed, or forced, to proceed towards its complete conversion rate.

4.2.2 Experimental Characterization to PDMS Curing

Introduced above, the hydrosilylation reaction of SiVi with a hydrosilane polysiloxane crosslinker creates a three-dimensional network. The rate of the reaction is a complex function of the curing temperature, catalyst nature and concentration, of inhibitor nature and concentration, and on the concentration of vinyl and SiH groups etc. For instance, RT 601 PDMS material, applied as waveguide cladding material in the thesis, under that conditions of 50 ppm (Pt) and in 1mm thick they can be completely cured within 5 min at 150 °C instead of 25 min at 70 °C. In details, the influences on rate of the reaction from catalyst concentration (Wacker EP), inhibition concentration (PT 88) and the concentration of base component and crosslinker were experimental investigated and illustrated below respectively in Fig. 4.3.

From these results, it is clear that platinum catalyst can improve PDMS curing evidently even if in quite few amounts. Then the presence of platinum will inversely affect the optical properties of the transparent PDMS system explained in Chapter 3 due to scattering of platinum colloid created by the extra Pt catalyst and medium sized molecular chain with uncrosslinked Si-Viny groups, so its concentrations should be controlled in one relatively low level. Inhibitor, organic temporal platinum catalyst deactivator, which can inhibit the quick curing due to its temporal deactivation and inhibition to platinum catalyst at room temperature, and it is helpful to extent the pot life of silicone rubber resins. When PDMS is thermally cured, the inhibitor will be evaporated as well and no extra influences on PDMS physical and chemical performances. Thus in the waveguide fabrication part, influences of concentrations of Si-H and Si-CH=CH_2, and temperature on PDMS curing will be investigated and studied as main points.

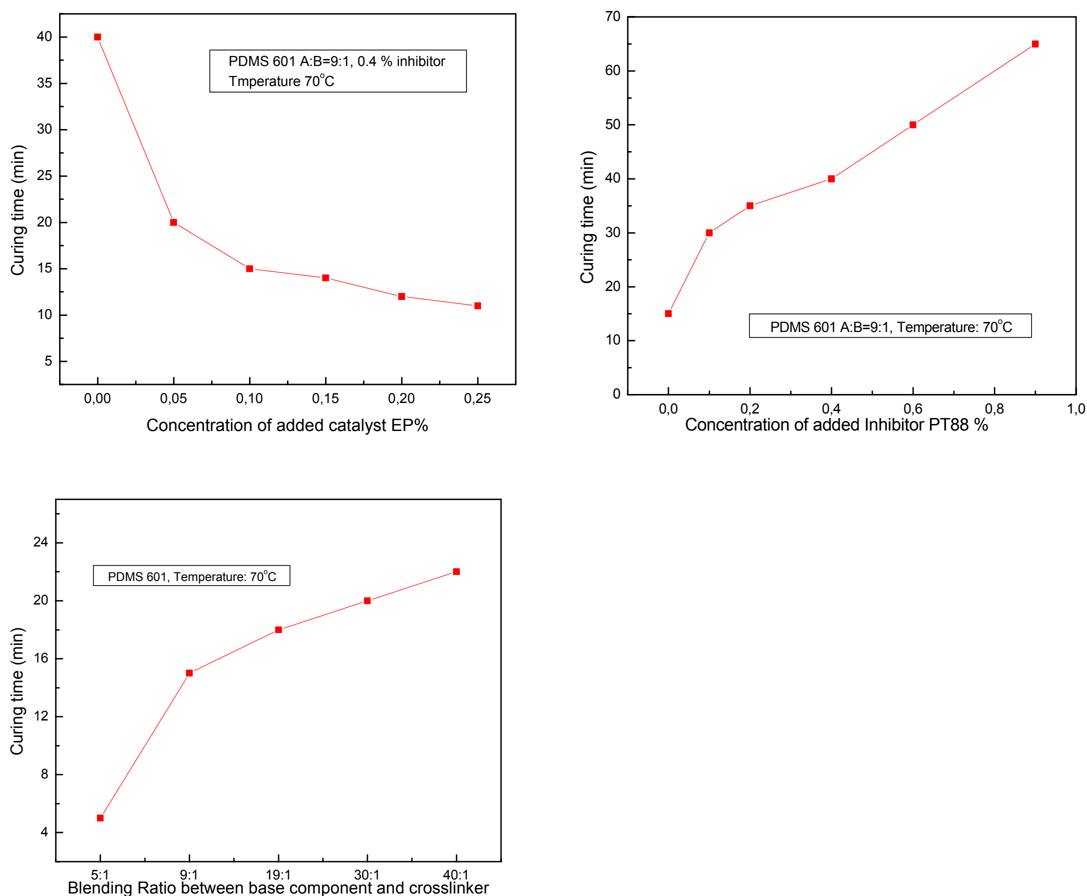

Figure 4.3 *Various influences factors on PDMS curing*

Actually, the conversion of Si-H and Si-CH=CH_2 bonds can be followed and monitored by infrared and Raman spectroscopies. The IR and Raman spectra of RT 601 PDMS base component (compound A), crosslinker (compound B) and the corresponding cured polymer with different blending ratio are shown in Figure 4.3 respectively. From these spectra, the absorbances of the Si-H and Si-CH=CH_2 bonds (2159 and 1597 cm^{-1}, respectively) are nicely isolated peaks and may be applied for determination of state of curing of PDMS, because the Si-CH_3 absorbance (1263 cm^{-1}) will remain the same throughout the reaction and can act as an internal standard. The results are listed in Table 4.1.

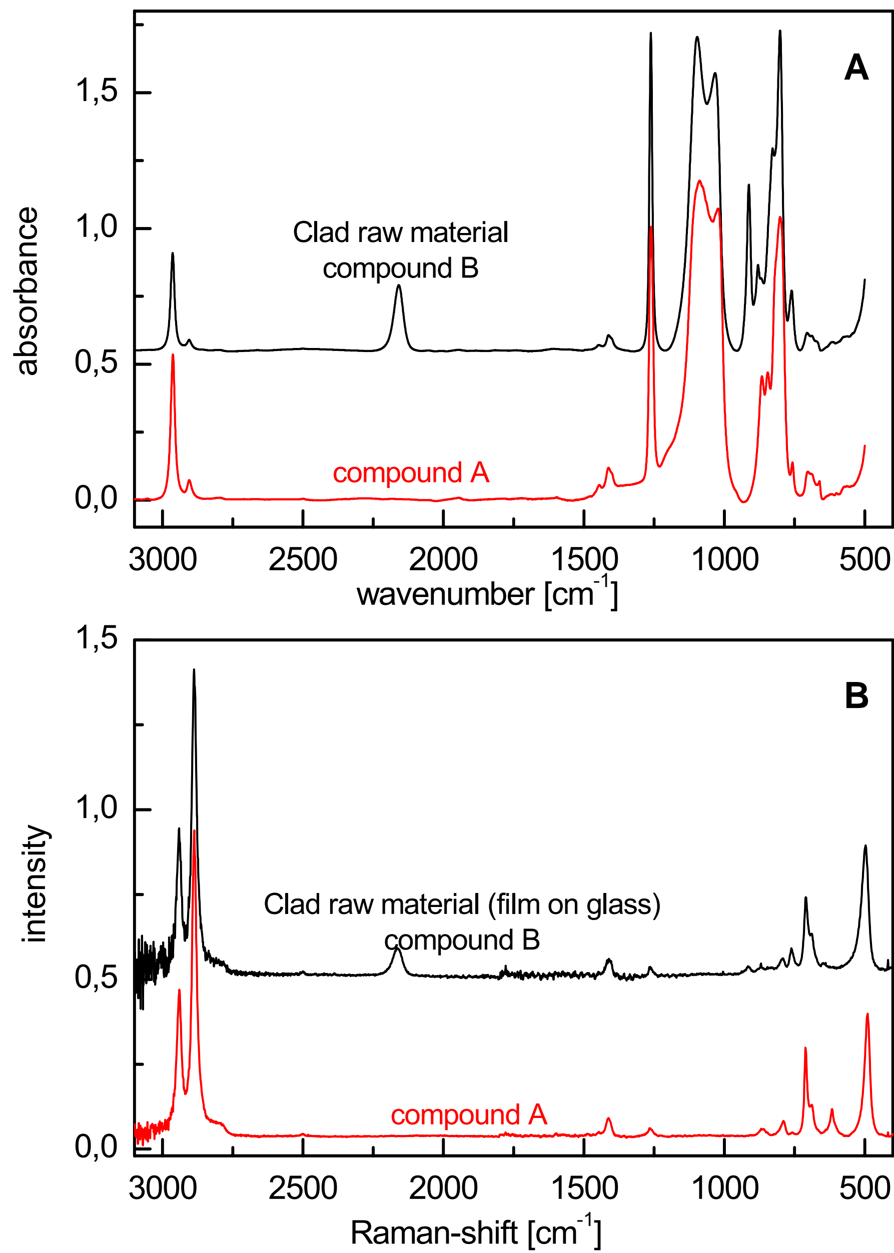

Figure 4.4A *FT-IR and FT-Raman spectra of PDMS prepolymers (cladding)*

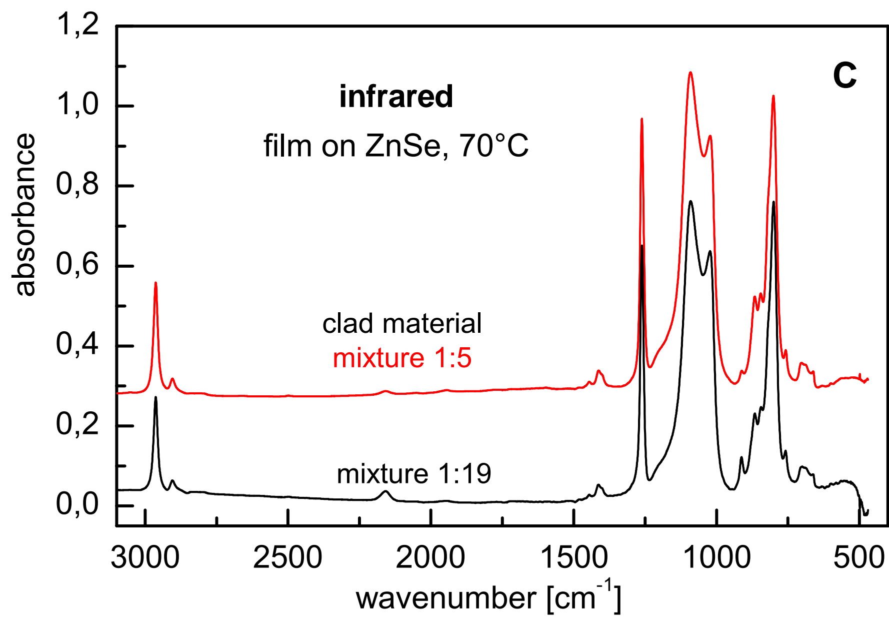

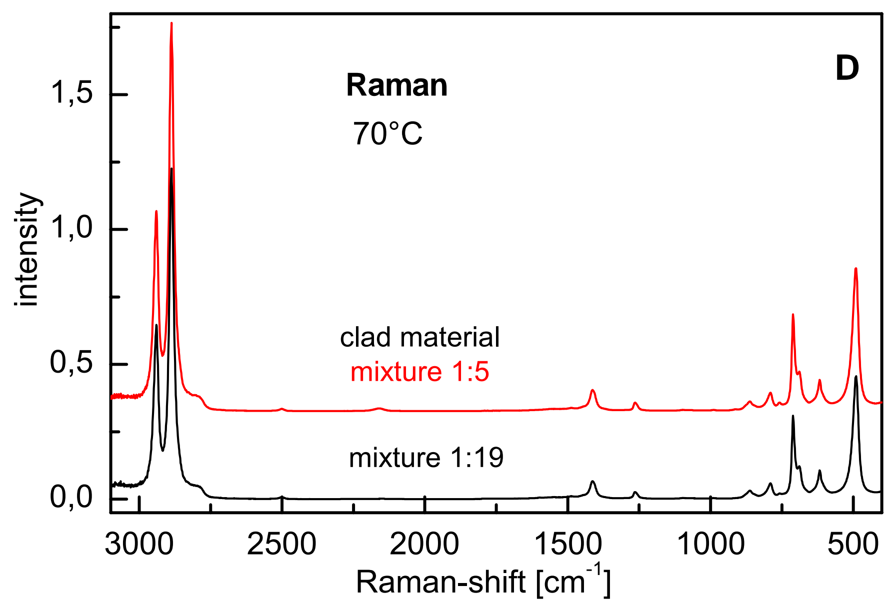

Figure 4.4B *FT-IR and FT-Raman spectra of PDMS crosslinked polymer (cladding)*

Table 4.1 *The conversion (FT-IR and FT-Raman) of the reactive groups after curing at 70 °C for 2 hrs for the PDMS networks*

PDMS blending ratio (A:B)	***Conversion Si-H (%)***	***Conversion Si-CH=CH₂ (%)***
19:1	79	72
5:1	87	78

With respect to 5: 1 blending ratio PDMS, it includes relatively more Si-H groups, whereas the conversion of the Si-H groups is higher than the conversion of Si-vinyl, it can be proposed to be a consequence of side reactions (post-cure) for which the following possibilities shown in equations 4.2 and 4.4. However, to 19: 1 blending PDMS, there are less Si-H groups reacted in post-cure stage and more is hydrosilylation crosslinking and thus the blending ratio is recommended for application of RT 601 cladding PDMS on waveguide fabrication for post-cure reaction can make PDMS network shrink and bring some by-products, e.g. bubbles.

Certainly the sensitivity for these Si-H side reactions is also strongly related with the presence of the platinum catalyst. They indicate that PDMS can potentially react with some polar components e.g. OH and carbonyl etc. on substrates through dehydration and hydrogen bonds (See Eq. 4.5 and 4.6) and enable PDMS bond with substrates under some specific conditions, which gives us hint that the PDMS might adhere to substrates through increasing the concentrations of Si-H groups and platinum catalyst for Pt catalyst can increase the velocity of post-cure reactions in some extents. It will be verified in the later parts.

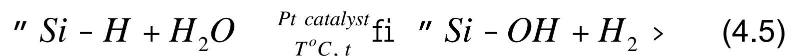

$$\equiv Si - H + H_2O \xrightarrow[T^oC,\, t]{Pt\ catalyst} \equiv Si - OH + H_2 \uparrow \qquad (4.5)$$

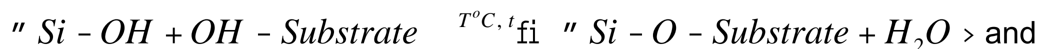

$$\equiv Si - OH + OH - Substrate \xrightarrow{T^oC,\, t} \equiv Si - O - Substrate + H_2O \uparrow \text{ and}$$

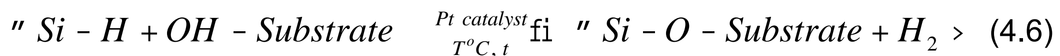

$$\equiv Si - H + OH - Substrate \xrightarrow[T^oC,\, t]{Pt\ catalyst} \equiv Si - O - Substrate + H_2 \uparrow \qquad (4.6)$$

Additionally from spectrum of 5:1 blending cured PDMS it indicates that the conversion of Si-CH=CH$_2$ bonds can be increased by using an excess of Si-H bonds.

Furthermore, temperature influence on PDMS curing is also investigated with one 19:1 blending PDMS. The measured spectra in different curing conditions are

shown in Fig. 4.5.

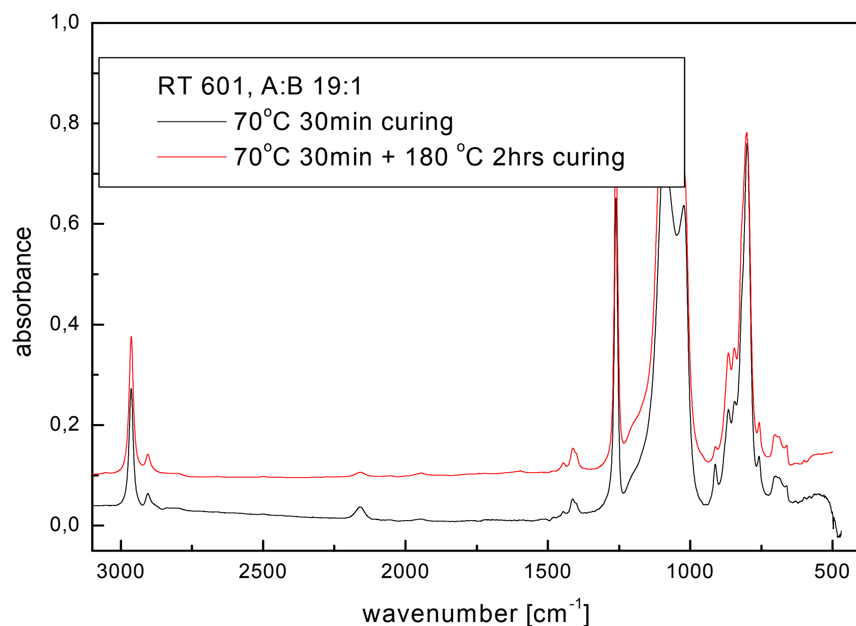

Figure 4.5 *FT-IR spectra of PDMS cured in different temperatures*

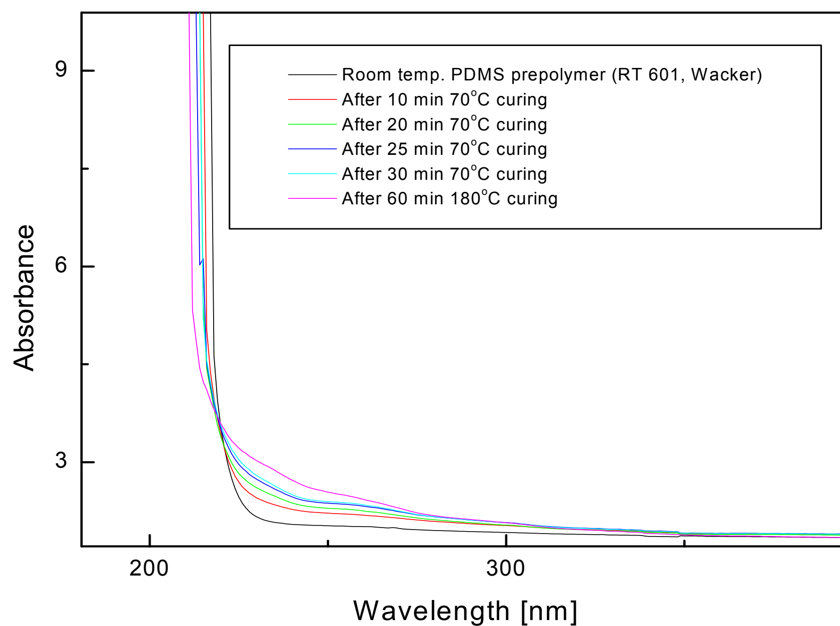

Figure 4.6 *UV-Vis spectra of cured PDMS at different temperatures*

After further 180 °C for 2 hrs curing the conversion ratio of Si-H is obviously is

increased to be 87 % and the conversion of Si-vinyl to be 78 % from respective 99 % and 62 %. We thought the further high temperature treatment not only leads to hydrosilylation crosslinking but the Si-H react with water diffused into PDMS through post-cure reactions.

Beside IR and Raman spectroscopies one easy way is to use UV-VIS spectroscopy on monitoring PDMS curing state, since Si-CH=CH_2 bonds have strong absorption peak at 260 nm arising from electronic transitions.[75] After curing, the absorption peak at 260 nm will shrink with the elimination of vinyl groups in PDMS and shift to deep UV region, which is shown in Fig. 4.6.

4.2.3 Identification of Curing Conditions for PDMS Waveguides Fabrication

The critical issue in PDMS waveguides fabrication is that it must keep core PDMS strongly adhere to both cladding PDMS layers and the first cladding bond strongly with second cladding layer without any by-products as well as its good structure fidelity of cores with the respective grooves in the casting mould. Through analysis above, within post-cure reactions PDMS probably adhere to substrates with the increase of the concentrations of Si-H groups, but by-products from these reactions can cause waveguides shrink and lots of bubbles in the waveguides layer as well. Therefore, in PDMS waveguides fabrication PDMS post-cure reaction should be avoided.

In chapter 4.2.2, curing of RT 601 cladding PDMS has been studied with UV-VIS, IR and Raman spectra, and we found that 19:1 blending can make it have more hydrosilylation crosslinking and thus the blending ratio between base component and crosslinker is set to be 19: 1. To core PDMS (SLM 77522), due to its relatively shorter molecular chain and some specific structures applied for refractive index tuning we set it to be 9:1 after analysis of IR spectra of core PDMS with different mixing ratio like last chapter. Except identifying the appropriate blending ratios to achieve more hydrosilylation in PDMS curing, the curing time and temperature will be very important factors to determine the bonding quality between PDMS core and cladding etc. Through lots of pull-off measurements on PDMS waveguides layers (as to detailed measurement methods, please refer to chapter 4.2.4 B) and their cross-section observation with microscopy we found 70 °C for 30 ± 5 min curing is the optimum condition for core PDMS (SLM 77522) curing and first cladding PDMS layer curing. Under such conditions, core PDMS layer can strongly adhere to both cladding PDMS layers and first cladding bond strongly with second

cladding layer with good structure fidelity from the mould groove. In the following half part, with measured FTIR spectra of core PDMS we will in detailed explain and analyze the reason that we select such parameters.

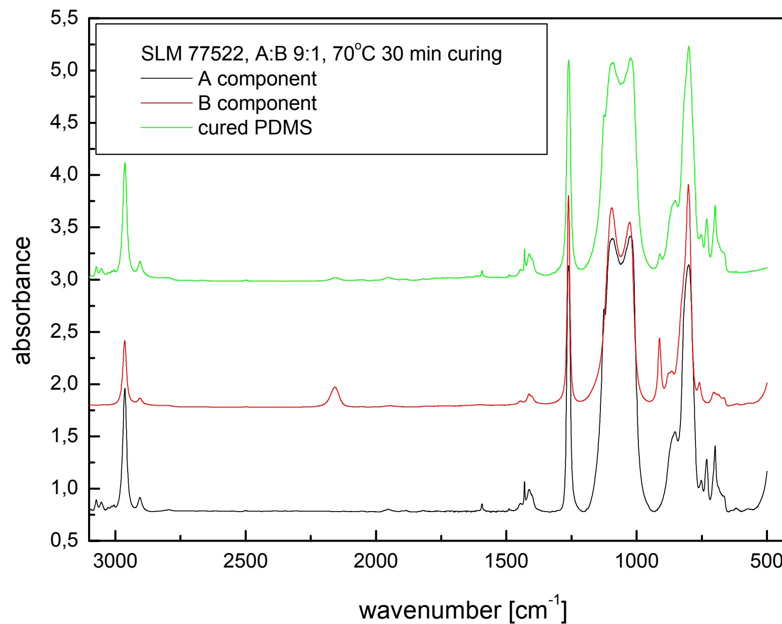

Figure 4.7 *FT-IR spectra of core PDMS prepolymers and cured polymer*

From the spectra, we found a low conversation of Si-H bonds (65 %) and Si-vinyl bonds (45 %) in core PDMS based on the 70 °C for 30 min curing conditions but such conversation is proved enough to keep its robust mechanical properties and also to be demoulded from casting mould easily. Due to relatively low conversation ratio, lots of residual uncured reactive groups on the top surface of core PDMS layer might continue to react with respective groups, e.g. Si-vinyl vs SiH in cladding PDMS prepolymer through hydrosilylation reaction when they are poured onto the core PDMS in waveguide fabrication. The new hydrosilylation reaction between them will make them integrated together after some time thermal curing. Due to the incomplete curing, the network of core PDMS is not so dense that some parts with short molecule chain including reactive groups e.g. Si-H in cladding PDMS prepolymer may diffuse into core PDMS and react with Si-vinyl groups in core PDMS through hydrosilylation crosslinking, and finally make core and cladding bond strongly through chemical bonds. Whilst, after curing at 70 °C for 30 min of first cladding PDMS, its 99 % and 62 % conversation ratios of Si-H and Si-vinyl also can ensure it to form good bonding with second cladding PDMS layer for the

same mechanism. After pouring the 2nd cladding layer onto core and first cladding layer, it is suggested to make a little longer e.g. 1 - 2 hours curing to the whole realized waveguides, to keep further complete hydrosilylation reaction and reach better mechanical properties of the whole PDMS layer.

Then, as we found, the relatively larger mismatch between Si-H and Si-vinyl in 9: 1 core PDMS than 19: 1 cladding PDMS shown in Fig. 4.4 and beside the higher ratio of SiH bonds it can be explained as follows. Owing to the bulkiness of the phenyl group added to core PDMS for higher refractive index to keep optical waveguiding- and the increase in the number of branching (crosslink) points, the Si-vinyl and Si-H groups become more spatially hindered and have a fewer possibilities to react with each other. The higher conversions of the Si-H groups here should be a consequence of side reactions in post-cure stage. More Si-H side reactions will take place with an increasing amount of branching, because more end groups are present and capable of reacting with the Si-H groups.

4.2.4 Mechanical Characterization

A. Relationship between molecular curing and mechanical properties of PDMS

Beside characterization with UV-VIS, IR and Raman spectrocopies, the state of curing of PDMS polymers can be directly reflected to their mechanical properties, e.g. tensile strength and elongation ratio at break, for they are strongly related with PDMS molecular chain length and crosslinking density. Thus PDMS polymers based on different curing conditions are prepared for the experimental verification.

Due to PDMS intrinsic low Young's modulus and high possion ratio, one mechanically optimized PMMA based casting mould (see Fig. 4.8) is designed based on FEM (Finite Element Method) mechanical simulation (Length: 110 mm; Width: 35 mm; Length of narrow part: 40 mm; Width of narrow part: 12 mm; Curve of neck place: 98 ± 1°) and fabricated with high precision diamond based micromilling machine. In order to avoid the shear strength during measurement, bottom and sidewall of mould are specially treated with UV exposure to achieve lower roughness (Ra< 20 nm). Furthermore during fabrication the PDMS layer in two wide side parts will be kept 1.5 - 2.5 mm thicker than the narrow part for they will sustain larger force when pressed by two clamps during pull test (See Fig. 4.8). The pull speed is 0.02 mm/ s. To every test item, 8 samples are prepared for measurement. The results are listed in Table 4.2.

Table 4.2 *Mechanical properties of PDMS with different blending ratio and temperature treatments*

	19:1 PDMS (70 °C 2 hrs)	***5:1 PDMS (70 °C 2 hrs)***	***19:1 PDMS (70 °C 2 hrs + 180 °C 2hrs)***
Tensile strength (MPa)	1.42 ± 0.29	1.23 ± 0.34	1.49 ± 0.32
Elongation at break (%)	158 ± 7.92	112 ± 6.47	147 ± 0.29

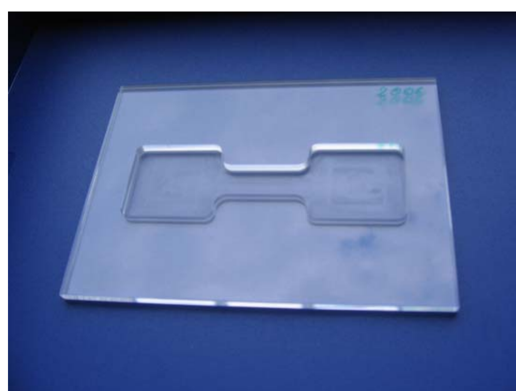

Fig. 4.8 *Casting mould for tensile strength measurement and set-up of pull off test*

In terms of aforementioned spectra analysis, it is clear that access of Si-H can obviously affect the PDMS robustness and elasticity properties due to post-cure reaction, for which causes much shorter molecular chain in PDMS network and relatively lower crosslinking density. The continuous high temperature curing indeed can increase the robustness of PDMS but the intrinsic good elasticity of PDMS elastomer is reduced, which is due to the post-cure reactions. Further hydrosilylation crosslinking can make Si-vinyl containing molecular chain react with Si-H containing molecular chain to form PDMS linear network structural unit and increase the crosslinking density and material intrinsic strength. However the post-cure reaction between Si-H with water etc. can decrease the materials elasticity due to its side reaction and low molecular chain properties.

B. Limit strength in PDMS waveguides layer

In terms of PDMS waveguide fabrication method and curing conditions (70 °C for 30 min curing to core and first cladding, and 70 °C for 2 hrs curing to second cladding layer, i.e. the whole waveguides layer), the bulk PDMS waveguides layer including core and cladding is prepared. However, it is difficult to identify one appropriate method to correctly measure the limit strength of PDMS waveguides layer, for the actually used two-component PDMS prepolymer is well known for its reluctance to adhere to most of the substrates against curing. Then, as we knew cured PDMS can form good and strong bonding with glass sheets after O_2 plasma exposure and thermal treatment, so samples shown in Fig. 4.9 are prepared with two low roughness glass sheets (Middle part without metal chuck). They are separately put into O_2 plasma chamber for 0.5 - 1 min exposure and after that, pressing them together and drive the air bubbles out from their interfaces, then putting into 160 °C oven for 2 - 3 hrs thermal curing. After that the PDMS will strongly bond with the glass sheets. The glass sheets can be as a mechanical holder and inserted into two suitably sized metal chucks to be connected with force sensor (see Fig. 4.8). Then pull-off method can be used for identifying the limit strength of the bulk waveguides layer for intrinsic strength of glass is far stronger than PDMS applied here. After pull-off tests, it is found that strength limit of such PDMS waveguides layer is about 0.8 MPa and the damage of sample normally happens in the middle of waveguide cores for core PDMS applied here (SLM 77522) has relatively low tensile strength (0.57 MPa, and through adjusting the molecular chain length the intrinsic tensile strength can be improved to 2 MPa). Direct separations between core and both cladding layers, and first cladding and second cladding layer are not observed, which proves the core and cladding layers, first cladding and second cladding layers have been crosslinked each other to be one integration.

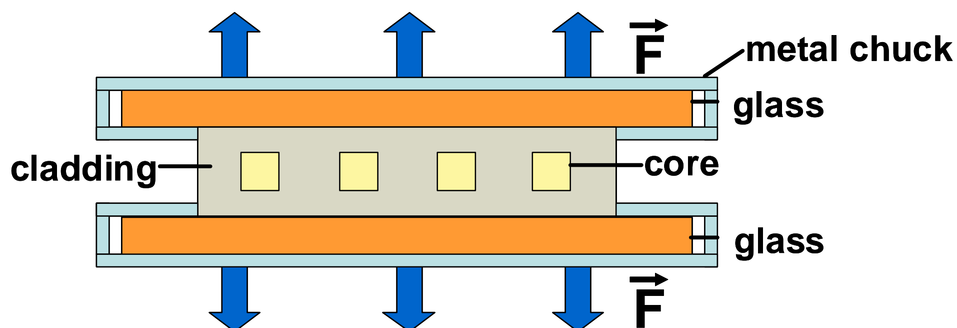

Figure 4.9 *Cross-section of test specimens for determination of limit strength in PDMS*

waveguides layer

In conclusion, more hydrosilylation will improve PDMS crosslinking density and intrinsic mechanical properties which is also expected in PDMS waveguide fabrication, and then post-cure reactions also indicates that PDMS has potential to react with some polar components e.g. OH and carbonyl etc. on substrates through dehydration and hydrogen bonds under some specific conditions. After identifying the curing mechanism and various components functions in PDMS curing, based on different requests we have the capability to flexibly keep balance between main hydrosilylation and post-cure reactions through controlling curing temperature, the ratios of Si-H, Si-vinyl, inhibitor and platinum catalyst etc. Through adjusting curing parameters, the limit strength of PDMS waveguides layer can be directly up to the core material itself. Appropriate methods are identified to correctly measure the intrinsic tensile strength of PDMS polymer and the limit strength in PDMS waveguides layer.

4.3 Development of Surface-Adhesion-Promoter and Substrates Etching

The integration of multimode PDMS waveguides into conventional printed circuit boards is indeed very attractive because of low cost and easy manufacture. However, the actually used two-component PDMS prepolymer is well known for its reluctance to adhere to most of the substrates, especially to FR4 and copper, two most widely used substrates in general PCB manufactures. Unfortunately this property prevents the realization of self-packaged EOCB. Then according to our aforementioned research results about optical properties and loss contributors in PDMS and PDMS curing mechanism, in the chapter, from two aspects of surface adhesion promoter (SAP) development and substrates activation we will discuss how to realize the EOCB self-packaging under no extra influences on good optical, thermal, and mechanical properties of PDMS based EOCB.

In this chapter, FR4-boards, Kapton^{TM} (polyimide, HN series from DuPont), copper coated FR4 boards and ED copper (Electrical Deposited as barrier layer for preventing outgas from some polymer based PCB substrates) are selected as PCB candidates' materials for research.

4.3.1 Basic Concept for Surface-Adhesion-Promoter Synthesis

To achieve good adhesion between PDMS and PCB substrates special Surface-Adhesion-Promoters (SAP) has to be developed. Though such RTV 2 PDMS is reluctant to adhere to most of the substrates, in terms of results in chapter 4.2 we found that PDMS has potential to react with some polar components e.g. OH and carbonyl etc. on substrates in post-cure stage through increasing the concentrations of platinum catalyst and Si-H groups. Additionally, by keeping balance between main hydrosilylation and post-cure reactions by controlling Pt concentrations, curing temperature and the ratios of Si-H and Si-vinyl etc., the PDMS polymers in terms of different requests, e.g. hardness, elasticity and bonding quality with substrates etc. may be synthesized respectively.

However, not like polymer substrates i.e. FR4 and Kapton, we can easily improve the concentrations of OH and carbonyl groups etc. on their surfaces through dry and wet etching which will be introduced in the following parts. With respect to PCB copper (Zinc covered copper, in chapter 4.3.3 it will be in detailed introduced) and ED copper, they are metals and obviously different with these polymer substrates, due to the highly ionic character of the metal-O bonds the covalent linkage to the siloxane group is chemically difficult. As we knew, Zinc has some catalyzing function to addition curing two components polysiloxane and Si-H bond can be added oxidatively to the zinc (0) atom and form colloid hydride Zinc containing ligand when the Si-H concentration and curing temperature are both high enough, and consequently they can be bonded together chemically. Thus it is necessary to protect the Zinc layer when it is micro-etched with $Na_2S_2O_8$ for organic contamination cleaning. To SAP applied for Zinc covered PCB copper, high concentration of Si-H groups and curing temperature are expected. However, with respect to ED copper, this method cannot be used any more for copper has no catalyzing function on such polysiloxane curing. In order to increase the possibility of reaction between SAP and copper substrates, the pure ‘post-cure’ reaction is expected for increasing the reaction possibility and thus the concentration of Si-viny groups in SAP should be as low as possible, additionally the surface of ED copper after organic contamination cleaning is proposed to be cleaned only with N_2 gas blowing not by drying in to avoid copper surface oxidized.

Based on such basic concepts to different boards, various surface adhesion promoters (SAP) containing different concentrations of Pt (0) catalyst ranging from 0.001 to 2 wt% and inhibitor ranging from 0.15 to 6 wt%, and different ratio between Si-H and Si-vinyl ranging from 1: 0 to 1: 100 are synthesized successfully in our Lab under that no any phase incompatibility and crystallizations exist, in addition the viscosity of SAP also can get controlled to be less 300 mPas for

meeting different fabrication requests, e.g. spray coating.

In the following parts, according to their different surface molecular structures, topography and distribution of polar components on substrates, their influences on bonding strength between SAP layer and PCB layer will be investigated in details after different etching treatments.

4.3.2 Identifications of Substrate Surface Molecular Structures and Appropriate Etching Methods

A. FR4

FR4 laminate is the usual base material from which plated-through-hole and multilayer printed circuit boards are constructed. It is the most versatile laminate and composite, this is a continuous glass woven fabric base impregnated with an epoxy resin binder whose synthesis is shown in Fig. 4.10.

It has extremely high mechanical strength, good dielectric loss properties, and good electric strength properties, both wet and dry. While the potential for environmental legislation is lessening in Europe (WEEE & RoHS),[76] primarily because Tetrabromo-Bisphenol A (TBBA) is not on the banned list, polybrominated aromatic compounds are still considered undesirable. The incineration of FR4 boards containing polybrominated aromatic compounds produces noxious Hydrogen Bromide (HBr) gas, which is corrosive.[77-79] Plastic materials that contain polybrominated biphenyls or polybrominated diphenyl ethers can be converted (oxidized) to dioxin or furan, respectively.80 Like introduced in chapter 3, they can not only harmer human but optical waveguides for they contain many vinyl groups which can absorb light near 850 nm wavelength.

While these specific flame retardants are not typically used in FR4 based PCBs, the perception is that PCBs will produce dioxin and furan derivatives upon thermal degradation. Toshiba has published data that indicates that no dioxins are formed upon incineration of PCBs using non-brominated resins with Phosphorous and inorganic based (some filler) chemistries.[81] “Green” labels are more common now in Europe. The European Community will most likely require OEMs to “take-back” electronic equipment. Future waste-management of PCBs containing halogens (and other environmentally unfriendly compounds) will most likely be costly. The main chemical families used for non-halogenated flame retardants are Phosphorous compounds, nitrogen compounds (including Polyamides and

Polyamines), oxy-acid sources like Boric, Sulfuric, and Phosphoric, and inorganic fillers and compounds containing Aluminum, Magnesium, or Red Phosphorous. Triazine derivatives are also effective flame-retardants.[80-82] In the thesis, FR4 boards (halogen free - non-brominated) were purchased from Isola GmbH, Düren, Germany.

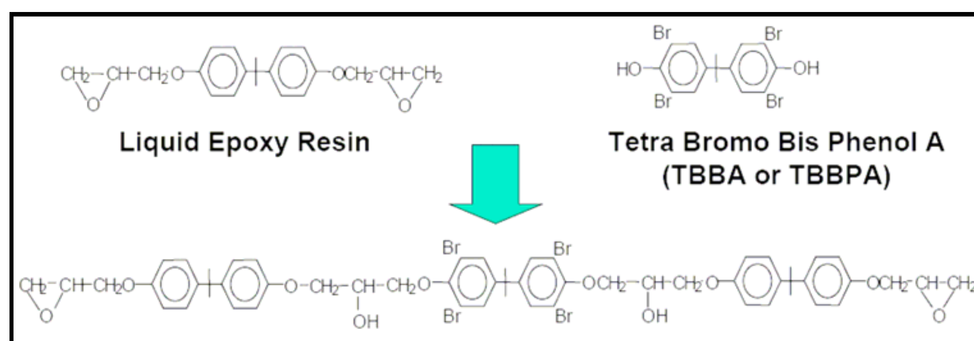

Figure 4.10 *Basic synthesis concept of FR4*

Low pressure plasma treatment is probably the most versatile surface treatment technique to improve polar components concentrations on polymer substrates. It has become an important industrial process for modifying polymer surfaces which is usually confined to the top several hundred angstroms and does not affect the bulk properties. Oxygen and oxygen-containing plasmas are most commonly employed to modify polymer surfaces. In oxygen plasma, two processes occur simultaneously: etching of the polymer surface through the reactions of atomic oxygen with the surface hydrocarbon groups, giving volatile reaction products; and the formation of oxygen functional groups at the polymer surface through the reactions between the active species from the plasma and the surface atoms e.g. C-OH, C=O, O-C=O, C-O-O, and CO_3 etc. on the surface.[83-84] The balance of these two processes depends on the operation parameters of a given experiment. Actually many processes including O_2 plasma activation like introduced above followed by a surface graft polymerization. However, due to the restriction of high price of high vacuum plasma instruments, other appropriate low cost treatments are also necessary to be identified, e.g. wet chemical etching. Compared with plasma (vacuum) processes, these treatments are more preferred industrially. In the thesis, an alkaline oxidizing solution containing 1.25 - 2 mol/ l $KMnO_4$ and 1.25 - 2 mol/ l NaOH heating at 70 to 85 °C is applied as wet etchant to activate surfaces of polymer substrates, e.g. FR4 and Kapton (polyimide based) due to its potential on activating and modifying the carbon containing polymers surfaces physical and chemical characteristics. The function can be explained as follows

from equation 4.7 to 4.9.

Main reaction: 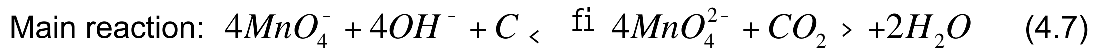
$$4MnO_4^- + 4OH^- + C \downarrow \rightarrow 4MnO_4^{2-} + CO_2 \uparrow + 2H_2O \quad (4.7)$$

In addition, the following reactions which happen on etchant itself should be avoided:

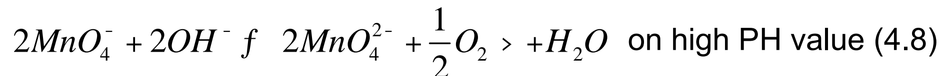
$$2MnO_4^- + 2OH^- \rightarrow 2MnO_4^{2-} + \frac{1}{2}O_2 \uparrow + H_2O$$ on high PH value (4.8)

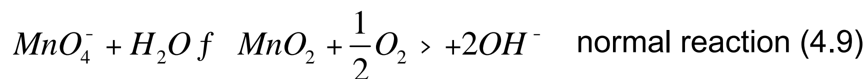
$$MnO_4^- + H_2O \rightarrow MnO_2 + \frac{1}{2}O_2 \uparrow + 2OH^-$$ normal reaction (4.9)

In the wet etching, concentrations of MnO_4^- and OH^-, etching time and temperature will be the main deterministic factors. To ensure the etchant used repeatedly, first the concentrations of KMO_4 and NaOH cannot be so high, and additionally the electrochemical method combing with heating together also can be used to make them react in the reverse orient and avoid the deposition of MnO_2.

To study the influences of the effect of the O_2 plasma exposure and $KMnO_4$ etching on the final bonding strength, before and after the two etching on FR4-boards their surface molecular structure were both analyzed by FTIR/ ATR spectroscopy. Measured spectra are shown in Fig. 4.11. Among the most intense absorption peaks are those associated with -OH stretching (3700-3100 cm^{-1}), alkyl group (2960-2975 cm^{-1}), carbonyl group stretching (1720 cm^{-1} out of phase and 1780 cm^{-1} in phase), ester group (1739 and 1179 cm^{-1}), C=C in aromatic ring (1506 cm^{-1}), ether groups (1236, 1111, 1019 and 806 cm^{-1}), and epoxy group (914 cm^{-1}) etc.[85-87]

As seen in Fig. 4.11, in untreated FR4 substrate surfaces there also exist a few polar components, e.g. -OH and carbonyl, and lots of low surface energy non-polar alkyl groups. These few polar components on pure FR4-boards should enable reactions with –SiH containing groups in PDMS in terms of covalent and hydrogen bonds. However, the low surface energy of the alkyl groups on FR4-substrates can prevent the PDMS prepolymer wetting on FR4 substrate. To enhance the wettability of FR4-substrates and to improve the concentration of polar components, e.g. OH groups on it, low temperature O_2 plasma and $KMnO_4$ alkaline oxidizing solution (1.5 mol/ l $KMnO_4$ and 1.75 mol/ l NaOH) were applied. After 2 min and 10 min O_2 plasma exposure, and 30 min $KMnO_4$ wet etching on FR4 substrates, their spectra revealed that concentrations of various high surface energy polar oxygen complexes on the hydrophobic FR4 surface were increased, e.g. -OH and carbonyl groups etc. The concentrations change of oxygen complexes on FR4 surfaces is

due to the oxidation of FR4 surfaces by the two etching which is believed to proceed via a free radical, chain-reaction mechanism, whilst they also proves the two etching methods are both appropriate and effective on activating FR4 surfaces. The liquid solution etching by $KMnO_4$ can substitute to O_2 plasma for industrial application on FR4 etching and surface activation.

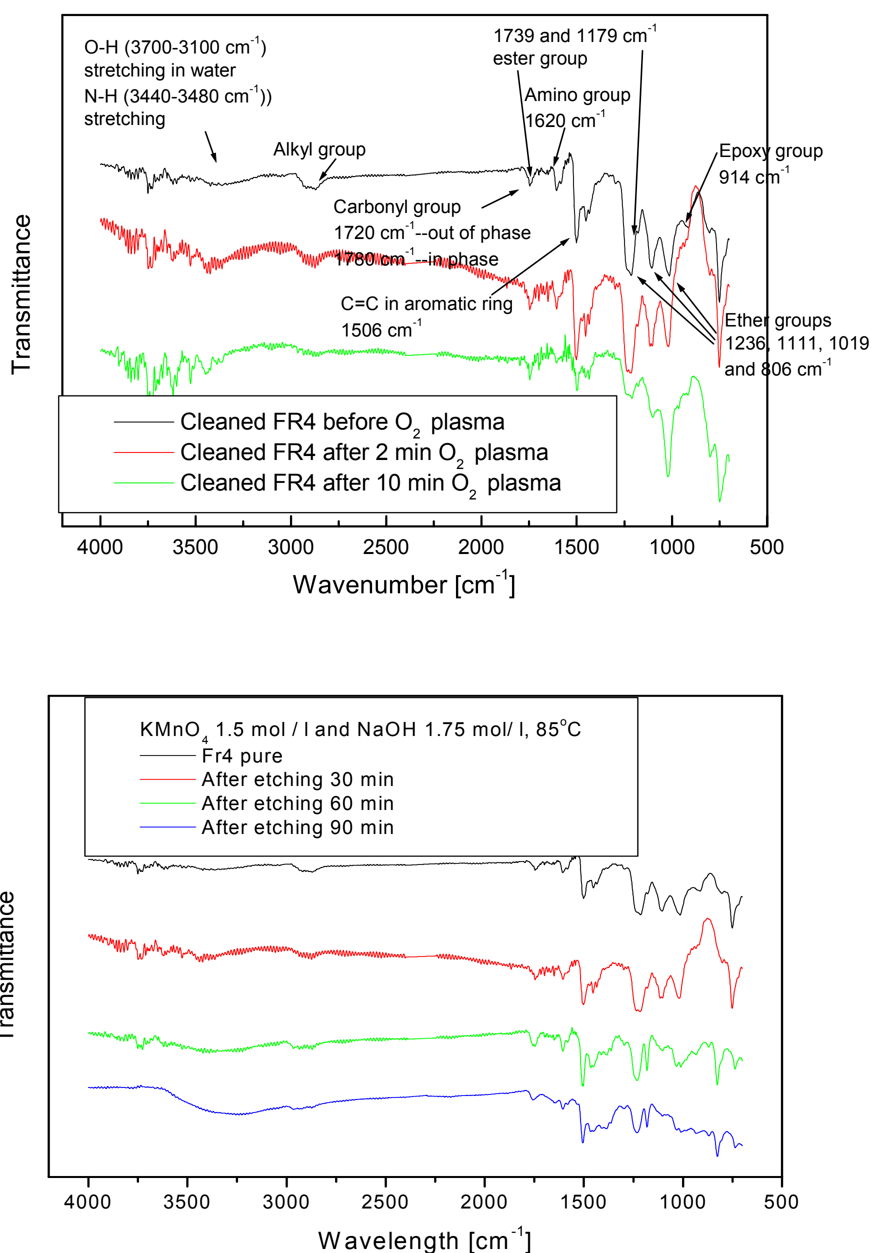

Figure 4.11 *FTIR/ ATR spectra of FR4 surface before and after different etching*

B. Kapton

The chemical structure of Kapton^{TM} is shown in Fig. 4.12.[88] It has an amine $–NH_2$ group attached to the diphenyl ether group at various positions (ortho or meta). To Kapton, O_2 plasma exposure and $KMnO_4$ etching are also applied for etching only adjusting the O_2 gas from 20 % (to FR4) to 50 % and etching liquid solutions to be $KMnO_4$ of 1.75 mol/ l and NaOH of 2 mol/l due to Kapton's more robust molecular structures compared with FR4. To study the influence of the effect of the O_2 plasma exposure and $KMnO_4$ etching on the final bonding strength, the surface molecular structure of Kapton-board before and after the dry and wet etching were both analyzed by FTIR/ ATR spectroscopy and shown in Fig. 4.13.

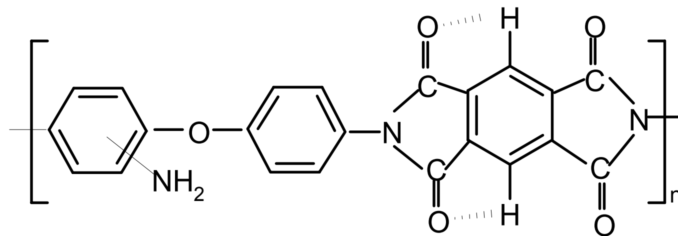

Figure 4.12 *Chemical structure of Kapton^{TM}*

In terms of the spectra shown in Fig. 4.13, the characteristic absorption bands of kapton were assigned: 3700-3100 cm^{-1} (-OH stretch), 3637, 3575 and 3479 cm^{-1} ($-NH_2$ stretch), 3100-3000 cm^{-1} (-CH in aromatic stretch), 1780 cm^{-1} (cyclic imide -C=O in phase), 1712 cm^{-1} (cyclic imide -C=O out of phase), 1609 cm^{-1} ($-NH_2$ deformation bending), 1502 cm^{-1} (aromatic ring C=C), 1370 cm^{-1} (imide -CN), and 1236, 1111, 1013, 807 cm^{-1} (ether).[89-91] As seen from the spectrum after 30s O_2 exposure, there are not largely different in the absorption of imide -CN group and aromatic C=C group. The absorption bands at 3700-3100 (-OH stretching peaks) cm^{-1}, 1780 cm^{-1} (in phase C=O) and 1236, 1111, 1013, 807 cm^{-1} (ether group) are slightly increased. Then the absorption bands at 3100-3000 cm^{-1} (-CH in aromatic stretch), 3637, 3575 and 3479 cm^{-1} ($-NH_2$ stretch), and 1712 cm^{-1} (cyclic imide -C=O out of phase) is decreased, and the decrease of aromatic C-H band and $–NH_2$ are due to due to the loss of $-NH_2$ on the diphenyl ether group, and then the decrease of cyclic out of phase -C=O is possible due to the cleaning of organic contamination from the Kapton foil. To the spectrum of after 1 hour $KMnO_4$ etching, it has similar etching effects on Kapton surfaces but stronger, esp. OH groups, which got obviously increased.

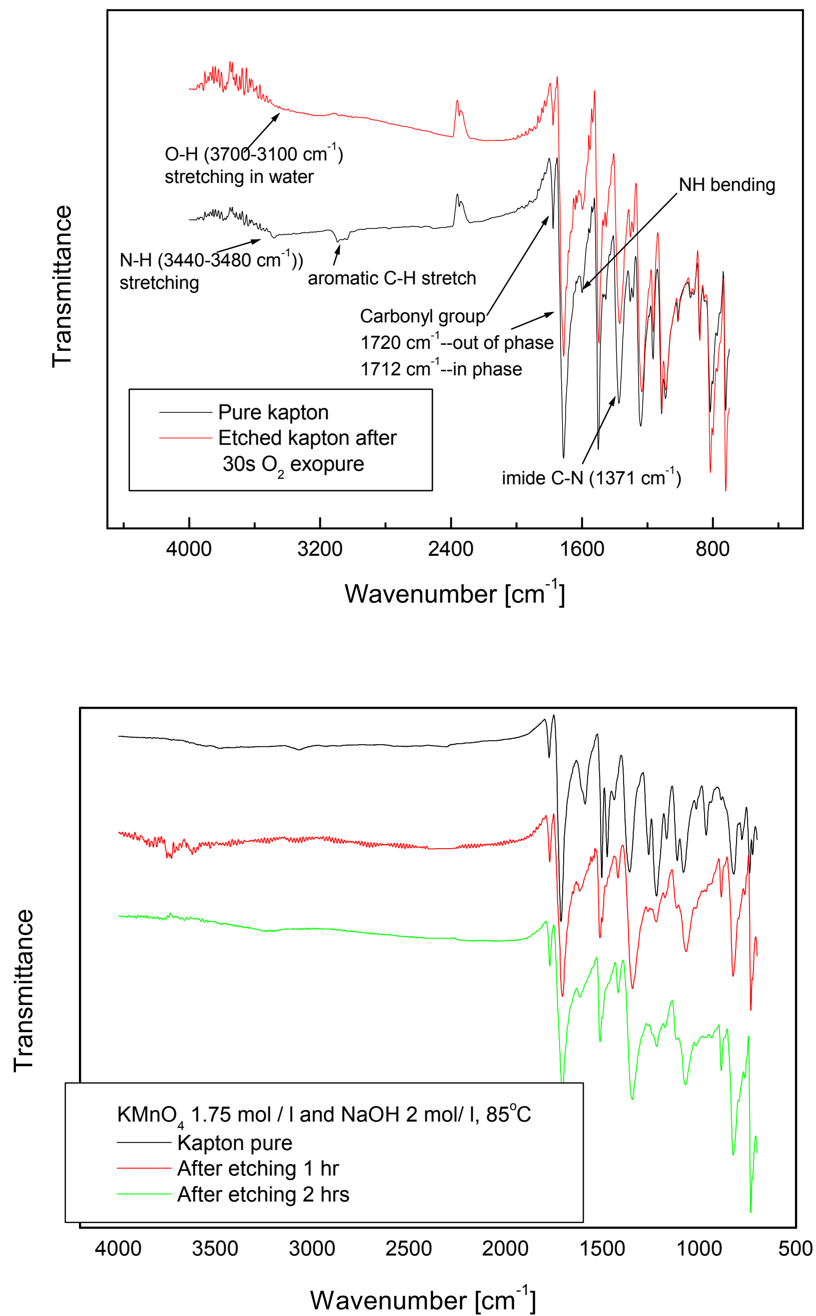

Figure 4.13 *FTIR/ ATR spectra of Kapton surface before and after different etching*

Anyway, it indicates that reactive free radicals were formed by O_2 plasma exposure and $KMnO_4$ etching on the Kapton surface, colloid with the surface of Kapton, which introduced the oxygen-containing functional groups. In the process, free

radicals at the polymer surface were created by hydrogen abstraction in the O_2 plasma exposure and $KMnO_4$ etching. Then, these followed the formation of alkoxy radicals from the reaction of near-surface alkyl radicals with atomic oxygen, and they led to the formation of carbonyl groups etc. Also, like to FR4 substrates, the liquid etching solution including $KMnO_4$ can substitute to O_2 plasma for industrial application on Kapton etching and surface activation.

C. Copper

In the thesis two kinds of copper based metals are applied in EOCB fabrication as EOCB carriers. One is the normal PCB copper (purchased from normal PCB vendors) and the other is ED copper (Electrical Deposited). Due to high purity and stable crystal structure of ED copper, here we will focus more on PCB copper and its surface elements distribution. In order to investigate the surface elements distribution of PCB copper, XPS/ AES (Auger electron spectrum) is applied for identification. In general, X-ray photoelectron spectroscopy (XPS) is widely used to obtain information about the elemental composition and the oxidation state of the elements being examined. Often the surface composition of a solid differs, at least to some degree, from the bulk composition. The high surface sensitivity provided by XPS is the greatest asset of the method in comparison with other surface analytical methods, esp. for metals. XPS/ AES spectrum and depth profile of pure PCB copper are illustrated in Fig. 4.14.

From the spectrum and depth-profile of copper surface, Zn and its oxidation state ZnO may be found everywhere and actually or say that a Zinc layer is on the copper layer. In order to investigate the real depth of this Zinc layer, Ar^+ sputtering is applied through driving out the surface element with high energy Ar^+ backscattering. It is found that about 20-50 nm Zinc layer (up to different PCB vendors) is on the copper layer which is treated as passivation layer for protecting copper from oxidization. Additionally about 10 % carbon is also found in the elements distribution, where small parts of them should be CO_2 absorption and most of them should be the organic contaminations.

To remove some organic contamination from surface under the precondition not damaging Zn passivation layer and obtain chemically pure and uniform surface for achieving better interface adhesion with PDMS, a kind of wet etching solvent called SENO 3207 ($Na_2S_2O_8$, Kepets) is used as the pre-treat etchant due to its relative low etching speed and the PH of etchant is adjusted at 4.0 - 4.3.

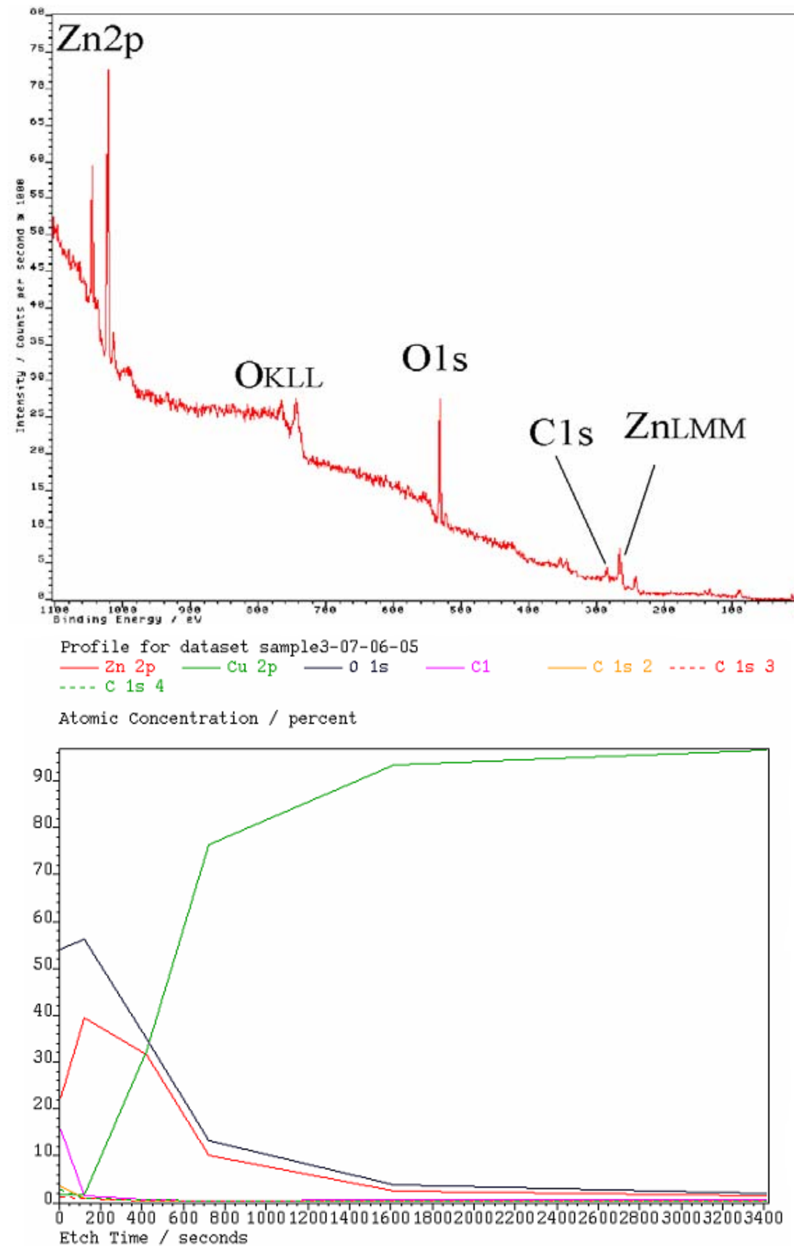

Fig. 4.14 *XPS spectrum of PCB copper surface of Cu-Fr4 and depth-profile prior to etching*

The micro-etching mechanism can be illustrated below shown in equation 4.10:

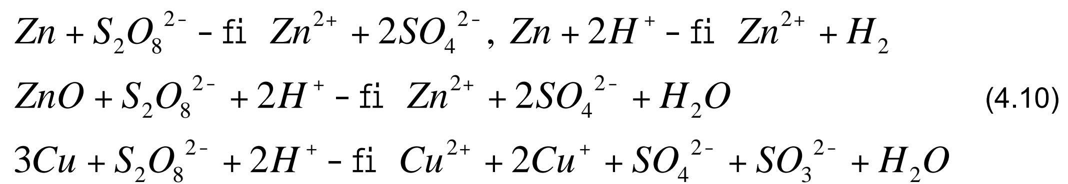

$$Zn + S_2O_8^{2-} \rightarrow Zn^{2+} + 2SO_4^{2-},\ Zn + 2H^+ \rightarrow Zn^{2+} + H_2$$
$$ZnO + S_2O_8^{2-} + 2H^+ \rightarrow Zn^{2+} + 2SO_4^{2-} + H_2O \qquad (4.10)$$
$$3Cu + S_2O_8^{2-} + 2H^+ \rightarrow Cu^{2+} + 2Cu^+ + SO_4^{2-} + SO_3^{2-} + H_2O$$

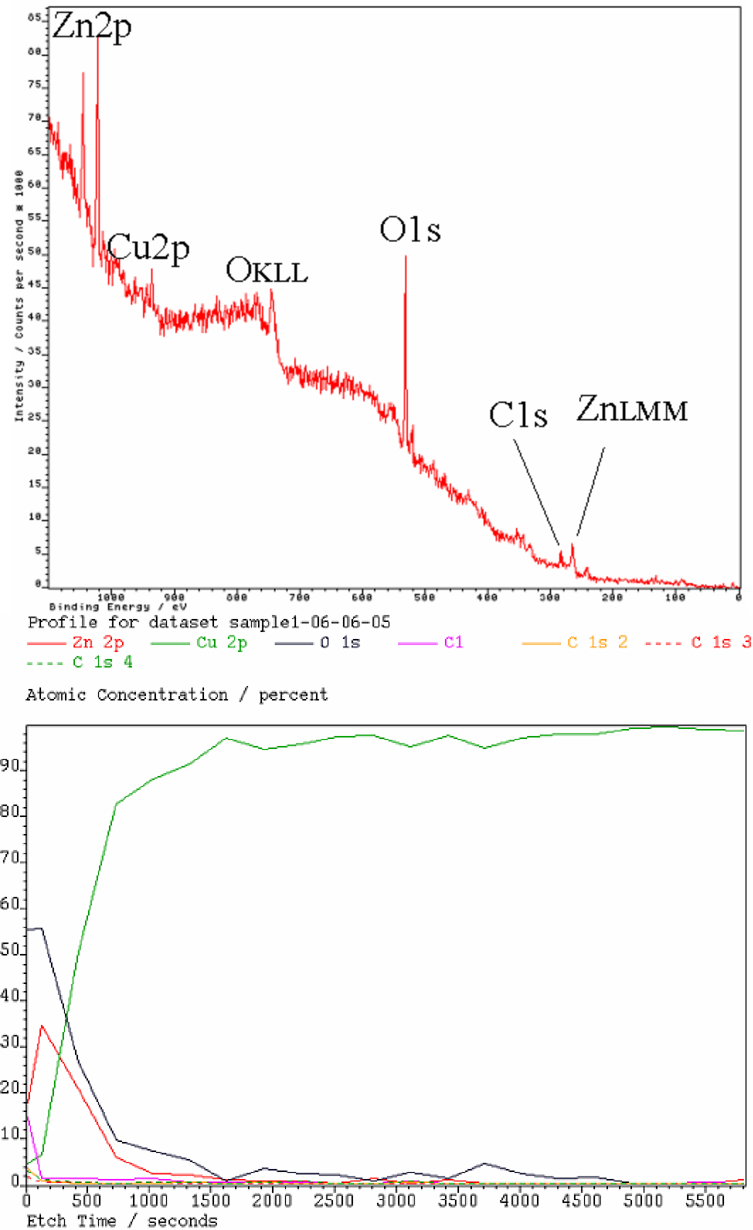

Fig. 4.15 *XPS spectrum of copper surface of Cu-Fr4 and depth-profile after etching*

One PCB copper sample surface after 30s etching with 1 mol/ l $Na_2S_2O_8$ is checked with XPS spectrum and shown in Fig. 4.15. From their depth profiles, obviously Cu2p peak appears and C element amount is decreased due to removing of contamination compared with untreated PCB copper, but certainly the protection layer of Zinc also gets a little affected but not serious, which can get controlled through the etching time, concentration of etchant and PH value etc.

Additionally, for ED copper is also easily oxidized in air and we propose that it also should be etched with $Na_2S_2O_8$ before application in EOCB fabrication and the etching time is about 30 - 40 seconds.

4.3.3 Effect of Treatments on Surface Roughness

The positive effect of various etching treatments on the bonding strength between adhesives, like SAP and substrates is in part due to the chemical surface effects described in the previous chapter, but as well due to micro mechanical modifications of the surface. The reason is an increase of micro-roughness on the surface which leads to enlarged mechanical interlocking areas.

Good bonding occurs when the adhesive is able to penetrate into surface undulations like pores, holes and crevices. This causes the adhesive to mechanically lock into the surface of the substrate. For this to occur, the adhesive should be able to spread or wet the surface effectively and also possess the proper rheological properties to penetrate into the pores of the surface.

White-light-interferometer was used to quantify the roughness change on these PCB substrate-surfaces caused by various etching treatments. The arithmetic average surface roughness of substrates at different etching times is shown in Fig. 4.16. Obviously, there is no significant change on the FR4 and Kapton-substrate roughness after 10 min of O_2 plasma etching, and the copper-substrate roughness after 10 min wet etching as well.

Different with them, $KMnO_4$ containing oxidizer has a more profound influence on roughness. Roughness of FR4 and Kapton substrates both increase monotonously with an increase of oxidizing time due to large increase of oxygen contents at the surface, e.g. acid and ketone functions which are also shown in Fig. 4.11 and 4.13. However, to the two substrates the etching velocities are different due to their molecular structures. With respect to FR4 substrate, the increase of roughness is nearly linear with time for $KMnO_4$ oxidative treatment until a certain time, indicating a constant speed of roughness increase. The higher the speed of roughness increase, the smaller the treatment time at which the linear increase of roughness stops.

The constant speed of roughness formation indicated the existence of a pseudo-steady state for the polymer breaking down group scheme probably. Actually, the similar phenomena have also been reported recently, since the O/ C ratio is independent of the oxidation time.[61] In addition, to Kapton there even exists

one maximum with etching time increase, after which the roughness lowers slowly again. We think the pseudo-steady state and maximum lowers with increasing speed of roughness formation and hence may be also associated to diffusional limitations of the oxidizer, which influences the roughness evolution. The surfaces of FR4 and Kapton before and after $KMnO_4$ etching are observed with SEM as well, which is shown in Fig.4.17. Obviously, microcavities appear with longer etching times, which is possibly for the polar groups in these patches on substrates surfaces react with oxidizers and cause the formation of cavities. Pits of the order of a micro fraction appear in the surface of the polymer, as is well know from catalyses, pore diffusion is relatively slow and can easily limit reaction speeds. The polymer surface is constantly being etched away, and the cavities are formed by small differences in etching speed of the polymer. The pits are formed in the zones with highest oxidation speed. However, diffusion of the oxidizer through the pore is difficult and will limit the reaction speed as the pore depth increases. Due to these diffusional limitations, there exists one pseudo-steady state and the roughness will reach a maximum. This is probably the case for the fast $KMnO_4$ oxidation.

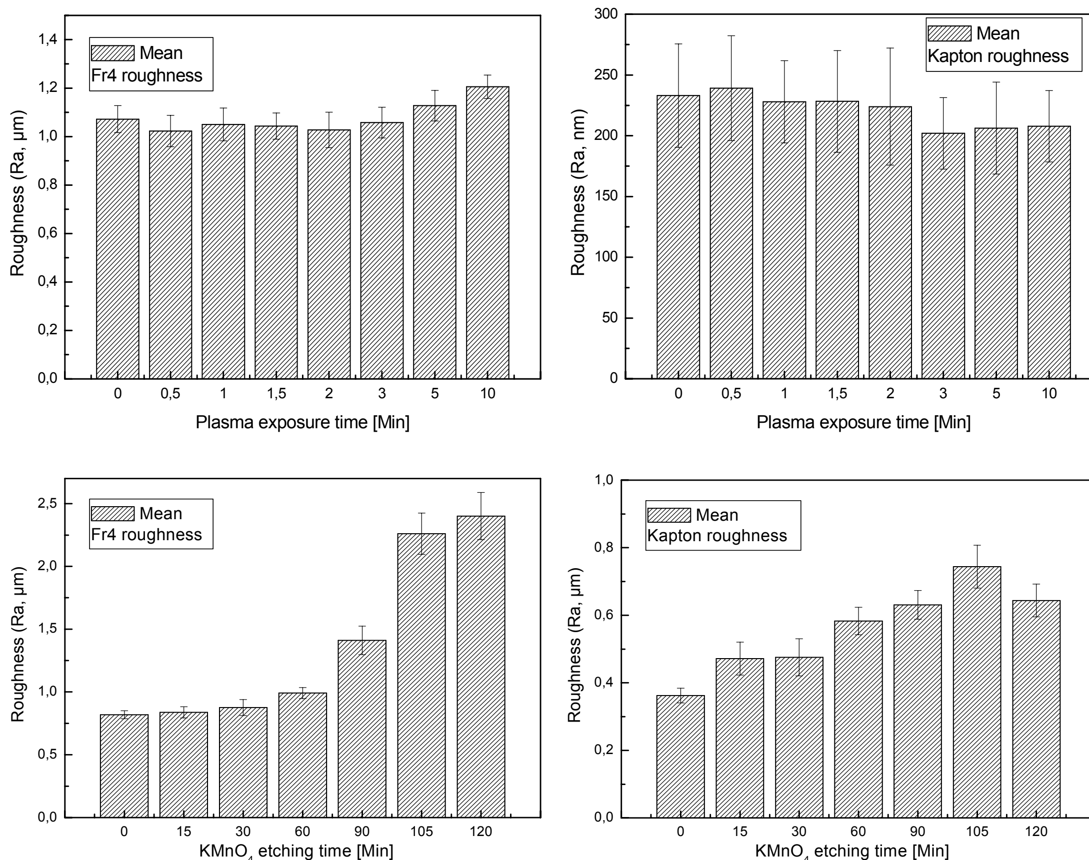

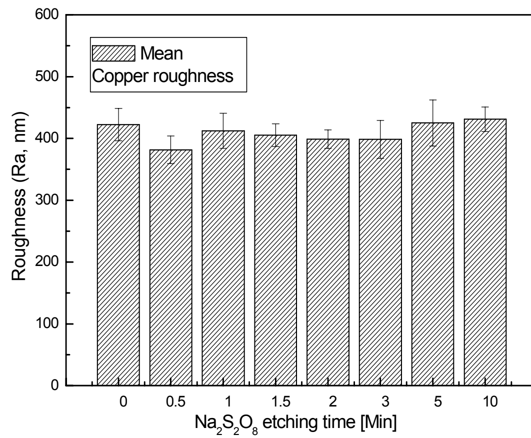

Figure 4.16 *Effect of various etching on PCB substrates roughness*

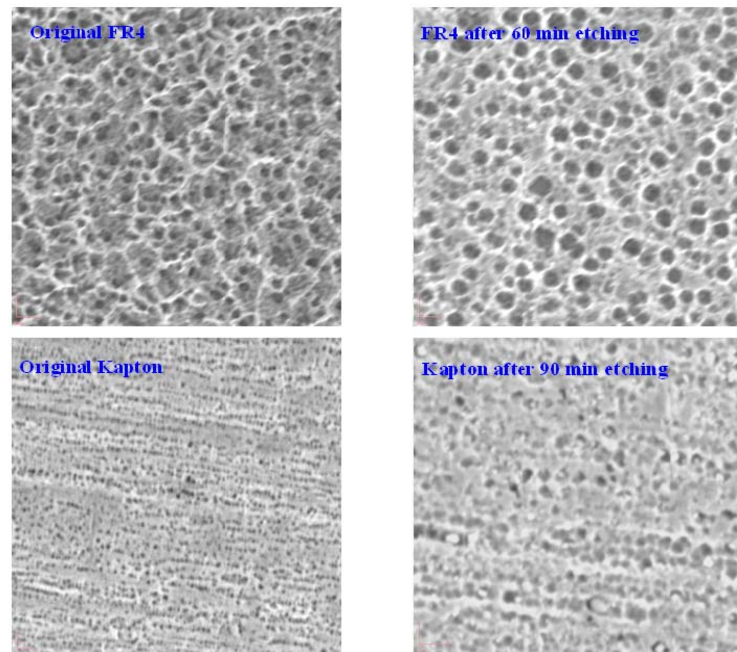

Figure 4.17 *SEM images of FR4 and Kapton boards before and after etching*

4.3.4 Effect of Surface Etching on Surface Free Energies of Substrates

A. Polymer substrates

FR4 and Kapton-surfaces are chemically activated by O_2 Plasma and $KMnO_4$ etching resulting in enhanced surface wettability and an improved concentration of

polar components. These can be determined by surface free energy analysis. A further advantage of the knowledge of the surface free energy is the following: when the values of surface free energies of solid polymers, esp. respective different components' surface energy value (e.g. polar or dispersive components), are close to those of liquid polymers e.g. SAP, the liquid polymers will have maximum wetting on the solid polymers. Therefore, it is necessary to identify the relationship between etching times and surface energy changes on FR4 and Kapton, so that we can modify the relevant SAP viscosity and surface energy to meet different substrates. Measurement of contact angles yield data, which reflect the thermodynamics of a liquid/ solid interaction. Surface free energy of a solid can be characterized and deduced from contact angle measurements between liquid and solid surfaces. The surface free energy of etched FR4 and Kapton-boards was determined using a sessile drop method combined with a microscope-camera system. Two different wetting liquids, i.e. distilled water and diiodomethane (nonpolar liquid), were selected for contact angle measurements.

The obtained contact angles are used to deduce the surface energy of the solid. In the estimation of surface free energy of polymer solids (FR4 and Kapton), the extended Fowke's equation and Young-Dupre's equation are widely used.[93] This approach divides the surface energy into two components, dispersive and polar, and uses a geometric mean approach to combine their contributions. The resulting equation (Eq. 4.11) when combined with Young's equation yields.

$$\gamma_l(1+\cos\theta) = 2\left(\sqrt{\gamma_{lp}\cdot\gamma_{sp}} + \sqrt{\gamma_{ld}\cdot\gamma_{sd}}\right),\ \gamma_l = \gamma_{ld} + \gamma_{lp} \text{ and } \gamma_s = \gamma_{sd} + \gamma_{sp} \quad (4.11)$$

where θ is the contact angle, γ_l is liquid surface tension and γ_s is the solid surface tension, or free energy. The addition of d and p in the superscripts refer to the dispersive (also called London dispersive) and polar components of each. The total free surface energy is merely the sum of its two component forces. The values of γ_{lp} and γ_{ld} are listed in Table 4.3. The values of γ_{sp} and γ_{ld} can be calculated based on the measured contact angles and the values of γ_{lp} and γ_{ld}.

Table 4.3 *London dispersive and polar components of wetting liquids surface tension, measured at 20 °C (mJ/ m^2)*

Wetting liquid	***γ_{lp} (mJ/ m^2)***	***γ_{ld} (mJ/ m^2)***	***γ_l (mJ/ m^2)***
H_2O	51.0	21.8	72.8
CH_2I_2	50.42	0.38	50.8

Fig. 4.18 illustrates the results of surface free energies of the FR4 and Kapton-boards with respect to different etching times. The surface of untreated FR4 and Kapton-substrate is very hydrophobic, because of its low surface free energy, but hydrophilic after O_2 plasma exposure times of about 1 min (FR4), 30 seconds (Kapton), and wet etching of 15 min (FR4 and Kapton both).

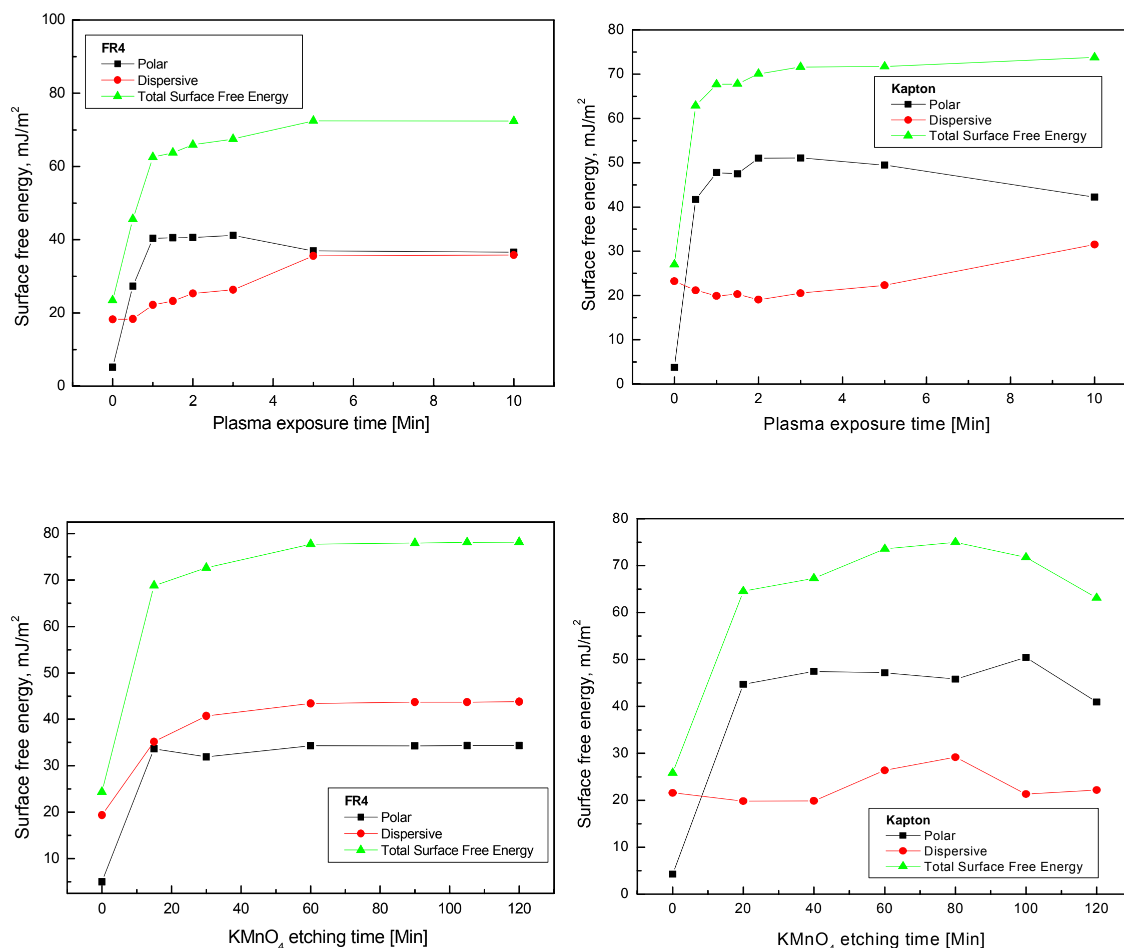

Figure 4.18 *Surface free energies of the FR4 and Kapton-boards*

From Fig. 4.18 it is clear that polar components concentrations on FR4 and Kapton both have been largely increased after O_2 plasma exposure times of about 1 min and 0.5 min, and wet etching of about 15 min respectively, actually which are also related with and verified in their FT-IR spectra (Fig. 4.11 and 4.13). From those spectra, though the continuous etching can improve surface energy, whilst also damages the inner molecules of boards from surface due to the penetrated oxidizers (see Fig. 4.17), which will form one loose layer with poor mechanical

properties on bulk substrates and in reverse is disadvantageous to bond with SAP actually. The SAP will be able to form bonding with some polar components on FR4 and Kapton substrates through dehydration reaction and diploe-diploe interaction etc. and the maximum wetting happens on the condition that values of surface free energies of FR4 and Kapton, esp. respective different components' surface energy value (e.g. polar or dispersive components) are close to SAP respective components. So, Combing with analysis of Fig. 4.11 and 4.13, we can propose the boards' treatment conditions in general. With respect to O_2 plasma exposure, the etching times to FR4 and Kapton are proposed to be 1 - 2 min and with respect to $KMnO_4$ etching, the times are shifted to be 20 - 30 min.

B. Copper substrates

Different with polymers substrates, beside the identification of various components surface energy and the relationship with etching times it is very important to identify one appropriate method to check the cleaning of organic contaminations on PCB copper substrate. So in the estimation of surface free energy of copper substrates, one Acid-Base (van Oss) equation and Young-Dupre's equation are used. It is proposed that the surface energy is composed of three components: lifshitz-van der Walls component γ^{LW} including electromagnetic interaction, oscillation temporary dipoles interaction, and permanent and induced dipoles interaction; Lewis acid component (γ^{+}), which is related with the organic concentration on substrate; and Lewis base component (γ^{-}).[84] Their relationship is given by equation 4.12:

$$\gamma = \gamma^{LW} + 2(\gamma^{+} \cdot \gamma^{-})^{1/2} \qquad (4.12)$$

Due to three unknown parameters, three standard liquids (Water, ethylene glycol and diiodomethane) were used for measuring the surface energy and its three components of copper. Their surface energy and components are listed in Table 4.4.

Table 4.4 *Surface tension of three liquids, measured at 20 °C (mJ/ m²)*

Wetting liquid	*γ^{LW} (mJ/ m²)*	*γ^{+} (mJ/ m²)*	*γ^{-} (mJ/ m²)*	*γ (mJ/ m²)*
H_2O	21.8	25.5	25.5	72.8
CH_2I_2	50.8	0	0	50.8
HOC_2H_4OH	29.0	1.9	47	47.9

Based on Young-Dupre's equation and Eqn. 4.12, the three components of surface energy of coppers are calculated after measuring the contact angles of the three liquids on them. The results are shown in Fig.4.19 where the green curve is related with general organic contamination for only it contains acid components. If magnifying, it can be observed to be decreased gradually with etching. Combing with the previous XPS analysis (see Fig. 4.14 and 4.15), we propose 1 - 2 min $Na_2S_2O_8$ etching time for copper treatment. Additionally the similar results are also achieved to ED copper.

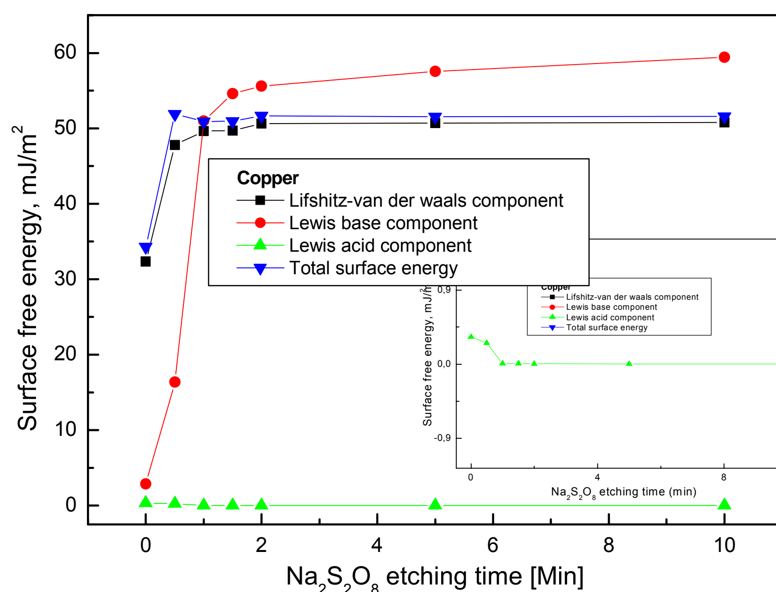

Figure 4.19 *Surface free energies of PCB copper*

4.3.5 Influence from Hydrophobic Recovery on Treated PCB Substrates

The significant factor causing the limitation of the wettability and adhesion properties of substrates surfaces is the hydrophobic recovery of the etched surfaces. Hydrophobic recovery is a phenomenon that originates from the natural, thermodynamically driven tendency of surfaces to lower their free energy which can be shown by contact angle measurement on the treated polymer surfaces versus time. Actually, the decay of the contact angle change after treatments has been proposed to form by several mechanisms. They include recontamination by hydrocarbon onto polymer surfaces, the reorientation of polymer chains so as to bury covalently bonded polar functional groups, the migration of additives toward

the surface, and the diffusion of low molecular weight oxidized materials or called LMWOM towards the surface of the material. However the reorientation of polar moieties should be able to happen quickly, less than one minute, and thus the explanation is unlikely. The exudation of additives and LMWOM diffusion are both not likely either, because it is impossible that FR4 and Kapton substrates themselves contain lots of LMWOM like PDMS.[94-95]

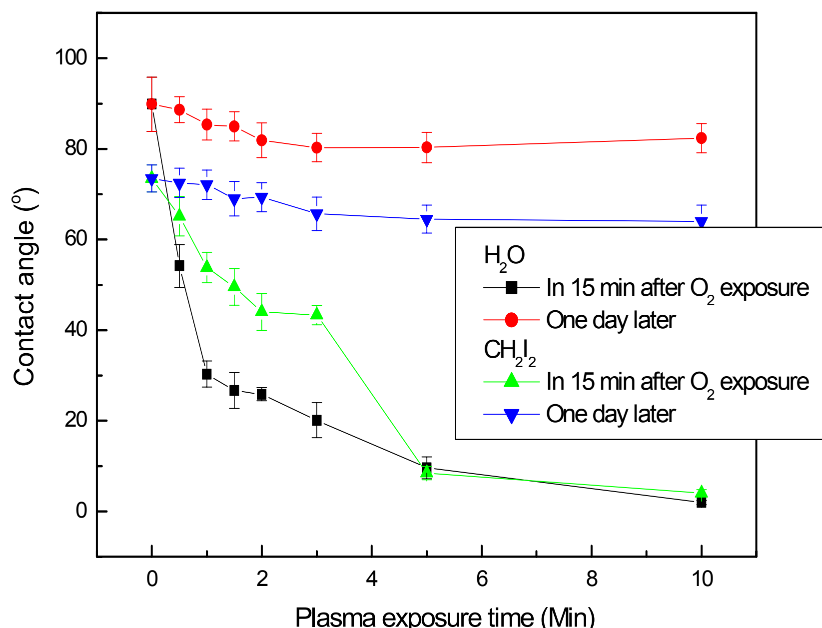

Figure 4.20 *Decay of contact angle change with time*

Fig. 4.20 shows the experimental results of contact angles of distilled water and diiodomethane on O_2 plasma etched FR4-boards after 15 min and one day later. The contact angles of the liquids on the etched FR4-boards after one day show great increase. The wettability of surfaces nearly returns the original samples.

In addition, 180° peel-off tests (it will be in detailed introduced in the following chapter 4.4.2) were done with one-day stored O_2 plasma etched FR4-substrates again. It is found that the bonding strength between one specially synthesized SAP and FR4 is greatly decreased due to hydrophobic recovery. Also, it was verified that the 1.5 min O_2-plasma etched FR4-substrates can exhibit a good bonding together with the SAP within a period of 3 hours after the plasma treatment, which might be a reasonable time frame for a production line. Similar results are obtained for Kapton and coppers as well. In the table 4.5, the reasonable time frame is given according to different boards and etching methods.

Table 4.5 *Valid time frame for boards use in EOCB fabrication after etching*

	O_2 plasma	***$KMnO_4$***	***$Na_2S_2O_8$***
FR4	3 hrs	One day	N.A
Kapton	2 hrs	One day	N.A
PCB Copper	N.A	N.A	1 hr
ED copper	N.A	N.A	1 hr

In the case, the main reason possibly causing the increase of contact angle of H_2O and CH_2I_2 on the one-day stored FR4 and Kapton boards is the recontamination of the surface by hydrocarbon. On FR4 and Kapton boards they both consist of some low surface tension hydrocarbon structures besides hydrophilic polar groups e.g. cyclic imides and carbonyl etc. and they can have high affinity with hydrocarbon contamination after O_2 plasma treatment or $KMnO_4$ etching. The hydrocarbon with lower surface tension will enable the increase of contact angles and make surfaces hydrophobic.

4.4 Development of EOCB Fabrication based on SAPs and Compatible Etching Treatments

4.4.1 Basic Concept

In the aforementioned chapters we have identified the basic concept for SAPs synthesis and compatible methods for boards etching. Also, in chapter 3, we have identified that Pt catalyst, vinyl and phenyl groups can affect the PDMS optical properties and then actually in most SAPs products, they contain some Pt catalyst and vinyl containing polysiloxanes for obtaining better solvent compatibility and improving their dehydration reaction with substrates etc. In addition, in terms of EOCB fabrication steps, SAPs or SAPs mixed PDMS can possibly bond with casting mould after curing if treating them directly as cladding materials though we may tune its refractive index for waveguiding. Furthermore, the storage of treated substrates through aforementioned etching methods is also a critical issue restricting their practical application on EOCB production due to hydrophobic recovery. So, in order to avoid the influences from SAPs on optical waveguiding and extend the pot life of etched substrates, we propose to directly coat SAPs on

activated PCB substrates through spray coating or rolling etc. By controlling the curing temperature and time of SAP, the cured SAP layer can easily bond with cladding PDMS prepolymer through hydrosilylation reactions due to its consisting of Si-H groups and Pt catalyst as well. The cured SAP is as coating layer on PCB substrates and thus additionally, it also can prevent the activated surfaces from hydrophobic recovery to extend the pot life of these substrates longer.

Moreover, the bonding between SAPs and boards happens on the post-cure stage and there exist some by-products after the reactions, e.g. H_2O and H_2 (see Eqn. 4.5 and 4.6). So the thickness of SAP layer is expected to be as thin as possible for elimination of bubbles on SAP layer. However, through experiments, we found that 70 μm thick cladding PDMS RT 601 (9: 1 mixture) can be cured at 90 °C after 20 min on copper substrate, but in 10 days it cannot be cured when the thickness is decreased to be 10 μm. Then, with the increase of Pt catalyst concentration it can be solved. The detailed experimental result is shown in Fig. 4.21. From the figure, with the increase of Pt catalyst concentration it is observed that the curing time is decreased dramatically. Further, the experiment is redone on non-polar components PDMS polymer surfaces and it is found the 10 μm thick PDMS layer can be easily cured in 60 min without any extra addition of Pt catalyst.

Compared with some similar results in other publications, we conclude that the possible reason is that the Pt catalyst in thin layer polysiloxanes is attached by polar components on substrates surfaces to the substrate surfaces and consequently affects hydrosilylation reaction. Specially, with respect to some FR4-like polymers which contain some electron donating compounds, for example organosulphur and amine etc. they can deactivate, inhibit and capture the Pt catalyst in PDMS and affect their curing.[71] Thus it is absolutely necessary to improve the concentration of Pt catalyst in various SAPs when they will be applied as thin layer coating onto such substrates. Moreover, compared with relatively thicker layer another advantageous of thin SAP layer- lower than 1 μm- is the limited mechanical influences on PCB substrates e.g. bow due to the Young's modulus and possion ratio mismatches.

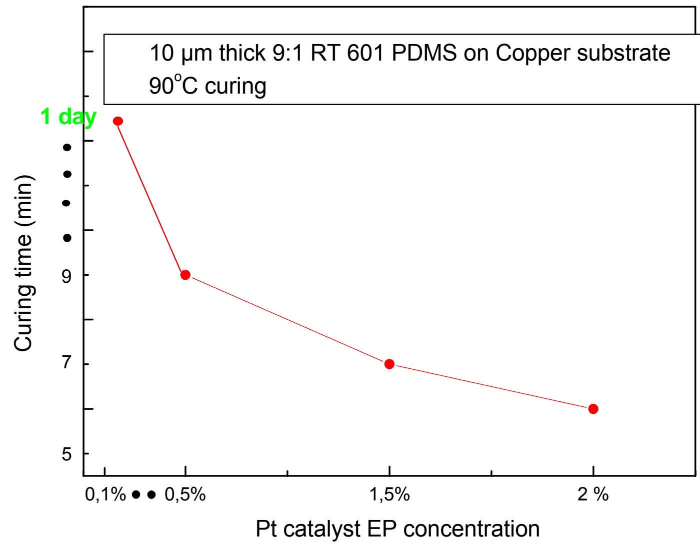

Figure 4.21 *Thin layer PDMS curing on copper substrate*

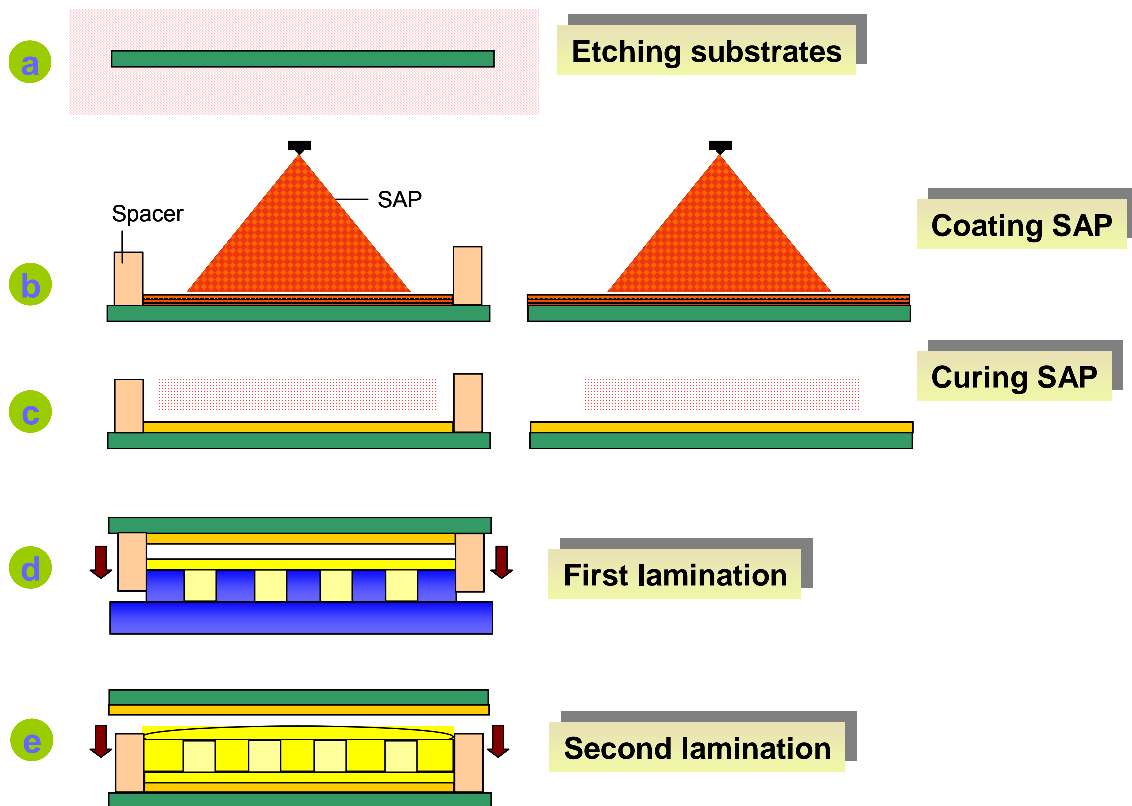

Figure 4.22 *EOCB fabrication combining with SAP technique and boards etching*

The detailed procedure is shown in Fig. 4.22. Presently, this method is being transferred to worldwide first EOCB production project: Prospeos.

Based on the studied PDMS curing mechanism, the non-complete crosslinking of polysiloxanes can make them easily bonded with other polysiloxane prepolymer. So the determination of SAP layer curing condition is very vital to realize the EOCB packaging. The SAP layer cannot be fully cured; otherwise it will be difficultly bonded with liquid cladding PDMS against curing, but also not is too few, which will possibly lead to bubbles in cladding PDMS due to the post-cure reaction in cladding PDMS.

4.4.2 Determination of SAP Components and Etching Conditions

To examine the correlation between etching conditions on substrates and SAP components, one simple but effective 180°-peel-off test with pulling speed of 0.1 mm/ s was proposed and conducted (see Fig. 4.23) to identify the optimum treatments conditions to PCB substrates, SAP components and curing time etc.

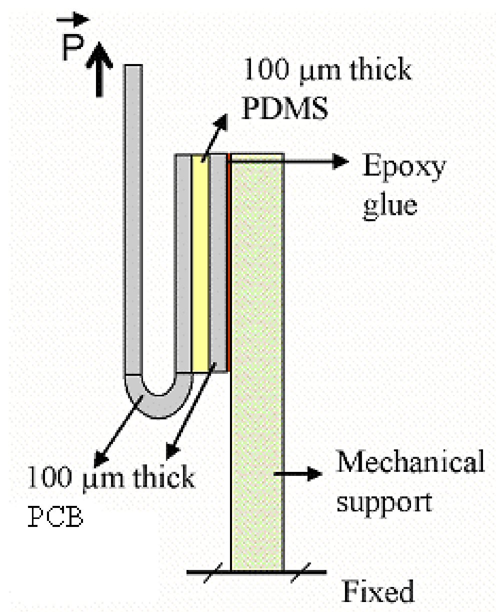

Figure 4.23 *Schematic of 180°-peel-off test*

In the thesis, commercial RT 601 (Base component including Si-viny group called RT 601-A and crosslinker including Si-H groups called RT 601-B), H-Siloxane (methylhydrogen polysiloxane with trimethylsilyl endgroups), Catalyst EP (Pt

catalyst, 1, 1, 3, 3-Tetramethyl-1,3-Divinyldisiloxan- -platincomplex), PT 88 (Inhibitor) and AK 35 (Silicone oil for adjusting the viscosity of SAP) are selected as various basic constituents for SAPs synthesis and all of them are purchased from Wacker Chemie, Burghausen.

The prepared peel-off test sample is a Substrate-SAP-cladding PDMS-SAP-Substrate sandwich structure. Its dimensions are 10 cm in length, 1.5 cm in width, SAP layers thicknesss are both less than 1 µm and 100 µm in cladding PDMS thickness. As suggested by the name, peel-off test involves peeling of the top 100 µm thick FR4, Kapton, Zinc covered copper and ED copper coated PCB layers by fixing the bottom 100 µm thick layer on a stable mechanical support. From the measured peel force the peel energy (G_{IC}) can be determined through the following Eqn. 4.13 assuming that the extension of the peel strip is negligible.[96]

Peel-off energy equation:

$$G_{IC} = P(1 - \cos\theta)/b = 2P/b \text{ (for } \theta = 180^{\circ}) \quad (4.13)$$

where P is the peel force, θ is the peel angle and b is the width of the test sample. The average residual SAP area - i.e. unpeeled SAP area on both substrate boards - is observed as well. With respect to different boards, the different SAPs are synthesized and applied for sample preparation.

Through lots of experiments and combining with the proposed results in chapter 4.3, hereby we propose the treatments conditions, SAP components and SAP layers curing condition in EOCB fabrication as follows summarized in Table 4.6.

Table 4.6 *Summarized optimum conditions for EOCB fabrication*

	Components	***Parameter of PCB materials***			
		FR4	***Kapton***	***Zinc-Copper***	***ED copper***
SAP components	RT601-A: B	5: 1	5: 1	9: 1	N.A
	Catalyst EP	2 %	2 %	1 %	2 %
	Inhibitor	8 %	8 %	8 %	7 %
	H-Siloxan	10 %	10 %	15 %	91 %
PCB-Material	Polymer-O_2 Plasma	1.5 min	1 min	N.A	N.A

Etching methods	Polymer-$KMnO_4$	30 min	40 min	N.A	N.A
	$Na_2S_2O_8$	N.A	N.A	1.5 min	1 min
SAP layer curing conditions (90 °C)	Polymer-O_2 Plasma	8 - 10 min	10 - 12 min	N.A	N.A
	Polymer-$KMnO_4$	10 min	10 - 12 min	N.A	N.A
	$Na_2S_2O_8$	N.A	N.A	12 - 15 min	15 - 20 min

4.4.3 Characterization to Fabricated EOCB

A. Mechanical characterization

The mechanical stability of fabricated EOCBs depends in a crucial way on the interfacial strength between the optical PDMS layer and the SAPs layer, and beteeen SAPs layer and PCB layer. If not strong enough, thermal stress resulting from coefficient of thermal expansion (CTE) and Young's modulus mismatch will cause delamination and therefore damage. The pull off test is widely used to test the adhesion of coatings to substrates. The prepared sandwich structure shown in Fig. 4.24 included a 200 μm thick cladding PDMS layer (19: 1) laminated between two SAPs coated various PCB carriers. The sample dimensions were 7 cm in length and 1.5 cm in width. After preparation, they were glued to an aluminium holder and measured under a pull speed of 0.02 mm/ s.

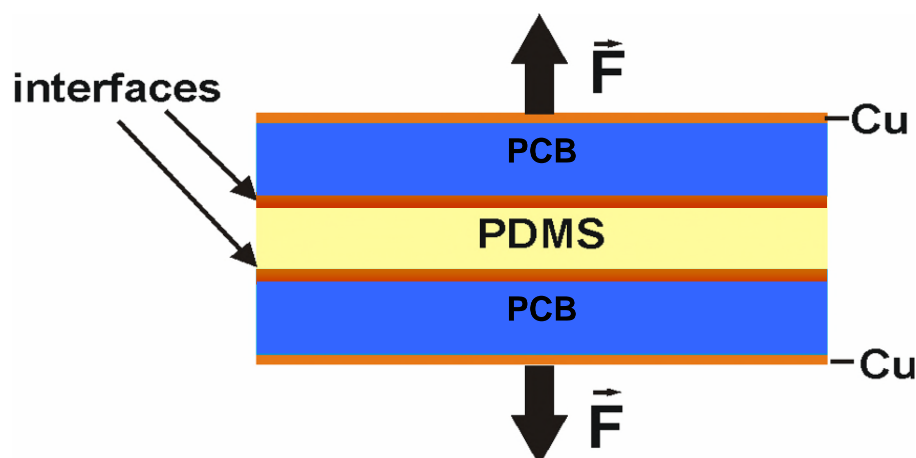

Figure 4.24 *Schematic of pull-off test*

The measurement results are indicated in Table 4.7. The PRAA (largest percentage of residual adhesion area) of all samples is more than 95 %. By comparing these values with the measured stability limit of pure PDMS (1.35 ± 0.33 MPa) it is clear that the stability limit of the prepared samples is determined by the intrinsic material stability of cladding PDMS layer and not by the interface properties between SAPs and PCB substrates, and SAPs and cladding layer. A little larger pull strength of laminate than pure cladding PDMS is possible due to the following reasons. Some excess compounds in SAPs can indeed help cladding PDMS fully crosslinking e.g. Pt catalyst, in addition the thin layer crosslinking is also different with large dimension bulk sample and it can have more dense crosslinking in plane. The pull strength of copper and Kapton packaged samples is larger than FR4 packaged sample, because they have no inhibition effects on Pt catalyst and can ensure the cladding PDMS higher curing density.

Table 4.7 *Test results of Pull strength of laminate*

Test samples	*Pull strength of laminate (MPa)*	
	70 °C 2hrs curing	*180 °C 2hrs curing*
Cladding PDMS	1.35 ± 0.33	1.42 ± 0.29
PCB Copper/ PDMS	1.38 ± 0.29	1.44 ± 0.32
ED Copper/ PDMS	1.41 ± 0.28	1.43 ± 0.21
FR4/ PDMS (O_2 exposure)	1.34 ± 0.32	1.36 ± 0.26
Kapton/ PDMS (O_2 exposure)	1.39 ± 0.23	1.44 ± 0.21
FR4/ PDMS ($KMnO_4$ etching)	1.35 ± 0.29	1.38 ± 0.26
Kapton/ PDMS ($KMnO_4$ etching)	1.42 ± 0.26	1.46 ± 0.27

B. Ultrasonic scanning

Multilayer EOCB including not only more optical layers but also electronics layers will be the main development trend in the future. It means that general EOCB layer will be laminated with various PCB layers through high vacuum, high press and high temperature lamination process, e.g. to FR4: 0.3 bar, 180 °C for 2 hrs and 16 kp/ cm^2. In addition, in PCB manufacture, high vacuum plasma is also applied widely for via and PTH (Plated Through Hole) cleaning. So it will be very dangerous that air bubbles like defects exist in optical layer and interfaces which can cause EOCB delamination and even damage. During EOCB fabrication, some

air bubbles or water molecules in air can probably flow into PDMS and form defects. In the thesis, one non-destructive ultrasonic scanning method is proposed to identify the defects due to their different sonic transimission velocity in air, PDMS and PCB substrates. Through selecting appropriate scanning frequencies, it cannot only identify the sizes of defects but position them in EOCB by amplitude and depth analyses. With the help of the intensity and the distance traveled by the reflected waves, two kinds of reports namely, amplitude and depth analyses can be produced. The amplitude report shows the intensity of the reflected waves where as the report for depth shows the distance (depth) through which the waves are penetrated.

The ultrasonic device is provided with a transmitter and a receiver. A uniform beam of ultrasonic waves are cast on to the sample from one side. The waves penetrate through the board if there are no flaws or errors. On the other hand, if there are any flaws at some locations, the waves at those particular locations would reflect back.[97]

These reflected waves will be received by the receiver. Using the time taken for the to and fro traveling of the waves and the velocity of the ultrasonic waves, the distance could be calculated. The intensity of the reflected waves could also be known, which is, in fact, inversely proportional to the distance traveled.

The ultrasonic scanning report may have different colors which vary from red to violet. Different colors in the report indicate different amplitude/ depth at respective locations of the board. The reports are provided with a scale of colors (VIBGYOR) with the help of which the amplitude/ depth at particular locations could be studied. The scale provided in the amplitude report shows the intensity of the waves received by the receiver in terms of percentage. For instance, 100 % in the report implies that the waves are reflected from the outer surface of the board without penetrating into it.

As the waves penetrate deeper in to the board, the intensity will be gradually decreased. The scale provided in the depth report shows how deep the waves are penetrated into the board in terms of millimeters (in this EOCB case). To put it in another way, the length of the scale is nothing but the thickness of the board. The color with the minimum value indicates that the waves are reflected from the top surface of the board without penetrating into it. Whereas the color with the maximum indicates that the waves are completely penetrated to the other end of the board and reflected back.

In order to verify the validity of this method, one preliminary test to EOCB (Copper coated FR4-PDMS-Copper coated FR4) with ultrasonic scanning analysis has been performed and shown in the figures below.

Fig. 4.25 is the amplitude report of the sample. As the main focus of this thesis is on the optical layer of EOCB, it is better to observe the amplitude at the interfaces of the optical layer with the layers above and below it. As the velocity of the ultrasonic waves and the distance (depth) of the interfaces are known, the amplitude at the interfaces could be observed by calculating the time at which the ultrasonic waves cross the interfaces approximately.

It could be noticed from the figure that there are three samples of EOCB in this case. The part of the board outside the three samples is the excess board considered for marginal purposes. The interpretation of this part could be neglected. The focus is only on the EOCB samples. The PDMS regions in the figure are in blue color which indicates that the intensity of the ultrasonic waves is about 70 % to 80 %. The PDMS regions are almost uniform (with the same color), which means that there are no air bubbles in that region. The yellowish and aqua regions where the intensity of the ultrasonic waves is about 30 % to 50 % could be air bubbles in this case. The air bubbles inside the sample are dangerous and could lead to unexpected consequences. Therefore, it is always important to avoid air bubbles between the layers. To 3rd EOCB sample in Fig. 4.25, along with the bottom half margin the color shows that there are possible air bubbles. In the following, the assumption is also verified through cutting the sample and observing the cross-section with microscope.

Additionally, Fig. 4.26 shows the depth report for the sample. From the scale below the figure it can be understood that the ultrasonic waves have penetrated more through the green regions. The distance/depth traveled by the waves in the PDMS region is less due to relatively larger sonic impedance in PDMS.

Anyway, in analyzing the depth report, it is important to know that the sample has layers of different materials and the ultrasonic waves travel with different velocities through the materials with different properties. Because of this, the point or the layer from which the waves are being reflected could not be properly studied. Moreover, this analysis could lead to fallacious interpretations and assumptions due to its less penetration in PDMS area. Hence, depth analysis is not recommended as main analysis method on EOCB defect detect.

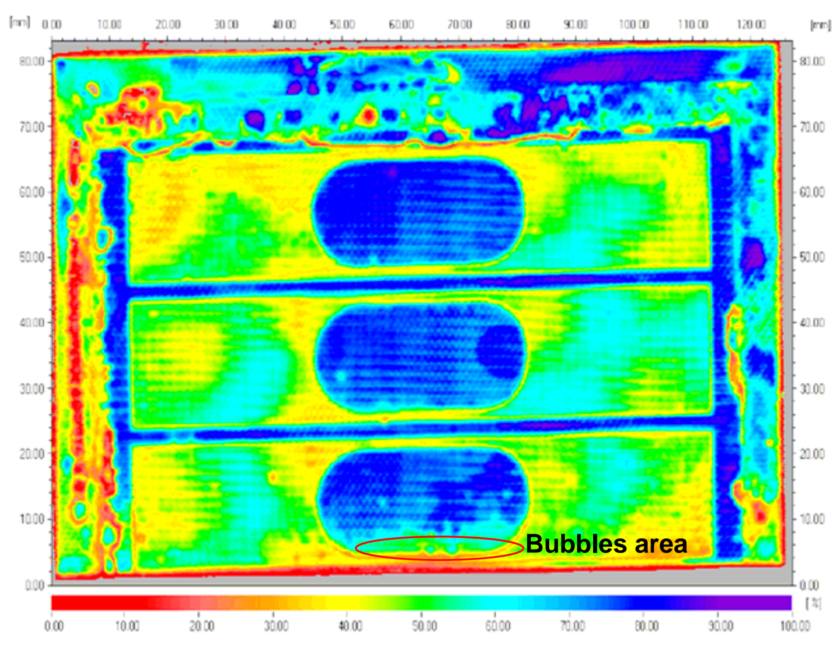

Figure 4.25 *Ultrasonic Scanning report – Amplitude Analysis*

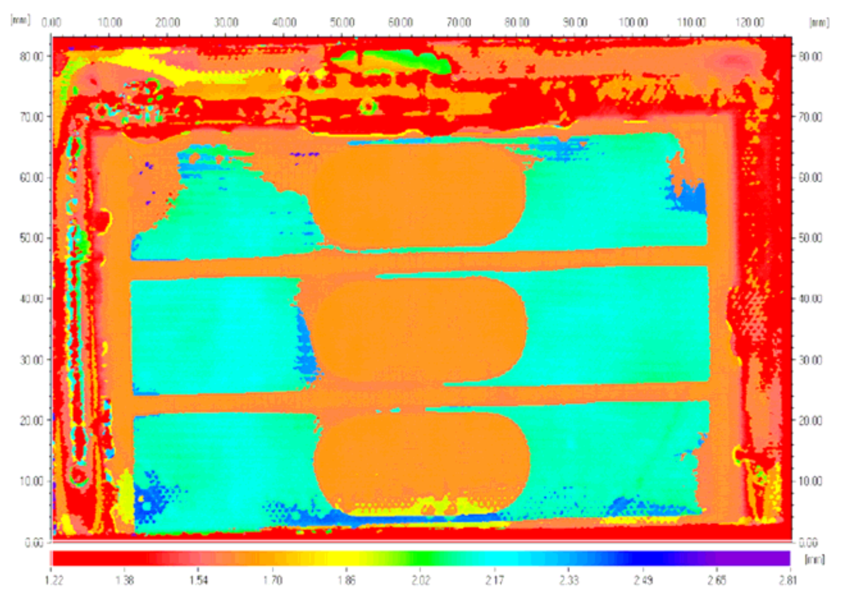

Figure 4.26 *Ultrasonic Scanning report – Depth Analysis*

C. Optical characterization

Optical waveguide transmission loss and mechanical stability are the two basic issues in EOCB specifications.

Here, the optical transmission loss of fabricated EOCBs has been measured at the standard wavelength for optical interconnects at 850 nm at different annealing conditions. Laser light was launched into the waveguides by a 50 μm GI fibre and detected by a 200 μm SI fibre. A transmission loss value of 0.035 dB/ cm was obtained which is almost that of a sample prepared without FR4 carriers (Fig.4.27, left column). After the measurement the sample was annealed at 180 °C for 2 hours which corresponds to the time and temperature conditions at multilayer PCB board lamination. The transmission loss shows a slight increase for the self-packaged EOCB to 0.04 dB/ cm and a decrease to 0.03 dB/ cm in case of the pure PDMS waveguide samples. This procedure is repeated at 260 °C for 1 min which represents the soldering condition.

As seen in Fig. 4.27, the waveguide loss of FR4 packaged EOCBs gets slightly increased compared with pure PDMS waveguide samples, but is still under 0.06 dB/ cm - even after annealing up to 260 °C/ 1min. Similar results are also obtained to Kapton, PCB copper and ED copper packaged EOCBs.

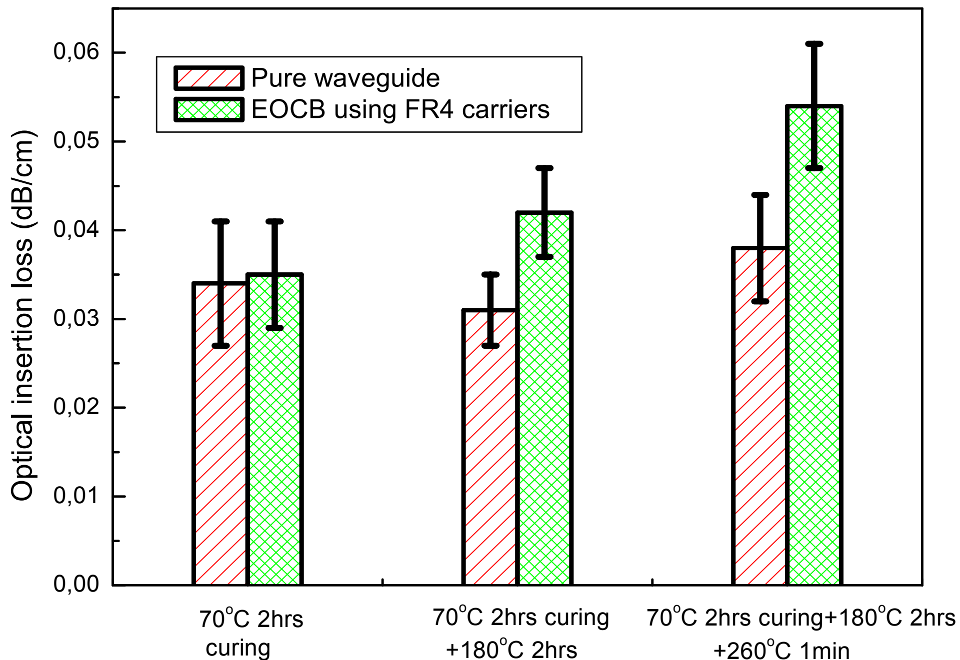

Figure 4.27 *Thermal stability of EOCB optical transmission loss*

In conclusion, fabricated EOCBs show sufficiently low optical transmission loss as

well as thermal stability to overcome standard PCB manufacturing conditions.

4.5 Environmental Stability of Realized EOCB

Electrical-optical circuit boards are investigated worldwide to overcome the problems arising from high speed signal transmission in high power computing systems. In previous chapters, most of the research work reported is focused on materials, fabrication technologies and identification to characterization methods etc. However, for an industrial implementation of EOCBs, a reliable production technology as well as a corresponding quality management must be developed. In the part the environmental stability of the optical and mechanical properties of fabricated PDMS based EOCBs based on SAP coating and board etching technologies is presented. The test methods are based on the standards for optical components in telecommunications (Telcordia) and general PCB tests (IPC and IEC).

4.5.1 Environmental Accelerated Testing Design

The concept of accelerated testing is to compress time and accelerate the failure mechanisms in a reasonable test period so that product reliability can be assessed. The only way to accelerate time is to stress potential failure modes. These include electrical and mechanical failures. Figure 4.28 shows the basic concept of stress testing. Failure occurs when the stress exceeds the product's strength.

In a product's population, the strength is generally distributed and usually degrades over time. Applying stress simply simulates aging. Increasing stress increases the unreliability (shown in Figure 4.28 as the overlap area between the strength and stress distributions) and improves the chances for failure occurring in a shorter period of time.

This also means that a smaller sample population of devices can be tested with an increased probability of finding failure. Stress testing amplifies unreliability so failure can be detected sooner. Accelerated life tests are also used extensively to help make predictions. Predictions can be limited when testing small sample sizes. Predictions can be erroneously based on the assumption that life-test results are representative of the entire population. Therefore, it can be difficult to design an efficient experiment that yields enough failures so that the measures of uncertainty in the predictions are not too large. Stresses can also be unrealistic. Fortunately, it

is generally rare for an increased stress to cause anomalous failures, especially if common sense guidelines are observed.[98]

Anomalous testing failures can occur when testing pushes the limits of the material out of the region of the intended design capability. The natural question to ask is: What should the guidelines be for designing proper accelerated tests and evaluating failures? The answer is: Judgment is required by management and engineering staff to make the correct decisions in this regard. To aid such decisions, the following guidelines are provided:

1). Always refer to the literature to see what has been done in the area of accelerated testing.

2). Avoid accelerated stresses that cause “nonlinearities,” unless such stresses are plausible in product-use conditions. Anomalous failures occur when accelerated stress causes “nonlinearities” in the product. For example, material changing phases from solid to liquid, as in a chemical “nonlinear” phase transition (e.g., solder melting, intermetallic changes, etc.); an electric spark in a material is an electrical nonlinearity; material breakage compared to material flexing is a mechanical nonlinearity.

3). Tests can be designed in two ways: by avoiding high stresses or by allowing them, which may or may not cause nonlinear stresses. In the latter test design, a concurrent engineering design team reviews all failures and decides if a failure is anomalous or not. Then a decision is made whether or not to fix the problem. Conservative decisions may result in fixing some anomalous failures. This is not a concern when time and money permit fixing all problems. The problem occurs when normal failures are labeled incorrectly as anomalous and no corrective action is taken.

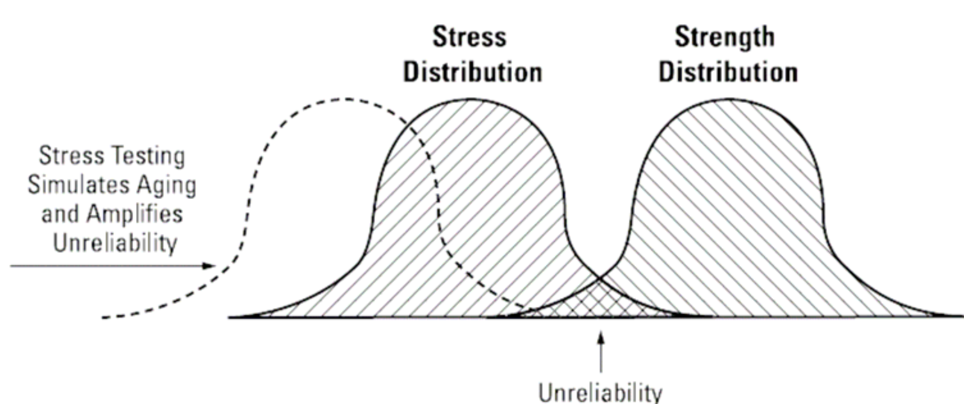

Figure 4.28 *Principal of accelerated test*

However, presently there are no any existing environmental stability standard test procedures for EOCBs, in the thesis for the first time we define the test procedures by combining general PCB test methods (e.g. IPC-TM-650 and IEC 99) together with standard test methods for optical components in telecommunications (e.g. Telcordia standards GR-1220 and GR-1209) as test methods for verification of EOCBs environmental stability. From these methods and standards, based on our experiences and knowledge to EOCB materials and products, and similar literatures on PDMS based products environmental tests the following test items significantly related with environmental stability have been identified:

A. Tests against reliability during fabrication

1) Lamination conditions: 180 °C for 2 hrs., 16 kp/ cm^2 (To FR4);

2) Solder floating: 3 times 10 s solder floating at 260 °C.

B. Tests against reliability during operation

1) Damp heat: 40 °C, 93 % humidity, 96 hrs.;

2) Dry heat: 150°C for 3 - 10 days (depending on the specific EOCBs application environments);

3) Thermal shock: -50 °C - 125 °C, 100 cycles;

Except for the exposure to dry heat, all other tests have been performed at a professional PCB test house (Microtec GmbH, Stuttgart).

4.5.2 Determination of Simulating Aging Time and Samples Sizes

To estimate test time compression and devise test plans that include sample size requirements, both acceleration models and statistical analysis are required.

A. Determination of simulating aging time

1). Dry Heat Operating Life Acceleration Model

In High-Temperature Operating Life testing, devices are subjected to elevated temperature under bias for an extended period of time. Often, it is assumed that the dominant thermally accelerated failure mechanisms will follow the classical Arrhenius relationship. The traditional dry heat Arrhenius acceleration model is provided in Eqn. 4.14. The Arrhenius function is important. It is not only used in reliability to model temperature-dependent failure-rate mechanisms, but it also

expresses a number of different physical thermodynamic phenomena. In Equation 4.14, we see that this factor is exponentially related to the activation energy. As the name connotes, in the failure process there must be enough thermal energy to be activated and surmount the potential barrier height of value E_a. As the temperature increases, it is easier to surmount this barrier and increase the probability of failure in a shorter time period. Thus, the activation energy parameter expresses a characteristic value that can be related to thermally activated failure processes. Each failure process has associated with it a barrier height E_a. In practice, when trying to estimate acceleration factor without knowing this value for each potential failure mechanism, a conservative value is used. For example, 0.7 eV is typically used for IC failure mechanisms and appears to be somewhat of an industry standard for conservatively estimating test times. With respect to EOCB products, high temperature stability PDMS (up to 300 °C) is integrated into PCB and obviously the activation energy is not determined by PDMS but its surrounding PCB materials so we will continue to keep the value for calculation of temperature acceleration factor in the model. That is, a low value will overestimate the test times and/or sample sizes needed to meet test objectives.

Obviously, the other important considerations are the actual use and stress temperatures. These estimates may also have errors. For example, to accurately assess time compression in testing, a device's junction temperature rise under bias needs to be taken out.[98]

$$A_T = Exp\{\frac{E_a}{K_B}[\frac{1}{T_{use}} - \frac{1}{T_{stress}}]\} \qquad (4.14)$$

$$Test\ Time = Life\ Time / A_T$$

Notation: A_T=Temperature acceleration factor, T_{stress}= Test temperature (K), T_{use}=Use temperature (K), E_a= Activation energy, and KB=8.6173e-5 eV/ °K (Boltzmann's constant).

In terms of the definition for dry heat test to EOCB, test time is 96 hours, test temperature is 150 °C and use temperature is supposed to be 25 °C.

From Eq. 4.14, the acceleration factor is:

A_T = Exp {(0.7 eV/ 8.6173 × 10–5eV/ °K) × [1/(273.15 + 25) –1/(273.15 + 150) °K]} = 3128.99

From Eq. 4.14, the test time of 96 hours can simulate:

Life Time= Test Time × A_T = 96 × 3128.99 = 300,353 hours = 34.3 years.

2). Temperature-Humidity-Bias (THB) Acceleration Model (Damp heating)

In THB, test devices are put at elevated temperatures and humidity under bias for an extended period of time. One of the most common THB models used in the industry is a 1989 Peck model shown in Equation 4.15. This includes a relationship between life-and-temperature (Arrhenius model) and life-and-humidity (Peck model), so that the product of the two separable factors yields an overall acceleration factor. When Peck originally proposed this model, he reviewed all published life-in-humidity conditions versus life at 85 °C/ 85% RH for epoxy packages. His results found good agreement with the model. Fitted data found nominal values for Ea to lie between 0.77 and 0.81 and nominal values between 2.5 and 3.0 for m.[98]

Notation: A_{TH} = temperature-humidity acceleration factor, R_{stress}=relative humidity of test, R_{use}=nominal use relative humidity, and m=humidity constant (To normal IC chip and PCB, it was set to be 2.66. For PDMS is a hydrophobic materials and has a good water resistant properties 2 times more than epoxy applied for packaging in IC chip, in the model we set it to be 5.2.).

$$A_T = Exp\{\frac{E_a}{K_B}[\frac{1}{T_{use}} - \frac{1}{T_{stress}}]\}$$

$$A_H = (\frac{R_{stress}}{R_{use}})^m \qquad (4.15)$$

$$A_{TH} = A_T \cdot A_H$$

$$Test\ Time = Life\ Time / A_{TH}$$

In terms of the definition for damp heat test to EOCB, test time is 96 hours, test temperature and humidity are 40 °C and 93 % RH and use temperature temperature and humidity are 25 °C and 40 % RH.

From Eq. 4.15, The temperature acceleration factor is:

A_T = Exp {(0.7 eV/ 8.6173 × 10–5eV/ °K) × [1/(273.15 + 25) –1/(273.15 + 40) °K]} = 3.69

The humidity acceleration factor is

$A_H = (93\ \%RH / 40\ \%RH)^{5.2} = 80.43$

Therefore, the combined temperature humidity acceleration factor is:

A_{TH} = 80.43 × 3.69= 296.8

From Eq. 4.15, the test time of 96 hours can simulate:

Life Time= Test Time × A_T = 96 × 296.8 = 28,492 hours.

3). Temperature Shock Acceleration Model

In Temperature shock, test devices are subjected to a number of cycles of alternate high and low temperature extremes. This cyclic stress produced in temperature shock is related to thermal expansion and contraction undergone in the material. To relate field usage to accelerated test conditions, the most widely used model in industry is the Coffin-Manson model. This is a simple model used for estimating the temperature shock and cycle acceleration factor (see Eq. 4.16).

Reasonably estimating the acceleration factor depends on the failures being caused by fatigue subject to the Coffin-Manson law for cyclic strain versus the number of cycles to failure. Values between 2 to 4 have typically been reported in the literature for K. These values are related to the specific design. A value of 2.5 is commonly used for solder-joint fatigue, while 4 is often reported for IC interconnection failures. The lower value (2.5) is a good value for conservative estimates.

Additionally, for Tg of PDMS in under -50 °C and the decomposition temperature is up to 300 °C, hereby, to EOCB products K we choose 3.5 for estimation of the life time.[98]

$$A_{TS} = \left(\frac{N_{use}}{R_{stress}}\right) = \left(\frac{\Delta T_{stress}}{\Delta T_{use}}\right)^{K} \quad (4.16)$$

Notation: Test: -50 to 125 °C, Nominal= -5 °C to 25 °C and K= 3.5,

$A_{TS} = (T_{Stress}/ T_{Use})^K$ = (175 °C/ 30 °C)$^{3.8}$= 479.4, and tem times cycles for one day. Test cycles are 100 and thus for 10 days. So the simulating aging time is 4794 days and about 13 years.

B. Determination of samples sizes

There are numerous types of accelerated tests. Any test that in some way accelerates environmental use conditions is an accelerated test. Two of the most common types of accelerated tests used in industry are catastrophic and

failure-free testing. In a catastrophic accelerated test, a frequent objective is to estimate the failure rate at a use condition. DMT is based on failure-free testing. The main objective of a DMT (Design Maturity Testing) test is to determine whether a design will meet its reliability objective at a certain level of confidence. This requires that a statistically significant sample size be tested in a number of different stress tests. However, at this point, we would like to illustrate how to conservatively plan a DMT to demonstrate that a particular reliability objective can be met.

In the part, it will plan accelerated tests for a failure-free DMT to demonstrate that EOCB will meet its reliability objective of 400 FITs (Failure in Time, one FIT is equal to one device failure in 10^9 device-hours of operation) at the 90 percent confidence level. To estimate the sample size required to show that this component is failure-free of any dry heat, damp heat and temperature shock type failure modes. The acceleration factors found above will be used for design.

In the design, we assume that each test will check for different failure modes. This means that each test is allocated a portion of the failure rate. One allocation plan is assigned, where damp heat-, temperature shock-, and dry heat-type failure modes were assigned 50 percent, 20 percent, and 30 percent, respectively, of the total reliability. Using this plan, the 400 FITs are broken up with 200, 80, and 120 FITs to THB, TC, and HTOL tests, respectively. At this point, a single-sided chi-square estimate for sample-size planning can be used.

Once reliability objectives are established, sample sizes can be planned with statistical confidence. To determine a statistical sample size to meet a particular reliability objective at a specific confidence level, it is common to use a chi-square, χ^2, confidence estimate, given by (See eq. 4.17).[98]

$$N = \frac{\chi^2(\gamma, 2Y + 2)}{2\bar{\lambda} A t} \quad (4.17)$$

Where, N = the sample size, λ = the upper-bound or failure-rate objective, Y = the number of failures (nominally zero), t = the total test time, A = the estimated test/failure mode acceleration factor, and γ= the confidence level (nominally 90 %).

For example, the Thermal Shock values are:

Y=0 Faliures, χ^2(90 %, 2) = 4.605, λ = 120 FITs = 1.2 e-7 failure/ hour, A = 479.4 (from calculation on Temperature Shock Acceleration Model) and t = 10 cycles × 24 hours = 240 equivalent test hours.

Thus, N = 4.605/ (2 × 0.8 e-7 × 479.4 × 240) = 251 waveguides = 21 EOCB (For in terms of our mould, every EOCB will include 12 waveguides)

Using this same approach for the other tests, the results are summarized in Table 4.8.

In order to check the influence of the PCB carrier materials on the optical waveguide loss, samples with and without different carrier materials have been prepared. About in terms of reliability objective of 400 FITs and defined minimum sample sizes, samples based on etched FR4, Kapton and copper coated FR4 substrates and respective SAPs are fabricated in terms of the procedure shown schematically in Fig.4.21. The sample sizes for lamination simulating and solder floating are both set to be 5 EOCBs, i.e. in the level of 60 waveguides for the two simulating temperatures are both lower than the decomposition temperature of PDMS and the lasting times are very short as well. The thickness of the PDMS waveguide layer is about 200 μm resulting in a total sample thickness (including the two PCB carrier layers) of about 400 - 600 μm. The dimensions of the samples prepared for the environmental tests are 10 cm × 1 cm, each carrying 12 parallel straight waveguides.

Table 4.8 *Minimum sample sizes for EOCB environmental stability tests*

Accelerated Test	***Acceleration Factor***	***Test Time (hours)***	***FITs***	***Sample Size***
Dry heat	3128.99	96	120	6
Damp heat	296.8	96	200	34
Temperature shock (100 cycles)	479.4	240	80	21
Lamination	N.A	N.A	N.A	5
Soldering floating	N.A	N.A	N.A	5

4.5.3 Optical Stability of EOCBs

The influence of all environmental tests on refractive indices (measured at 589 nm) of PDMS core and cladding is illustrates in Fig. 4.29 and three test procedures (damp heat treatment, thermal shock, and soldering float) on the optical waveguide

loss is summarized in Fig. 4.30 and results after simulating lamination has been illustrated in Fig. 4.27. For evaluation, 12 waveguides on each sample have been measured at 850 nm wavelength before and after each test. The tests have been performed with PDMS waveguide samples laminated between three different PCB carriers: uncoated FR4, copper coated FR4, and Kapton.

The results show that damp heat has no significant influence on the loss which is expected because of the good water resistant properties of PDMS material. Similar insignificant changes of the loss figures are observed after thermal shock treatments. This is explained by the high mechanical flexibility of the PDMS material. The influence of dry heat on the waveguide loss is documented in Fig. 4.31. The motivation for testing the waveguide samples against dry heat results from general PCB-requirements concerning their long-term durability at high-temperature operation conditions. Figure 4.31 shows the resulting waveguide loss figures before and after dry heat exposure. The waveguide loss remains stable up to about 4 days, after 5 days a loss increase of about 0.02 dB/cm is observed and after 10 days the total loss increase is about 0.03 dB/cm. We conclude that the waveguide transmission loss is quite sensitive to long time dry heat exposure (150 °C, 10 days). However, even at these strongest test conditions, the total waveguide transmission loss remains below 0.1 dB/cm which is a required target for most of the optical interconnect applications.

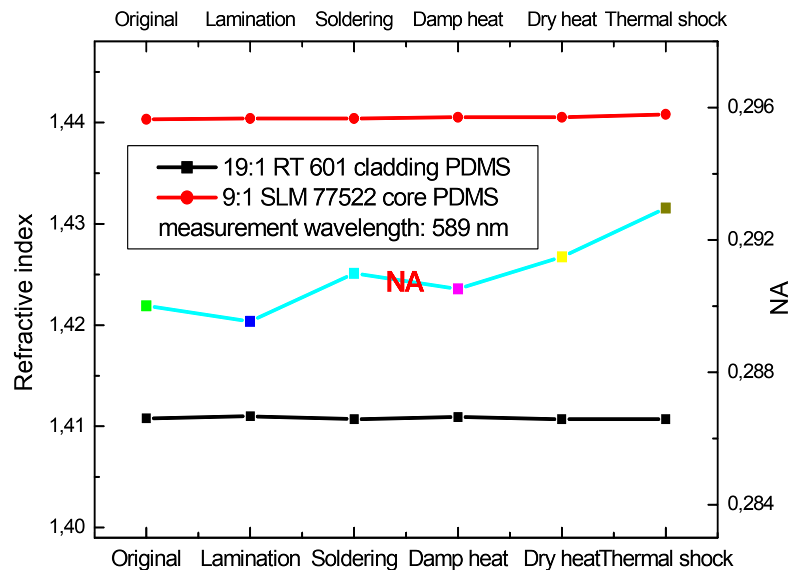

Figure 4.29 *Influence of different environmental conditions on optical wavguide materials refractive indices and NA*

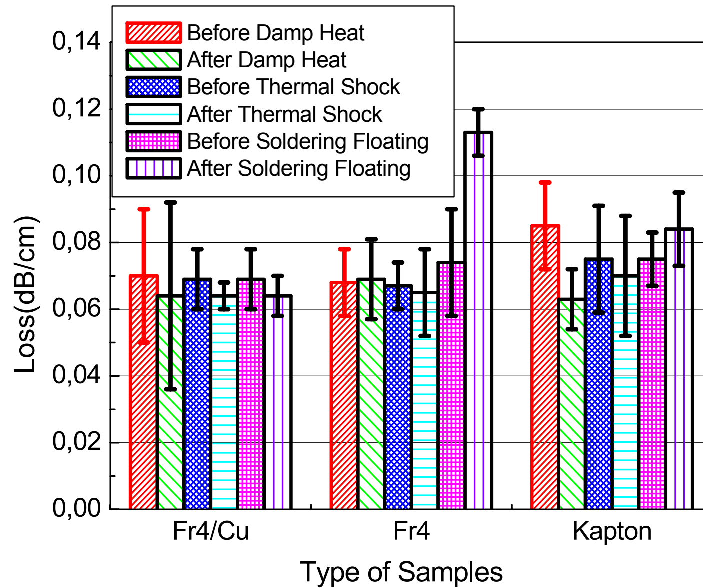

Figure 4.30 *Influence of different environmental conditions and different PCB-carrier materials on optical wavguide loss*

4.5.4 Mechanical Stability of EOCBs

The mechanical stability of fabricated EOCBs depends in a crucial way on the interfacial strength between the optical PDMS layer and the PCBs. If not strong enough, thermal stress resulting from CTE (Coefficient of Thermal Expansion) and Young's modulus mismatch will cause delamination and therefore damage. We have tested the mechanical stability of PDMS layers embedded between two copper coated FR4 laminates against the environmental test conditions indicated above by using a pull-off test described in detail in chapter 4.4.3. The obtained results for the maximum mechanical strength are shown in Table 4.9. By comparing the achieved values with the measured stability limit of pure PDMS (1.35 ± 0.33 MPa) it is clear that the mechanical stability limit of the prepared samples is determined by the intrinsic material stability of the PDMS layer and not by the interface properties. Similar results are obtained for laminates made from Kapton, uncoated FR4 and ED copper.

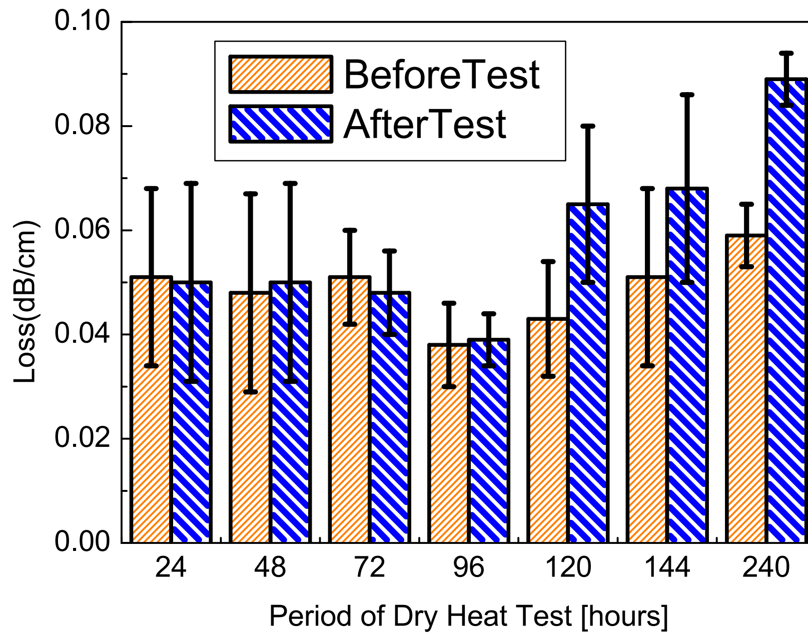

Figure 4.31 *Influence of dry heat treatment on optical waveguide loss*

Table 4.9 *Maximum mechanical strength after different environmental tests*

Test item	***Max. pull strength of laminate (MPa)***
70 °C 2hrs curing	1.35 ± 0.33
After lamination	1.44 ± 0.29
After thermal shock	1.41 ± 0.28
After damp heating	1.37 ± 0.32
After Dry heat	1.37 ± 0.31
After soldering float	1.42 ± 0.28

4.6 Summary of results of the chapter

In the chapter, a novel self-packaging method of PDMS based optical waveguide layers laminated to standard PCB carrier materials has been experimentally verified with identified optimum bonding conditions. The mechanical stability of the fabricated EOCBs is limited not by the interfacial bonding strength between PDMS and PCBs, but by the intrinsic mechanical stability. Reasonable environmental test procedures to check the optical and mechanical stability performances of EOCBs have been defined and implemented to PDMS-waveguide layer based EOCBs. Except the good mechanical stability the packaged EOCBs exhibit low and stable optical loss values (<0.1 dB/cm) even at extreme environmental conditions.

5 Summary and outlook

In the thesis work, combining with polysiloxanes based EOCB project: Prospeos (worldwide first industrial production of EOCBs within the frame of BMBF projects) optical aspects and mechanical aspects which mainly determine EOCB products' operation stability and reliability are analyzed and focused in detailed. Basic quality factors in the two aspects, including the influences of the materials, processes, and environments etc. on the optical, mechanical and thermal performance of the final EOCB product are identified and studied respectively in order to assure the EOCB products' quality and long-term reliability. Additionally, some basic quality monitoring methods as well as test and optimization procedures are identified and verified as well.

In details, first with respect to optical aspects of EOCBs, the impact factors on refractive indices of polysiloxanes materials were identified and verified in terms of bandwidth request from our customer and market requests. Furthermore, the absorption loss of polysiloxane in the spectral datacom and telecom region of 600 - 1600 nm was analyzed and summarized to be scattering loss and absorption loss due to molecular vibrational overtone and combination bands of the CH containing groups. In terms of the observed positions of fundamental, overtone and combination bands of CH containing groups' vibrations in the mid-IR and NIR spectra, anharmonicity constants including normal harmonic vibration frequencies have been determined and two empirical equations for estimating the significant intrinsic absorption loss wavelengths has been presented in terms of core and cladding two different PDMS based polymers. The results agreed well with the experimental data. Moreover, we derived two empirical equations between integral band strength and the intrinsic absorption loss based on the NIR spectral data of cladding and core two different PDMS based materials, which can be exploited also for the limit estimation of the optical loss in deuterated or halogenated such siloxane-based polymers applied in different datacom devices. Additionally, the PDMS waveguides were fabricated with low optical insertion loss at 850 nm and

1300 nm respectively, and of high thermal stability were also verified, which prove indeed two components thermal curing PDMS are very promising in production of datacom devices. In the end of this part, the impact factors on optical properties of EOCB products from process aspects were identified as well as the proposal of the optimum process conditions.

In the following, with respect to mechanical aspects of EOCBs, based on study of polysiloxanes curing mechanism, a novel self-packaging method of PDMS based optical waveguide layers laminated to standard PCB carrier materials has been identified and experimentally verified. Through experimental verification, it was found that the mechanical stability of the fabricated EOCBs is limited not by the interfacial bonding strength between optical layer and PCB layers but by the intrinsic mechanical stability of the PDMS material at about 1.35 MPa. Additionally, in part of design for reliability, ccombining general PCB test methods together with standard test methods for optical components applied in telecommunications, one reasonable reliability test procedure has been defined and practically implemented to check the optical and mechanical stability performances of EOCBs as well as the determination acceleration factors and sample sizes. After tests, it was found, except the good mechanical stability the packaged EOCBs exhibit low and stable optical loss values (<0.1 dB/cm) even at extreme environmental conditions.

In the future, apart from the costs control in EOCB production line e.g. from materials and processes etc., how to manage and control efficiently the identified quality factors with low cost in EOCB production will be very worthy expecting in terms of those basic quality requirements. Moreover, a topic, whatever must be further examined and considered in serious in the future, is just the realization of an appropriate and compatible passive coupling and packaging solution, which achieves optical loss as small as possible. Along with Prospeos project, a first worldwide foundation-stone of EOCB and its production was built. However in order to fully industrialize it and produce the eligible and reliable EOCB products, it is very important to establish series of inspections standards and evaluation criterions with respects to EOCB products.

6 Literatures

6.1 Applied literatures

1. BPA Consulting Ltd., „Worldwide market and technology trends for optical substrates and backplanes 2003-2010”, *BPA Report* no. 825, 2003.
2. Whitepaper: PCI Express Ethernet Networking. www.intel.com, date: 11.01.2007.
3. Miller, D A B., „Rationale and Challenges for Optical Interconnects to Electronic Chips”, *Proceedings of the IEEE 88*, Nr. 6, 2000, pp. 728-749.
4. Voges, E., Petermann, K. (Hrsg.), „Optische Kommunikationstechnik”, Springer-Verlag, 2002.
5. Bauer, J., Ebling, F., Schröder, H., „Verbindungstechnik New Generation“, *Elektronik Praxis,* 2005.
6. Huang, D, Sze, T, Landin, A, Lytel, R and Davidson, H L., „Optical Interconnects: Out of the Box Forever?”, *IEEE Journal of Selected Topics in Quantum Electronics*, Nr. 9, 2003, pp. 614-623.
7. Berger, C, Kossel, M A., Menolfi, C., Morf, T., Toifl, T. and Schmatz, M L., „High-density optical interconnects within large-scale systems”, *Proceedings of SPIE 4942*, 2003, pp. 222-235.
8. Kopetz, S., Rabe, E., Kang, W., and Neyer, A., „Polysiloxane optical waveguide layer integrated in printed circuit board”, *Electronics Letters* 40, Nr. 11, 2004, pp. 668-669.
9. Cai, D., Neyer, A., „Realization of Electrical-Optical-Circuit-Board self-packaging,” *Proceedings on 57th Electronic Components and Technology Conference, ECTC*, Reno, Nevada, USA, 2007, pp. 1368-1374.
10. Eldada L., „Polymer integrated optics: promise vs. practicality”, *Proc. Of SPIE 4642*, 2002, pp. 11-22.

11. Fa. Exxelis Ltd., Produktinformation Truemode Polymer, Internet: http://www.exxelis.com/products/truemode.php, 5.2.2007.
12. Bosman, E., Geerinck, P., Van Daele, P., „Optical connections on flexible subtrates", Proc. of SPIE, vol. 6185, 2006, pp. 60-67.
13. Wang, L., Wang, X, Chen, R.T., „Low-loss, thermally stable waveguide with 45° micromirrors fabricated by soft molding for fully embedded board-level optical initerconnects", Proc. of SPIE, vol. 5731, 2005, pp. 87-93.
14. Optical CrossLinks, Inc., „Multi-mode Circuit Board Components Optical Interconnections, Preliminary Product Brief", Internet: http://opticalcrosslinks.com, 7.11.2006.
15. DeGroot, J.V., Glover, S.O., Dyer, M.J., „Polymeric Optical Interconnect for Chip-to-Chip Communication", Proc. of the OFC 2005, Anaheim, USA, 2005, pp. OFD6.
16. Moynihan, M. et al., „Progress Towards Board-level Optical Interconnect Technology", Proc. of SPIE, vol. 5731, Photonics Packaging and Integration, 2005, pp. 50-62.
17. Schröder, H. et al., „Temperaturstabile Wellenleiter und optische Kopplung für elektro-optische Leiterplatten", Tagungsband der GMM/DVS-Tagung Elektrische Baugruppen, Aufbau und Fertigungstechnik, 2006, Fellbach, Deutschland.
18. Produktkatalog für micro resist technology Produkte. Internet: http://www.microresist.de/dl/booklet_d_lq.pdf, aufgerufen am 7.11.2006.
19. Kim, J.S., Kang, J.W., Kim, J.J., „Simple and Low Cost Fabrication of Thermally Stable Polymeric Multimode Waveguides using a UV-curable Epoxy", Jpn. J. Appl. Phys., vol. 42, 2003, pp. 1277-1279.
20. Fa. Luvantix CO Ltd., Internet: http://luvantix.com/specialty-EFIRON%20WR.htm, Letztes Update 1.4.2003, 5.2.2007.
21. Lamprecht, T., Horst, F., Dangel, R., „Passive Alignment of Optical Elements in a Printed Circuit Board", Proc. of the 56th Electronic Components and Technology Conference (ECTC), 2006, pp. 761-767.
22. Moisel, J., „Optische Backplanes für Avionik und Telekommunikation", it - Information Technology, Vol. 45, No.2, 2003, pp. 72-78.

23. Su, K., DeGroot, J.V., Lo, P.Y., „Siloxane Materials for Optical Applications", Proc. of SPIE, vol. 6029, 2006, pp. 318-325.
24. Graydon, O., „Photonics unlocks chip bandwidth bottleneck", Opto & Laser Europe (OLE), Oct. 2004, pp. 25-27.
25. Choi, C., Lin, L., Chen, R.T., „Flexible Optical Waveguide Film Fabrications and Optoelectronic Devices Integration for Fully Embedded Board-Level Optical Interconnects", IEEE Journal of Lightwave Technology, vol. 22, no. 9, 2004, pp. 2168-2176.
26. Ishii, Y., Koike, S., Ano, Y., „SMT-Compatible Large-Tolerance "OptoBump" Interface for Interchip Optical Interconnections", IEEE Transactions on Advanced Packaging, vol. 26, no. 2, 2003, pp. 122-127.
27. Lee, E.H., Lee, S.G., Park, S.G., „Fabrication and integration of VLSI micro/nano-photonic circuit board", Microelectronic Engineering, vol. 83, 2006, pp. 1767-1772.
28. Chen, Y.-M., Yang, C.-L., Cheng, Y.-L., „10 Gbps Multi-Mode Waveguide for Optical Interconnect", Proc. of the 55th Electronic Components and Technology Conference (ECTC), 2005, pp. 1739-1743)
29. Schröder, H. et al., „Polymer Optical Interconnects for PCB", Proc. of the IEEE int. Conf. on Polymers and Adhesives in Microelectronics and Photonics (Polytronic), Potsdam, Germany, 2001, pp. 337-343
30. Van Steenberge, G., Hendrickx, N., Van Daele, P., „Laser Ablation of Parallel Opical Interconnect Waveguides", IEEE Photonics Technology Letters, vol. 18, No. 9, 2006, pp. 1106-1108.
31. Endo, Y., Fujimoto, K., Hirano, K., „Optical Wave Guide Inserted Opt-Electronic Circuit Board with High Design Possibility", Hitachi Cable Review, no. 22, 2003, pp. 38-41.
32. Glebov, A. et al, „Optical Interconnect modules with fully integrated reflector mirrors", IEEE Phot. Tech. Letters, vol. 17, 2005, p. 1540.
33. Chang, G.-K. et al., „Chip-to-Chip Optoelectronics SOP on Organic Boards or Packages", IEEE Transactions on Advanced Packaging vol. 27, no.2, 2004, pp. 386-397.
34. Krabe, D. et al., „New Technology for Electrical/Optical Systems on Module and Board Level - The EOCB Approach -", Proc. of the 50th IEEE ECTC, Las

Vegas, USA, 2004, pp. 970-974.

35. Kim, J.-S., Kim, J.-J., „Stacked Polymeric Multimode Waveguide Arrays for Two-Dimensional Optical Interconnects", IEEE Journal of Lightwave Technology, vol. 22, No. 3, 2004, pp. 840-844.
36. Jokerst, N.M. et al., „Planar Lightwave Integrated Circuits With Embedded Actives for Board and Substrate Level Optical Signal Distribution", IEEE Transactions on Advanced Packaging, vol. 27, no.2, 2004, pp. 376-385.
37. Kim, J.T., Choi, C.-G., „Integration of a polymeric planar-lightwave-circuit chip based on a polymer microsystem and a UV imprinting technique", Journal of Micromechanics and Microengineering, vol. 15, 2005, pp. 1140-1146.
38. Uhlig, S., Fröhlich, L., Robertsson, M., „Polymer Optical Interconnects - A Scalable Large-Area Panel Processing Approach", IEEE Transactions on Advanced Packaging, vol. 29, no. 1, 2006, pp. 158-170.
39. Immonen, M., Wu, J., Kivilahti, J., „Influence of Environmental Stresses on Board-Level Integrated Polymer Optics", Proc. of the 55th Electronic Components and Technology Conference (ECTC), 2005, pp. 1653-1658.
40. Choi, C., Lin, L., Chen, R.T., „Flexible Optical Waveguide Film Fabrications and Optoelectronic Devices Integration for Fully Embedded Board-Level Optical Interconnects", IEEE Journal of Lightwave Technology, vol. 22, no. 9, 2004, pp. 2168-2176.
41. Shen, L.-C., Lo, W.-C., Chang, H.-H., „Flexible Electronic-Optical Local Bus Modules to the Board-to-Board, Board-to-Chip, and Chip-to-Chip Optical Interconnection", Proc. of the 55th Electronic Component and Technology Conference (ECTC), 2005, pp. 1039-1043.
42. Dasgupta, S. et al., „A Polymer Based Platform Technology for Integrated Photonics", Proc. of SPIE, vol. 5517, 2004, pp. 134-140.
43. Kopetz, S., Technologie optischer Lagen für elektrisch-optische Leiterplatten, Universität Dortmund, Diss. 2007. – Published soon.
44. Rabe, E., Technologien großformatiger Replikationsformen für elektrisch-optische Schaltungsträger, Universität Dortmund, Diss. 2007. – Published soon.
45. Michalzik, R., „Fiber Optic Data Communication: Technological Trends and Advances", Academic Press, 2002, pp. 216-269.

46. Neyer, A., Kopetz, S., Rabe, E., Kang, W., Tombrink, S., „Electrical-Optical Circuit Board Using Polysiloxane Optical Waveguide Layer", *Proc. of the 55th IEEE Electronic Components and Technology Conference (ECTC)*, Orlando, Florida, 2005, pp. 246-250.

47. Kopetz, S., Cai, D., Rabe, E., Neyer, A., „PDMS-based optical waveguide layer for integration in electrical–optical circuit boards", *Int. J. Electron. Commun. (AEÜ)*, vol. 61, 2007, pp. 163-167.

48. Groh, W., „Overtone absorption in macromolecules for polymer optical fibers," *Makromol. Chem.* 189, 1988, pp. 2861-2874.

49. Tanio, N., Koike, Y., „What is the most transparent polymer?", *Polymer Journal* 32, 2000, pp. 43-50.

50. Ballato, J., Foulger, S., Smith, D., „Optical properties of perfluorocyclobutyl polymers," *J. Opt. Soc. Am. B* 20, 2003, pp. 1838-1843.

51. Cai, D., Neyer, A., Kuckuk, R., Heise, H.M., „Optical absorption in transparent PDMS materials applied for multimode waveguides fabrication", *Optical materials*, in press.

52. Flipsen, T., Pennings A.J., and Hadziioannou, G., „Polymer optical fiber with high thermal stability and low optical losses based on novel densely crosslinked polycarbosiloxanes", *J. Applied Polymer Science* 67, 1998, pp. 2223-2230.

53. Yasuda, N., Yamamoto, H., Minami, S., Nobutoki, H., Wada, Y., and Yanagia, S., „Novel silicone polymeric material with high thermal stability for optical waveguides", *Jpn. J. Appl. Phys.* 41, 2002, pp. 624-630.

54. Usui, M., Hikita, M., Amano, T., Sugawara, S., Hayashida, S., Imamura, S., „Low-loss passive polymer optical waveguides with high environmental stability", *Journal of Lightwave Technology*14, 1996, pp. 2338 - 2343.

55. Kai, S., et al., „ Siloxane materials for optical applications", *Proceedings of the SPIE 6029,* 2006, pp. 318-325.

56. Ma, H., Jen A., and Dalton, L., „Polymer-based optical waveguides: materials, processing, and devices", Advanced Materials 14, 2002, pp. 1339-1365.

57. Conrady, A. E., „Applied Optics and Optical Design", Dover, New York, 1960.

58. Herzberger, M., „Colour correction in optical systems and a new dispersion formula", *Opt. Acta* 6, 1959, pp. 197-215.

59. Nakamura, S., Takasawa, N., and Koyamada, Y., „Comparison Between Finite-Difference Time-Domain Calculation With All Parameters of Sellmeier's Fitting Equation and Experimental Results for Slightly Chirped 12-fs Laser Pulse Propagation in a Silica Fiber", *J. Lightwave Technol.* 23, 2005, pp. 855-865.

60. Bekenstein, J. D., Schiffer, M., „Quantum Limitations of the Storage and Transmission of Information", *International Journal of Modern Physics C*, vol. 1, no. 4, 1990, pp. 355-422.

61. Cai, D., Neyer, A., Kuckuk, R., Heise, H.M., „ Raman, infrared and visible spectroscopy of PDMS for characterization of polymer optical waveguide material", in preparation.

62. Cai, D., Neyer, A., Kuckuk, R., Heise, H.M., „Optical properties of polydimethylsiloxane (PDMS) used for optical waveguides", in preparation.

63. Siesler, H., et al., „Near-infrared Spectroscopy", Wiley-VCH, 2002.

64. Bokobza, L., Buffeteau, T., Desbat, B., „Mid- and Near-Infrared Investigation of Molecular Orientation in Elastomeric Networks", *Appl. Spectrosc.* 54, 2000, pp. 360 – 365.

65. Y. Xia and G. Whitesides, „Replica molding with a polysiloxane mold provides the patterned microstructure", *Angew. Chem.* 37, 1998, pp. 550-575.

66. Simpson, T. R. E., Parbhoo, B., Keddie, J.L., „The dependence of the rate of crosslinking in poly(dimethyl siloxane) on the thickness of coatings", *Polymer* 44, 2003, pp. 4829-4838.

67. Iji M., Kiuchi Y., „Flame resistant glass-epoxy printed wiring boards with no halogen or phosphorus compounds", *Journal of Materials Science: Materials in Electronics*, Volume 15, Number 3, 2004, pp. 175-182(8).

68. http://www.isola.de/

69. Japanese Patent Publication Nos. 13508/ 1978 and 5836/ 1982.

70. Stephen J., „Siloxane Polymers", Prentice Hall, 1993.

71. http://www.wacker.com/

72. Shigeyoshi S., Mizoe, N., Sugimoto, M., „Theoretical Study of Platinum(0)-Catalyzed Hydrosilylation of Ethylene. Chalk-Harrod Mechanism or Modified Chalk-Harrod Mechanism", *Organometallics*, 17 (12), 1998, pp. 2510 -2523.

73. Giorgi, G., et al., „A theoretical investigation of the Chalk-Harrod and modified Chalk-Harrod mechanisms involved in hybrid integrated circuit building”, *Computational chemistry and molecular dynamics*, Volume 20, Issue 5, 2004, pp. 781-791.

74. Sakaki, S., „Theoretical Study of Reaction Mechanism of Hydrosilylation Reactions”, *Keiso Kagaku Kyokaishi*, VOL.1, NO.20, 2004, pp. 4-9.

75. Angioni, E., et al., „UV spectral properties of lipids as a tool for their identification”, *European Journal of Lipid Science and Technology*, Volume 104, Issue 1, 2002, pp. 59-64.

76. http://ec.europa.eu/environment/

77. Nissen, F., Griese, H., Middendorf, A., Muller, J., Potter, H., Reichl, H., „Environmental screening of packaging and interconnection technologies, Environmentally Conscious Design and Inverse Manufacturing”, *Proceedings. First International Symposium On Eco Design*, Volume 1, Issue 2, 1999, pp. 754- 759.

78. Mauerer, O., „Polymer Degradation and Stability”, *New reactive, halogen-free flame retardant system for epoxy resins*, Volume 88, Issue 1, 2005, pp. 70-73.

79. http://www.turi.org/

80. http://lhcb-tech-coor.web.cern.ch/lhcb-tech-coor/Safety/documents/FireTests-FR4.PDF.

81. http://lhcb-elec.web.cern.ch/.../ElectronicsInstallation/PCB_FR4/documents/Halogen_free_PCBS_status_March-04.pdf.

82. Segerberg, T., Gumaelius, L., Hessle, H., Ostensson, E., „Toxicological aspects of halogen free flame retardants based on denitrification inhibition tests”, *Proceedings of the 2000 IEEE International Symposium on Electronics and the Environment,* 2000, pp. 69-74.

83. Park, S., Lee, H., „ Effect of atmospheric-pressure plasma on adhesion characteristics of polyimide film”, *J.colloid and interface science*, Vol. 285, 2005, pp. 267-272.

84. Luo, S.J, Vidal, M., and Wong, C.P., „Study on surface tension and adhesion in electronic packaging”, *Proc 50th Electronic Components and Technology Conf*, Las Vegas, 2000, pp. 586-591.

85. Vladimirov, L., Oleinik, E., „FT-IR studies of thermal history effects on

molecular structure of epoxy resin systems”, *Microchimica Acta*, Volume 94, 1988, pp. 329-333.

86. Cherian, A., Varghese, L., Tachil, T., „Epoxy-modified, unsaturated polyester hybrid networks”, *European Polymer Journal*, Volume 43, Issue 4, 2007, pp. 1460-1469.
87. Hong S.-G.1; Wu C.-S, „DSC and FTIR analysis of the curing behaviors of epoxy/ DICY/ solvent open systems”, *Thermochimica Acta*, Volume 316, Number 2, 2002, pp. 167-175(9).
88. http://www.dupont.com
89. Lee S., Tien Y., Hsu C.F., „FTIR Analysis of Plasma Damage of Kapton”, *Plasmas and Polymers*, Volume 4, Numbers 2-3, 1999, pp. 229-239(11).
90. www.lle.rochester.edu/pub/review/v88/88_05_Optimizing.pdf
91. Lee, S., Tien, Y., „Spectroscopic investigations of plasma damage of kapton”, J*ournal of Vacuum Science & Technology B: Microelectronics and Nanometer Structures*, Volume 18, Issue 2, 2000, pp. 805-810.
92. Siau, S., Vervaet, A., Calster, A., „Influence of wet chemical treatments on the evolution of epoxy polymer layer surface roughness for use as a build-up layer”, *Applied Surface Science*, Volume 237, Issues 1-4, 2004, pp. 457-462.
93. Owens, D. and Wendt, R, „Estimation of the surface free energy of polymers,” *J.Appl.Polym.Sci.*, Vol. 13, 1963, pp. 1741-1747.
94. Guimond, S., Wertheimer, M.R., „Surface degradation and hydrophobic recovery of polyolefins treated by air corona and nitrogen atmospheric pressure glow discharge”, *J. Appl.Polym.Sci.*, Vol. 94, 2004, pp. 1291-1303.
95. Oosterom, R., Ahmed, T.J. *et al*, „Adhesion performance of UHMWPE after different surface modification techniques”, *Med Eng Phy.*, Vol. 28, 2005, pp. 323-330.
96. Song, R., Chiang M, et al, „Combinatorial peel tests for the characterization of adhesion behavior of polymeric films”, *Polymer*, Vol. 46, 2005, pp. 1643-1652.
97. http://www.ob-ultrasound.net/history-realtime.html
98. Crowe, D., Design for Reliability, CRC, 2001.

6.2 Own publications

A. Journals

1. Cai, D., Neyer, A., Kuckuk, R., Heise, H.M., „Optical absorption in transparent PDMS materials applied for multimode waveguides fabrication," Optical materials, in press.
2. Cai, D., Neyer, A., Kuckuk, R., Heise, H.M., „ Raman, infrared and visible spectroscopy of PDMS for characterization of polymer optical waveguide material", in preparation
3. Cai, D., Neyer, A., Kuckuk, R., Heise, H.M., „Optical properties of polydimethylsiloxane (PDMS) used for optical waveguides", in preparation.
4. Zhu, D., Cai, D. et al., „Environmental stability of PDMS-waveguides for electrical-optical circuit boards", Electron. Lett., vol. 5, 2007, pp. 627-628.
5. Kopetz, S., Cai, D. et al, „PDMS-based optical waveguide layer for integration in electrical-optical circuit boards", ÄEU-International Journal of Electronics and Communications, vol. 61, 2007, pp. 163-167.

B. Conference papers and posters

1. Cai, D., Neyer, A., „Realization of Electrical-Optical-Circuit-Board self-packaging," Proceedings on 57th Electronic Components and Technology Conference, ECTC 2007, Reno, Nevada, USA, 2007, pp. 1368-1374.
2. Cai, D., Neyer, A., Kuckuk, R., Heise, H.M., „Estimation of absorption loss in siloxane-based materials implemented as passive optical interconnects," Proceedings on Optical Fiber Communication, OFC 2007, Anaheim, California, USA, 2007, Techn. Digest, paper JWA 27.
3. Cai, D., Neyer, A., Kuckuk, R., Heise, H.M., „Near-infrared and visible spectroscopy of PDMS for characterisation of polymer optical waveguide materials," Proceedings on the XXVIIIth European Congress on Molecular Spectroscopy, Aug. 2006, Istanbul, Turkey.
4. Cai, D., Neyer, A., Kuckuk, R., Heise, H.M., „Optical absorption due to high overtone of molecular fundamental vibrations in PDMS materials applied for data communication," Proceedings on the 1st International Conference on Physics of Optical Materials and Devices, Sep. 2006, Montenegro.
5. Cai, D., Neyer, A., Kuckuk, R., Heise, H.M., „Optical spectroscopy applied on

characterization of PDMS for optical interconnects," Proceedings on the 4th International Conference on Advanced Vibrational Spectroscopy. Jun. 2007. Corfu Island, Greece.

6. Neyer, A., Rabe, E., kopetz, S., Zhu, D., and Cai, D., „Large-area replication technology for the production of electrical-optical circuit board," Proceedings on LEOS Summer Topical Meetings, Oregon, USA, 2007, pp.127-128.
7. Neyer, A., Rabe, E., kopetz, S., Zhu, D., and Cai, D., „Polymer multimode waveguides for integrated optics," Proceedings on European Conference of Integrated Optics, ECIO 2007, Copenhagen, Denmark, 2007, pp. 25-27.